Nagra
Nationale
Genossenschaft
für die Lagerung
radioaktiver Abfälle

Cédra
Société coopérative
nationale
pour l'entreposage
de déchets radioactifs

Cisra
Società cooperativa
nazionale
per l'immagazzinamento
di scorie radioattive

TECHNICAL REPORT 90-43

STRIPA PROJECT

SITE CHARACTERIZATION AND VALIDATION-BOREHOLE RADAR INVESTIGATIONS, STAGE III

E. SANDBERG
O. OLSSEN
L. FALK

ABEM AB, Uppsala, Sweden

NOVEMBER 1989

Parkstrasse 23 5401 Baden/Schweiz Telephon 056/20 55 11

Nagra
Nationale
Genossenschaft
für die Lagerung
radioaktiver Abfälle

Cédra
Société coopérative
nationale
pour l'entreposage
de déchets radioactifs

Cisra
Società cooperativa
nazionale
per l'immagazzinamento
di scorie radioattive

TECHNICAL REPORT 90-43

STRIPA PROJECT

SITE CHARACTERIZATION AND VALIDATION-BOREHOLE RADAR INVESTIGATIONS, STAGE III

E. SANDBERG
O. OLSSEN
L. FALK

ABEM AB, Uppsala, Sweden

NOVEMBER 1989

Parkstrasse 23 5401 Baden/Schweiz Telephon 056/20 55 11

Der vorliegende Bericht betrifft eine Studie, die für das Stripa-Projekt ausgeführt wurde. Die Autoren haben ihre eigenen Ansichten und Schlussfolgerungen dargestellt. Diese müssen nicht unbedingt mit denjenigen des Auftraggebers übereinstimmen.

Le présent rapport a été préparé pour le projet de Stripa. Les opinions et conclusions présentées sont celles des auteurs et ne correspondent pas nécessairement à ceux du client.

This report concerns a study which was conducted for the Stripa Project. The conclusions and viewpoints presented in the report are those of the authors and do not necessarily coincide with those of the client.

Das Stripa-Projekt ist ein Projekt der Nuklearagentur der OECD. Unter internationaler Beteiligung werden im Rahmen einer 3. Phase dieses Projektes von 1986-1991 Forschungsarbeiten in einem unterirdischen Felslabor in Schweden durchgeführt. Unter Anwendung des in den vorhergehenden Phasen 1 und 2 Gelernten sollen folgende Arbeiten realisiert werden:

- Anwendung verschiedener Felduntersuchungs- und Berechnungsmethoden, um den Wasserfluss und Nuklidtransport in einem unbekannten Felsvolumen des Stripagranites vorherzusagen und anschliessend zu überprüfen
- Evaluation verschiedenster Materialien und Methoden zum Abdichten wasserführender Klüfte im Stripagranit

Seitens der Schweiz beteiligt sich die Nagra an diesen Untersuchungen. Die technischen Berichte aus dem Stripa-Projekt erscheinen gleichzeitig in der NTB-Serie der Nagra.

The Stripa Project is organised as an autonomous project of the Nuclear Energy Agency of the OECD. Over the time period 1986-1991 (Phase 3 of the Project), an international cooperative programme of investigations is being carried out in an underground rock laboratory in Sweden. Building on experience gained in Phases 1 and 2, the following research will be carried out:

- Application of various site characterisation techniques and analysis methods with a view to predicting and validating groundwater flow and nuclide transport in an unexplored volume of Stripa granite
- Verification of the use of different materials and techniques for sealing water-bearing fractures in the Stripa granite

Switzerland is represented in the Stripa Project by Nagra and the Stripa Project technical reports appear in the Nagra NTB series.

Le projet de Stripa est un projet de l'Agence de l'OCDE pour l'Energie Nucléaire. C'est dans le cadre d'une troisième phase de ce projet allant de 1986 à 1991, que des travaux de recherches sont réalisés avec une participation internationale, dans un laboratoire souterrain de Suède. Il s'agit d'effectuer les travaux ci-dessous, en mettant en application ce que l'on a appris au cours des précédentes phases 1 et 2:

- Application de diverses méthodes de recherches sur le terrain et de calcul, pour prévoir puis contrôler l'écoulement de l'eau et le transport des nucléides dans un volume rocheux inconnu du granite de Stripa
- Evaluation des méthodes et des matériaux les plus divers, en vue de colmater des fractures aquifères du granite de Stripa

La Cédra participe à ces recherches pour la Suisse. Les rapports techniques rédigés à propos du projet de Stripa paraissent en même temps dans la série des Rapports Techniques de la Cédra (NTB).

ABSTRACT

The borehole radar investigation program Stage III of the SCV-site has comprised single hole reflection measurements with centre frequencies of 22 and 60 MHz. Single hole reflection measurement with both omni-directional and directional antennas have been performed in the boreholes C1, C2, C3 and the D-holes (D1-D6). Crosshole tomographic measurements as well as crosshole reflection measurements have been made between the boreholes C1-C2, W1-C1 and W1-C2. The range obtained in the single hole reflection measurements was approximately 100 m for the lower frequency (22 MHz) and about 60-70 m for the centre frequency 60 MHz. In the crosshole measurements transmitter-receiver separations from 20 to 120 m have been used.

The Stage III radar investigations have essentially confirmed the three dimensional description of the structures at the SCV-site. The conceptual model of the site which was produced based on the Stage I data included three major zones (GA, GB, and GH), two minor zones (GC and GI) and a circular feature (RQ). The major features are considered to be the most significant at the site and are all observed in the Stage III boreholes close to their predicted locations. The circular feature RQ has also been found in two of the additional tomograms at the predicted location. RQ is seen as a ringshaped feature in the attenuation tomograms and as a single spot anomaly in the slowness tomogram.

The results indicate that the zones are not homogeneous but rather that they are highly irregular containing parts of considerably increased fracturing and parts where their contrast to the background rock is quite small. The zones appear to be approximately planar at least at the scale of the site. At a smaller scale the zones can appear quite irregular.

Keywords: Borehole radar, directional antenna, fracture zones, granite

RESUME

Le programme de recherche par radar en trou de forage de la phase III sur le site SCV comprenait des mesures de réflexion à partir de forages uniques, avec des fréquences centrales de 22 et 60 MHz. De telles mesures ont été réalisées avec des antennes tous azimuts ainsi qu'avec des antennes directionnelles dans les forages C1, C2, C3 et D (D1-D6). Des tomographies entre forages ainsi que des mesures par réflexion entre forages ont été réalisées entre les forages C1-C2, W1-C1 et W1-C2. La portée obtenue lors des mesures par réflexion en forage unique a été de 100 m approximativement pour la fréquence la plus basse (22 MHz) et de 60-70 m pour la fréquence centrale de 60 MHz. Pour les mesures entre forages des distances de 20 à 120 m entre émetteur et récepteur ont été utilisées.

Les investigations par radar de la phase III ont pour l'essentiel confirmé la description spatiale des structures du site SCV. Le modèle conceptuel du site, élaboré sur la base des données obtenues lors de la phase I, comprenait trois zones majeures (GA, GB et GH), deux zones mineures (GC et GI) et un élément circulaire (RQ). Les éléments majeurs sont considérés comme les plus significatifs du site et ont tous été observés à proximité des locations prédites par les forages de la phase III. L'élément circulaire a lui aussi été trouvé par deux des tomogrammes additionnels à l'endroit prédit. RQ est identifié comme un élément annulaire par le tomogramme d'atténuation et1 comme une anomalie ponctuelle unique par le tomogramme de ralentissement.

Les résultats montrent que les zones ne sont pas homogènes mais qu'elles sont au contraire très irrégulières, présentant des parties fortement fracturées et d'autres dont le contraste avec les roches environnantes est très faible. Les zones, à l'échelle du site du moins, apparaissent comme approximativement planes. A plus faible échelle ces zones peuvent apparaître comme très irrégulières.

Mots clés: radar en trou de forage, antenne directionnelle, zone fracturées, granite.

ZUSAMMENFASSUNG

Das Bohrlochradar-Untersuchungsprogramm Phase III am SCV-Standort umfasste Reflexionsmessungen aus einzelnen Bohrungen (Singlehole) mit Mittenfrequenzen von 22 und 60 MHz. Die Singlehole-Reflexionsmessungen mit ungerichteten und gerichteten Antennen wurden in den Bohrlöchern C1, C2, C3 und in den D-Bohrlöchern (D1-D6) durchgeführt. Tomographische Crosshole-Messungen sowie Crosshole-Reflexionsmessungen wurden zwischen den Bohrlöchern C1-C2, W1-C1 und W1-C2 durchgeführt. Die Radar-Reichweite betrug bei den Singlehole-Reflexionsmessungen rund 100 m bei der tieferen Frequenz (22 MHz) und zwischen 60 und 70 m bei der Mittenfrequenz von 60 MHz. Bei den Crosshole-Messungen variierte der Abstand zwischen Sender und Empfänger zwischen 20 und 120 m.

Die Radaruntersuchungen der Phase III haben im wesentlichen die dreidimensionale Beschreibung der Strukturen am SCV-Standort bestätigt. Das auf den Daten der Phase I basierende Modellkonzept umfasst drei grössere Störungszonen (GA, GB und GH), zwei kleinere Zonen (GC und GI) und eine kreisförmige Struktur (RQ). Die grösseren Zonen werden als die wichtigsten Charakteristiken des Standorts betrachtet; in den Bohrlöchern der Phase III liegen diese Zonen nahe bei ihren vorausgesagten Positionen. Die kreisförmige Struktur RQ wurde auch in zwei der zusätzlichen Tomogramme an der vorausgesagten Position beobachtet. RQ wird als ringförmige Struktur in den Dämpfungs-Tomogrammen und als Einzelpunkt-Anomalie im "Slowness-Tomogramm" registriert.

Die Resultate weisen darauf hin, dass die Zonen nicht homogen sind, sondern äusserst irregulär, mit Bereichen erhöhter Klüftung und Bereichen, in denen der Kontrast zum Hintergrundgestein recht klein ist. Die Zonen scheinen etwa planar zu verlaufen, wenigstens im Grössenbereich der Bohrlochabstände. Im Detail können die Zonen ziemlich irregulär erscheinen.

Schlüsselworte : Bohrlochradar, gerichtete Antenne, Störungszone, Granit

SUMMARY AND CONCLUSIONS

The borehole radar investigation program of the SCV-site has comprised single hole reflection measurements with centre frequencies of 22, 45, and 60 MHz. The frequencies 22 and 45 MHz were used in the boreholes N2, N3, N4, W1, and W2 during Stage I. During Stage III reflection measurements with the centre frequency 22 MHz were made in C1, C2 and C3 and measurements with a newly developed directional antenna system at the centre frequency 60 MHz were made in the C (C1-C3) and D-holes (D1-D6).

Crosshole tomographic measurements have been made between the boreholes W1-W2, N2-N3, N3-N4, N2-N4, C1-C2, W1-C1 and W1-C2. Crosshole reflection measurements have also been made between the same boreholes. The reflection measurements were made with the transmitter fixed positions in each borehole while the receiver was moved in 1 m increments in the other borehole. The crosshole sections were measured with the centre frequencies 20 and 60 MHz, except N2-N4 which was measured only with the lower frequency and the Stage III sections (containing the C-holes) which were measured only with the high frequency. The entire measurement program has totalled over 20 000 rays.

The radar range obtained in the single hole reflection measurements was approximately 100 m for the lower frequency (22 MHz) and about 60 m for the centre frequency 45 MHz. In the crosshole measurements transmitter-receiver separations from 60 to 200 m have been used.

An integrated analysis has been performed of the radar results obtained from the four different measurement modes; single hole reflection, crosshole reflection, crosshole tomography and single hole reflection with directional antenna. From the processed radar data geometric information about the location and extent of major features has been extracted. The geometry of the boreholes during Stage I forced radar data to be collected in two different planes, i.e. the N2-N3-N4 and the W1-W2 planes. Both planes are semi-horizontal with the W1-W2 plane located above the other plane. During Stage III three more boreholes i.e. C1, C2 and C3 were drilled in fanlike positions close to W1 which made it possible to perform crosshole tomography measurement between W1-C1, W1-C2 and C1-C2. Single hole reflection measurements have also been performed in the six D-

holes (D1-D6). The D-holes are located at the 385 m level, they are parallel separated with only 1.5 m and drilled in the same direction as where the excavation drift is to be drilled.

The conceptual model of the site includes three major features (fracture zones) and two minor zones. The zones GA, GB, and GH are considered as major zones while GC and GI are of smaller magnitude. The zones can also be grouped according to their orientation. The zones with a northeasterly strike (N40°E) and a dip of approximately 40° to the South are GA, GB and GC. The zones GH and GI strikes N355°E and dip steeply (≈60°) to the East.

The results indicate that the zones are not homogeneous but rather that they are highly irregular containing parts of considerably increased fracturing and parts where their contrast to the background rock is quite small. The zones appear to be approximately planar at least at the scale of the site. At a smaller scale the zones can appear quite irregular.

One of the most extraordinary features in the attenuation tomograms is the circular feature (RQ) between boreholes N3 and N4 and between W1 and C2. These two planes intersect and RQ is seen at exactly the same place in both tomograms.

The circular feature, RQ, is located close to GB and it is suspected that the zone GB at least partly consists of the same type of porous rock. This idea is supported by the fact that a circular feature is also found in the C1-C2 tomogram close to the predicted position of GB. The feature RQ is remarkable because the circular shape is only evident in the attenuation tomograms, while the slowness tomograms show an anomaly in the center of the structure.

The radar investigations have given a three dimensional description of the structure at the SCV-site. A generalized model of the site was produced within the SCV-project Stage I and Stage II which included three major zones, two minor zones and a circular feature. These features are considered to be the most significant at the site. The interpretation within the SCV-project, Stage III, is in good agreement with these predictions. All major zones are found close to their predicted locations. Smaller features than the ones included in the generalized model certainly exist but no additional features comparable to the three major zones are thought to exist.

CONTENTS

LIST OF FIGURES

LIST OF TABLES

1989-11-20 18.42

1 INTRODUCTION

1.1 SITE CHARACTERIZATION AND VALIDATION PROJECT

The purpose of the Site Characterization and Validation (SCV) Project is to predict groundwater flow and nuclide transport in a previously unexplored volume of the Stripa granite. In the SCV Project the primary emphasis lies on the application of the technology developed in Phases 1 and 2 of the Stripa Project.

Measurements will be taken from boreholes and drifts and the data will be used to model the groundwater flow. Data collection and modelling is a multidisciplinary effort including geology, geophysics, hydrogeology, rock mechanics, and geochemistry. The predictions will be made using numerical models. The accuracy of these predictions will be assessed by excavating a drift and measuring the geometrical, water flow, and solute transport properties of the fractures in the drift.

The SCV project is arranged in five stages so that data collection (Stages I and III) is followed by model prediction (Stages II and IV) in an iterative manner. The last stage is validation where the more detailed prediction (Stage IV) is checked by a final period of data collection (Stage V). Thus during the course of the project there is a progressive interplay between modelling and data collection.

Included in Stage III are the following subprojects:

- Blasting of an access drift at the 385 m level
- Drilling of 9 additional investigation boreholes
- Core logging and fracture mapping in drifts
- Geophysical single hole logging
- Measurements on large core samples
- In situ Block test
- Borehole radar
- Borehole seismics
- Hydraulic investigations
- Hydrochemistry

A detailed description of the five stages mentioned

above is to be found in the Program Plan for the Stripa Project, Phase 3 (Stripa Project TR 87-09).

This report concerns the borehole radar investigations carried out during Stage III with the objective to verify the large scale features (fracture zones) identified in Stage I and give a more detailed description of the fractures in the vicinity of the validation drift. For details about the radar investigations during Stage I, see Olsson, Eriksson, Falk and Sandberg, 1988.

1.2 BOREHOLE RADAR INVESTIGATIONS

The borehole radar technique uses electromagnetic waves concentrated in a short pulse with a length in the rock of 2-10 m to obtain information about the structure of the rock. Radar wave propagation is sensitive to the electric properties of the rock, mainly the dielectric constant and the electrical conductivity. The variation of these properties is related to other physical properties of the rock which are of more direct interest to groundwater flow, such as porosity and fracturing. An essential aspect of the borehole radar method is that it combines a resolution on the order of meters with investigation ranges on the order of hundreds of meters. This means that detailed information can be obtained on structures located far from the boreholes. In some sense the radar gives the ability to "see" through the rock.

The borehole radar technique has been developed to its current level of sophistication during Phase 2 of the Stripa Project by a research group at ABEM, formerly at the Swedish Geological Co. (SGAB). The development efforts during Phase 2 comprised the construction of a new radar system, a comprehensive field testing program, development of interpretation techniques, and interpretation of the collected data (Olsson, Falk, Forslund, Lundmark, and Sandberg, 1987). The new radar system (RAMAC) can be applied both for single hole and crosshole measurements. Reflections are observed in both measurement modes and can be used to identify fracture zones or other inhomogeneities in the rock. A directional antenna system has been used in this Stage of the SCV project giving unique information about the orientation of fractures and fracture zones. The analysis of the crosshole data also included tomographic inversion of travel times and amplitudes. A combined analysis of results obtained by all four investigations modes will in most cases give reliable data on the three-

dimensional geometry of the geologic structure at an investigated site.

The borehole radar investigations made during Stage III of the SCV Project has comprised the following items;

Single hole reflection measurements have been made in the 9 boreholes (C1-C3 and D1-D6) at two different frequencies. A low frequency (22 MHz) has been used to identify the large scale features at distances of up to 100 m from the boreholes.

The high frequency (60 MHz) **directional antenna system** has been used to determine both the angle of intersection and the direction angle to the minimum of the reflection from a fracture zone. The directional antenna system has been developed as a part of the Stripa Project Phase 3 (for more details about the system see Stripa Project Quarterly Report July-Sept, 1988). The directional antenna system was not used in Stage I.

Crosshole reflection measurements have been made between 3 pairs of boreholes (C1-C2, W1-C1 and W1-C2) at the centre frequency 60 MHz. The total number of crosshole reflection scans is 12. (A borehole scan is a set of measurements where one probe (transmitter or receiver) is kept fixed in one borehole while the other probe is moved in another borehole where measurements are made at fixed increments. The increment is normally 1 m in crosshole reflection measurements.)

Crosshole tomographic measurements have been made in the planes spanned by the boreholes C1, C2 and W1 at the frequency of 60 MHz. The measurement program has included a total of 3 borehole sections. Tomographic inversion has been made of both travel time and amplitude data.

The report briefly describes equipment used, measurements performed and interpretation procedures. A detailed description of equipment and interpretation procedures is given by Olsson, Falk, Lundmark, Forslund, and Sandberg, 1987. The results obtained by each measurement mode are first discussed separately followed by an integrated interpretation of all radar results.

1.3 EXPERIMENTAL SITE

The location of the new site to be explored was selected in such a way that has it was possible to

drill the investigation holes from existing drifts. Five "boundary boreholes" have been drilled for preliminary characterization of the site: three holes towards the North (N2 - N4) of 200 m length and 60 m apart, and two towards the West (W1 - W2). These holes of 150 m length are roughly 70 m apart, see Figure 1.1. A 50 meter long vertical hole has been drilled at the end of the 3D-migration drift mainly for the purpose of measuring rock stresses. In Table 1.1. the position of the SCV Stage I boreholes in the local mine coordinates, bearing (from mine north), plunge (from horizontal plane), and length are given.

The boreholes drilled within the SCV Stage III are the C-holes and the D-holes. The main objective of the three C-holes, C1-C3, was to characterize a smaller volume around the Validation Drift in more detail. Two of the most significant zones at the SCV-site are GB and GH. These zones were likely to control the hydraulics in the central portions of the site and they had to be checked with respect to location and properties. The circular feature RQ was also an anomaly of interest and an attempt was made to locate the boreholes so that this feature was included in the Stage III investigations. The location of the Validation Drift was changed compared to original plans in order to intersect both GB and GH and to make the intersection as perpendicular as possible.

The boreholes were located in such a way that they originate from essentially the same point (close to the beginning of W1). In this way each pair of boreholes would define a plane and tomographic surveys between the holes would be possible. The two major zones would be intersected by a large number of boreholes which would facilitate detailed crosshole hydraulic testing of the zones.

Two of the boreholes were given a steep dip in order to provide better sampling in the vertical direction compared to what has been obtained from the boreholes drilled previously.

In Table 1.2 the positions of the C-holes in the local mine coordinates, direction, inclination and length are given.

The Validation Drift will intersect zones GB and GH at a relatively steep angle. The Validation Drift has been oriented in order to minimize the risk of it being nearly parallel to a major zone. The Validation Drift will be located at the 385 m level of the mine which is approximately in the middle of the investigated volume.

The D-boreholes outlines the Validation Drift. There are 6 boreholes, one in the centre surrounded by five symmetrically placed boreholes. The radius of the perimeter where the boreholes are located is 1.2 m.

The D-holes, D1-D6 were drilled from the end of the access drift at the 385 m level towards WNW. They are all parallel and of 100 m length and slightly dipping. Table 1.3 gives the positions of the D-holes.

The total length of the holes drilled within Stage I is 960 m and Stage III 1000 m. The holes are 76 mm in diameter and fully cored.

Table 1.1 Position of boreholes W1, W2, N2 - N4, and V3, in the local mine coordinates. Bearing from mine north (in degrees), plunge below horizontal plane (in degrees), length (m).

	W1	W2	N2	N3	N4	V3
Collar position:						
X	440.0	510.0	333.3	347.4	321.1	502.9
Y	1146.8	1147.4	1139.2	1079.1	1023.1	1149.7
Z	356.1	355.3	356.7	356.9	345.0	356.5
Bottom hole position:						
X	441.7	511.4	530.1	527.4	529.0	503.4
Y	1000.3	1000.8	1141.0	1082.6	1025.5	1149.7
Z	368.1	365.9	420.7	414.2	413.7	404.5
Collar deviation:						
Bearing	269.94	269.90	359.85	359.97	359.25	
Plunge	4.99	5.02	18.59	18.59	18.80	89.33
Bottom hole deviation:						
Bearing	271.39	271.19	0.87	2.20	2.12	
Plunge	4.13	3.32	17.31	17.01	17.47	89.49
Length	147	147	207	189	219	50

Table 1.2 Position of boreholes C1, C2 and C3 in the local mine coordinates. Bearing from mine north (in degrees), plunge below horizontal plane (in degrees), length (m).

	C1	C2	C3
Collar position:			
X	438.5	442.5	432.8
Y	1147.0	1147.0	1147.6
Z	356.2	356.3	355.9
Bottom hole position:			
X	435.6	509.4	462.8
Y	1029.0	1054.4	1056.6
Z	448.8	453.4	380.9
Collar direction:			
Bearing	267.94	305.35	287.42
Plunge	38.95	40.53	14.68
Bottom hole direction:			
Bearing	269.35	306.06	288.82
Plunge	37.52	39.91	14.36
Length	150	150	100

Table 1.3 Position of boreholes D1-D6 in the local mine coordinates. Bearing from mine north (in degrees), plunge below horizontal plane (in degrees), length (m).

	D1	D2	D3	D4	D5	D6
Collar position:						
X	439.1	437.9	438.3	439.7	440.1	438.9
Y	1127.9	1127.7	1128.1	1128.3	1128.4	1128.3
Z	383.3	383.6	382.3	382.3	383.6	384.4
Bottom hole position: (99 m)						
X	469.5	468.1	468.3	469.9	470.3	469.4
Y	1033.9	1033.6	1033.8	1034.2	1034.3	1034.3
Z	389.0	389.4	387.6	388.3	389.5	389.9
Collar direction:						
Bearing	287.45	287.41	287.35	287.39	287.45	287.47
Plunge	3.32	3.10	3.26	3.41	3.35	3.37
Bottom hole direction: (99 m)						
Bearing	288.39	287.75	287.95	288.26	288.25	288.50
Plunge	3.24	3.95	2.80	3.43	3.38	3.00
Length	100	100	100	100	100	100

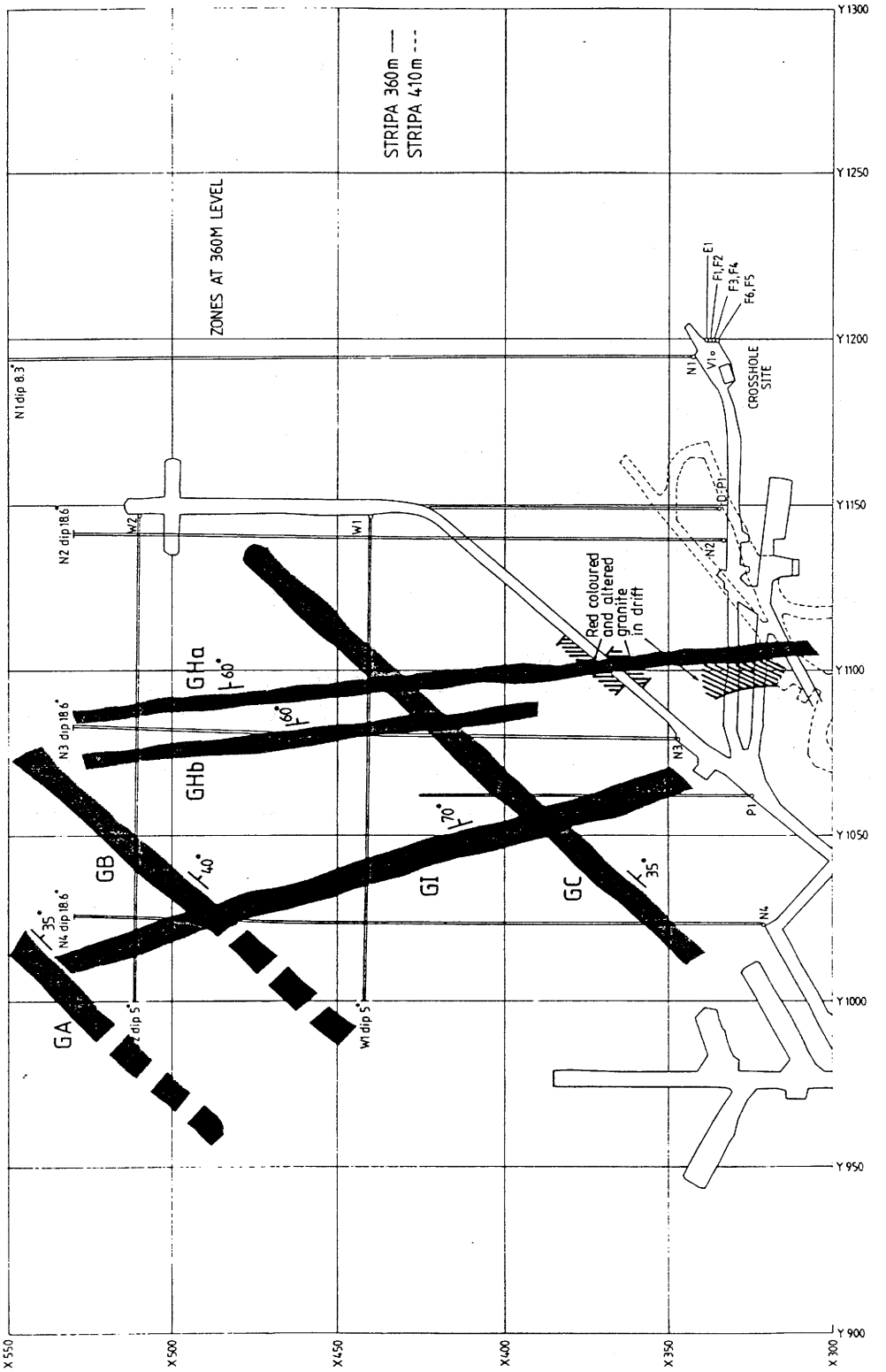

Figure 1.1 Plan view of the Stripa Mine at the 360 m level showing the position of the SCV-site, the Stage I boreholes and location of predicted zones.

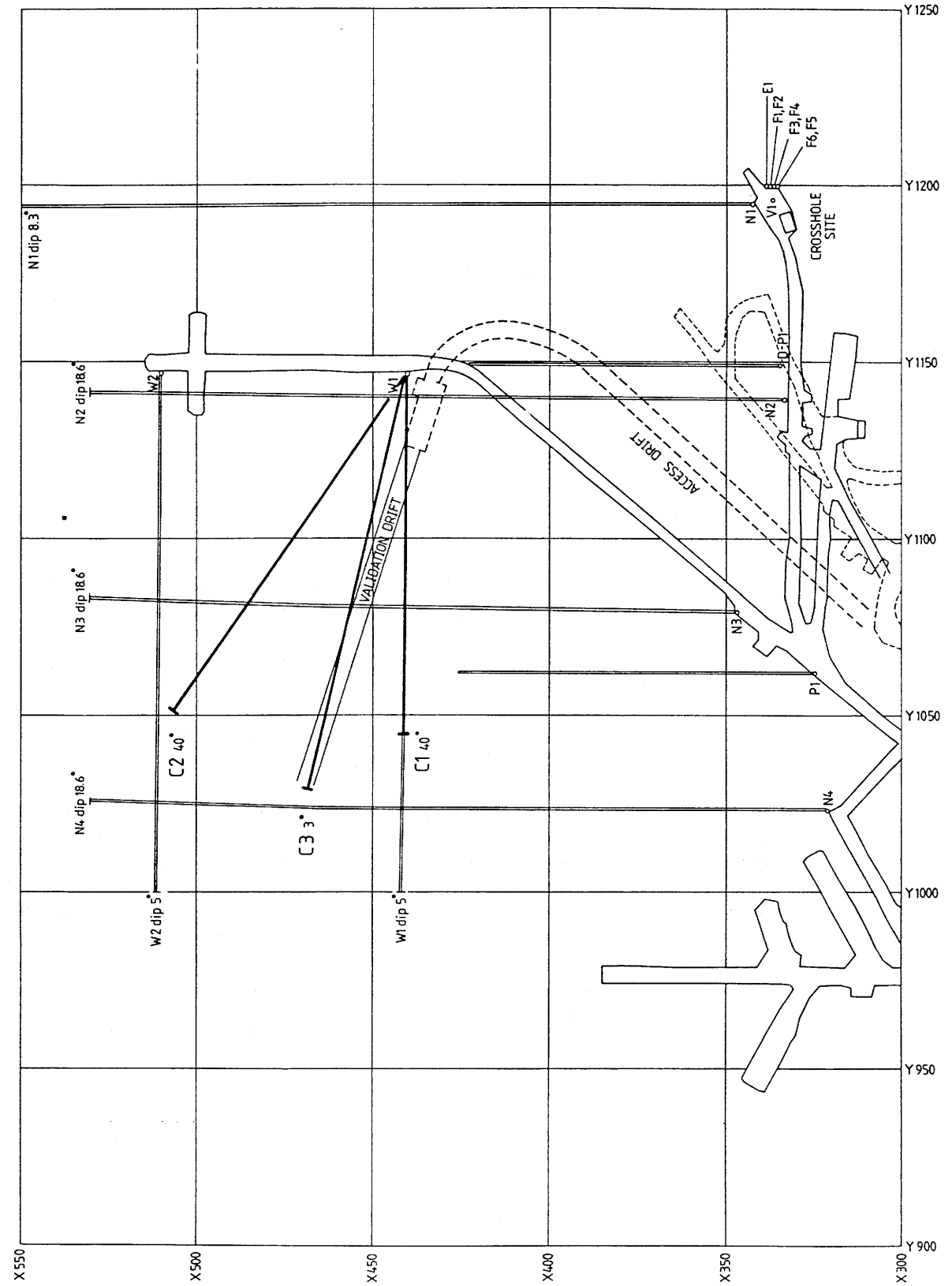

Figure 1.2 Plan view of the Stripa Mine at the 360 m and 385 m level showing the position of the SCV-site, the Access drift and the Stage III boreholes.

2 FIELD MEASUREMENTS

2.1 EQUIPMENT USED

The short pulse borehole radar system developed during Phase 2 of the Stripa Project and the directional antenna system developed within Phase 3 has both been used for these measurements.

The borehole radar system (RAMAC) consists of four different parts;

- a microcomputer with a 5 inch floppy disc unit and a 20 MB harddisk for control of measurements, data storage, data presentation and signal analysis.
- a control unit for timing control, storage and stacking of single radar measurements.
- a borehole transmitter for generation of short radar pulses.
- a borehole receiver for detection and digitization of radar pulses.

The newly developed directional antenna system is made compatible with the old dipole antenna system. Hence, the dipole antenna probes may be operated with the directional antenna control unit. The directional system consists in principle of the same units as the omnidirectional system. The modified parts are;

- the control unit which communicates on an extra two-way optical communication link with the directional receiver probe, used for selection of antenna and measurement of the orientation of the probe.
- the receiver probe which has four directional antenna elements and electronics for selecting one out of four antennas (looking in different directions) and a directional sensor. For one single measurement the receiver scans the four antennas and reads the directional sensor.

The RAMAC system works in principle in the following manner: A short current pulse is fed to the transmitter antenna, which generates a radar pulse that propagates through the rock. The pulse is made as short as possible to obtain high resolution. The

pulse is received by the same type of antenna, amplified, and registered as a function of time. The receiver may be located in the same borehole as the transmitter or in any other borehole. From the full wave record of the signal the distance (travel time) to a reflector, the strength of the reflection, and the attenuation and delay of the direct wave between transmitter and receiver may be deduced.

The recording of the signal is similar to that of a sampling oscilloscope, i.e. for each pulse from the transmitter only one sample of the received electric signal is taken at a specific time. When the next pulse is generated a new sample is taken which is displaced slightly in time. Thus, after a number of samples a replica of the entire signal is recorded. The sampling frequency and the length and position of the sampled time interval can be set by the operator.

Optical fibers are used for transmission of the trigger signals from the computer to the borehole probes and for transmission of data from the receiver to the control unit. The optical fibers have no electrical conductivity and will not support waves propagating along the borehole. Another advantage of optical fibers is that they can not pick up electrical noise and as the signal is digitized down-hole there will be no deterioration of the signal along the cable. The quality of the results will thus be independent of cable length.

There is no direct connection between the transmitter and the receiver. Both probes are instead connected directly to the control unit and the transmitter and the receiver can be put into the same as well as into separate holes. In other words, the radar may be used both for single hole and crosshole measurements. The system also provides absolute timing of the transmitted pulses and a calibrated gain in the receiver which makes it possible to measure the travel time and the amplitude of the radar pulses in a crosshole measurement and hence provide data for a tomographic analysis. The absolute time depends on the length of the optical fibers and is hence a quantity which has to be obtained through calibration for a given set of optical fibers. The technical specifications of the system are given in Table 2.1.

Table 2.1 Technical specifications of the borehole radar system.

General	
Frequency range	20-80 MHz
Total dynamic range	150 dB
Sampling time accuracy	200 ps
Maximum optical fiber length	1000 m
Maximum operating pressure	100 Bar
Outer diameter of transmitter/receiver	48 mm
Minimum borehole diameter	56 mm
Transmitter	
Peak power	500 W
Operating time	10 h
Length	4.8 m
Weight	16 kg
Receiver	
Bandwidth	10-200 MHz
A/D converter	16 bit
Least significant bit at antenna terminals	1 μV
Data transmission rate	1.2 MB
Operating time (Dipole/Directional)	10/4 h
Length	5.4 m
Weight	18 kg
Control unit	
Microprocessor	RCA 1806
Clock frequency	5 MHz
Pulse repetition frequency	43.1 kHz
Sampling frequency	30-3000 MHz
No of samples	256-4096
No of stacks	1-32767
Time window	0-11 μs

2.2 SINGLE HOLE MEASUREMENTS

In single hole measurements the transmitter and receiver are located in the same borehole. The transmitter and receiver are kept at a fixed separation by glassfiber rods. The transmitter-receiver array is moved along the borehole and measurements are made at fixed intervals. The measurement at each position takes about 30 seconds (70 seconds for the directional system) including the movement to the next measuring position.

Measurements have been performed at centre frequencies of 22 and 60 MHz. The centre frequency is essentially determined by the length of the antenna. The change of centre frequency includes a change of antennas in the borehole probes.

Data is first stored in binary format on an internal hard disk. After completion of the measurement of a borehole data is transferred to 5.25 inch floppy disks for backup or further processing on an other PC. Processing and display of data is made on a standard desktop computer (IBM PC/AT).

The reflection measurements performed as a part of the SCV Project, Stage III, are listed in Table 2.2. Included in the table is a list of the system parameters that can be varied during a survey.

Table 2.2 Data on single hole reflection measurements performed as a part of the SCV Project, Stage III.

Centre frequency:		22 MHz			
Sampling frequency:		227 MHz			
Number of samples:		512			
Bore-hole	Logged depth (m)	Point sep. (m)	Tr-Re sep. (m)	No. of stacks	Date logged
C1	13.1-140.1	1	15.4	256	881010
C2	13.1-139.1	1	15.4	256	881010
C3	13.1- 90.1	1	15.4	256	881020
Centre frequency:		60 MHz	Directional antenna system		
Sampling frequency:		480 MHz			
Number of samples:		512			
Bore-hole	Logged depth (m)	Point sep. (m)	Tr-Re sep. (m)	No. of stacks	Date logged
C1	9.1-142.5	1	7.4	128	881019
C2	9.1-142.1	1	7.4	128	881020
C3	9.1- 93.4	1	7.4	128	881019
W1	9.1-140.1	1	7.4	128	881103
D1	9.1- 93.1	0.5	7.4	128	881109
D2	9.1- 93.1	0.5	7.4	128	881108
D3	9.1- 93.1	0.5	7.4	128	881110
D4	9.1- 93.1	0.5	7.4	128	881110
D5	9.1- 93.1	0.5	7.4	128	881109
D6	9.1- 93.1	0.5	7.4	128	881108

2.3 CROSSHOLE MEASUREMENTS

In a crosshole measurement the transmitter and receiver are placed in separate boreholes. One of the probes is kept in a fixed position in one of the boreholes while the other probe is moved in the other hole where measurements are made with fixed intervals. A set of measurements where one probe is fixed in the first borehole and the other probe is moved along the length of the other borehole is termed a borehole scan. According to the reciprocity theorem the transmitter and receiver (omnidirectional) are interchangeable and it is irrelevant in which of the boreholes each probe is placed.

Crosshole reflection measurements have been made at one frequency; 60 MHz. Each crosshole reflection scan has been made with a measurement point separation of 1 m. The low value was chosen in order to avoid spatial aliasing. Two borehole scans have been made in each borehole. The points have been located near the top and near the bottom of each borehole. For each pair of boreholes (C1-C2, C1-W1, C2-W1) there has been two scans made from each borehole, thus making up a complementary data set where reflections close to both boreholes can be observed. The crosshole reflection measurements performed are listed in Table 2.3.

The borehole section C1-W1 was measured with the directional antenna system.

Table 2.3 Data on crosshole reflection measurements performed as a part of the SCV Project, Stage III.

Centre frequency: 60 MHz
Sampling frequency: 480 MHz
Number of samples: 512

Borehole fixed probe	Borehole moving probe	Logged depth (m)	Point sep. (m)	No. of stacks	Date logged
C1: 31.4 m	C2	31.4-141.4	1	256	881012
C1:144.4 m	C2	31.4-141.4	1	256	881012
C2: 31.4 m	C1	31.4-144.4	1	256	881012
C2:141.4 m	C1	31.4-144.4	1	256	881012
W1: 31.4 m	C2	31.4-142.4	1	256	881014
W1:144.4 m	C2	31.4-142.4	1	256	881014
C2: 31.4 m	W1	31.4-144.4	1	256	881014
C2:142.4 m	W1	31.4-144.4	1	256	881014
C1: 31.4 m	W1*	11.4-143.4	1	256	881102
C1:101.4 m	W1*	8.4-143.4	1	256	881102
W1: 31.4 m	C1*	11.4-138.4	1	256	881102
W1: 99.4 m	C1*	11.4-141.4	1	256	881102

*) indicates directional antenna receiver borehole

Crosshole tomography measurements have been made of all pairs of boreholes which define a plane. There are three possible pairs or borehole sections defined by the borehole layout described in Section 1.3. They are; C1-C2, W1-C1 and W1-C2. All sections have been measured at the radar frequency 60 MHz. The tomographic measurements were made with a point separation of 4 m in all boreholes. Tomographic analysis has been made of both travel times and amplitudes. Data on the crosshole tomography measurements are listed in Table 2.4.

Table 2.4 Data on crosshole tomography measurements performed as a part of the SCV Project, Stage III.

Centre frequency: 60 MHz
Sampling frequency: 480 MHz
Number of samples: 512
Number of stacks: 256

Bore-hole 1	Logged depth (m)	Point sep. (m)	Bore-hole 2	Logged depth (m)	Point sep. (m)	No. of rays
C1	31.4-143.4	4	W2	31.4-143.4	4	841
W1	31.4-143.4	4	C1	31.4-143.4	4	841
W1	31.4-143.4	4	C2	31.4-143.4	4	841

3 RESULTS FROM SINGLE HOLE REFLECTION MEASUREMENTS

3.1 INTERPRETATION PROCEDURE

The principle of a single hole reflection measurement is depicted in Figure 3.1. The transmitter and receiver are lowered or pushed into the same hole while the distance between them is kept constant. The result is displayed in the form of a diagram where the position of the probes is shown along one axis and the propagation distance along the other axis. The amplitude of the received signal is shown in a grey scale where black corresponds to large positive signals, white to large negative signals and grey to small signals.

The distance to a reflecting object is determined by measuring the difference in arrival time between the direct and the reflected pulse. The basic assumption is that the speed of propagation is the same everywhere. The two basic patterns are point reflectors and plane reflectors as shown in Figure 3.1.

From the radar reflection measurements it is possible to determine the angle of intersection between the hole and a fracture plane and also the point of intersection. This is done with the aid of a theoretically computed nomogram (Olsson, Falk, Forslund, Lundmark, and Sandberg, 1987). The information from the omni-directional antenna is cylindrically symmetric. Consequently one can not obtain the complete orientation of a fracture plane from measurements in a single borehole using the dipole antenna system. However, with the directional antenna system this is now possible. The absolute orientation can be determined from the directional antenna measurements.

The final interpretation of both the dipole and directional single hole measurement is done by plotting a curve representing all possible orientations of the normal of a plane using the Wulff projection given the restriction that the angle of intersection between the plane and the borehole and that the minimum obtained from the directional antenna has a specified value, i.e. the same technique is actually used for the results from the directional antenna system; all possible orientations of the normal of a plane given the azimuth angle. The combined results gives an uncertainty (two possible

solutions) depending on the phase of the dipole antenna and the phase of the directional antenna reflection. In practice, when a radar image contains many reflections and the radar pulse is ringing it can be very difficult to determine the phase. For more details about the interpretation of directional antenna measurements see Stripa Project Quarterly Report July-Sept, 1988. Points where curves representing the same reflector, observed from both the dipole and directional system and in several different boreholes, intersect are candidates for the correct orientation of the plane. For more details about single hole interpretation see Olsson, Falk, Forslund, Lundmark, and Sandberg, 1987.

The major source of error with the single hole method of analysis is that there is an uncertainty in the identification of the reflectors from the different boreholes. This type of analysis evidently relies on that the same reflector has been correctly identified in the respective boreholes. If this is not the case the results will be in error. The directional antenna removes this uncertainty.

Other sources of error are errors in the identified intersection and azimuth angles and the assumption that fracture zones are planar over the distances concerned.

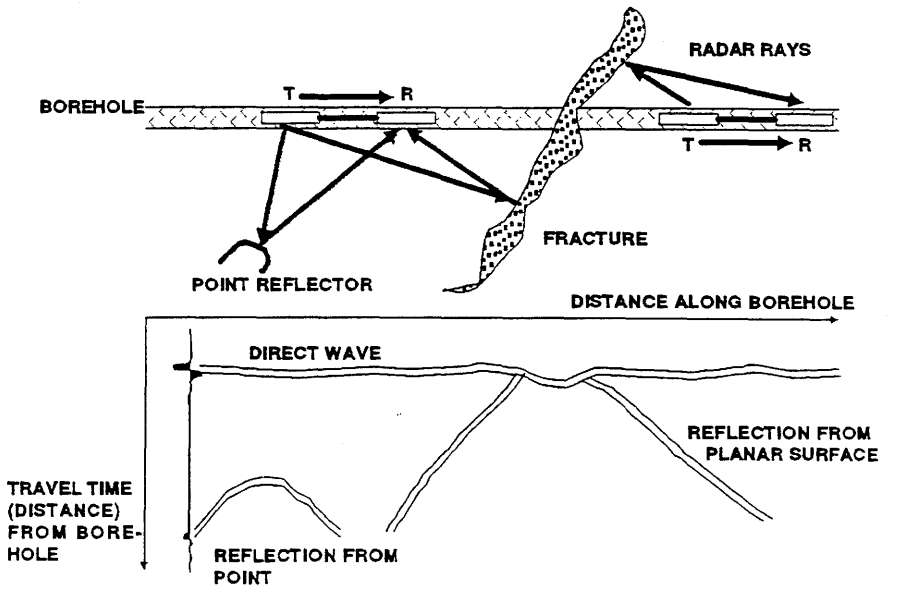

Figure 3.1 The principle of the borehole reflection radar and the characteristic patterns generated by plane and point reflectors.

3.2 DATA PROCESSING

The raw data registration contains some noise and spurious signals generated by the receiver electronics which have to be removed in order to improve the quality of the radar maps.

First a DC-level offset is removed from the data then a combined band pass and correlation filter has been applied in order to remove a low frequency oscillation present in the raw data. The correlation filter also removes some high frequency noise (Olsson et al 1987).

The results from the reflection surveys at Stripa are displayed as bandpass filtered data in Appendix. The cutoff frequencies for the 60 MHz measurements are 14 and 94 MHz and for the 20 MHz measurements 7 and 44 MHz respectively.

3.3 RESULTS FROM THE BOREHOLES

The preliminary predictions (Olsson, Black, Gale and Holmes, 1988) based on measuring geology, fracture characteristics, stress, single borehole geophysical logging, radar, seismics and hydrogeology resulted in four major zones GA, GB, GH and GI and one minor zone GC. These predictions have been used in this report to verify the orientation and extent of the zones. The zones identified in radar measurements are named RA, RB, RH, RC and RI.

3.3.1 Presentation of results

The most significant reflectors identified in the radar reflection maps from each borehole (Appendix A) have been listed in tables. The tables include the intersection of the reflector with the borehole, the angle of intersection, α, the minimum azimuth angle, ß, between the reflector plane and the borehole, and the relative strength of the reflex. The strength of each reflex is given in arbitrary units on a scale from 1 to 3, where 3 corresponds to the strongest reflexes. The rating of the reflexes is qualitative and based on the judgement of the person doing the interpretation.

The radar response caused by a fracture zone normally consist of two linear segments (cf. Figure 3.1) which have been termed upper and lower side reflexes. Here, upper refers to the reflex which occurs at the

smaller borehole depth. Sometimes a reflex is observed only from one side and at only one of the frequencies measured. The occurrence of the reflexes is indicated in the tables. If an interval is given for the borehole intersection this indicates that the fracture zone has a significant thickness and the depths given indicate the boundaries of the zone. The accuracy in intersection depth is about ±2 m. The accuracy in the intersection angles is estimated to less than 5° for angles less than 40° and to about 10° for larger angles.

The tables also include a column termed "Zone". This column identifies the reflectors which belong to the zones of significant extension which have been identified in the integrated interpretation of all radar data (Chapter 6). The results obtained from each borehole are discussed briefly in the following Sections.

3.3.2 Borehole C1

The radar range obtained in borehole C1 and also the other holes at the SCV-site is approximately 100 m for the lower frequency (22 MHz). In the 60 MHz (Directional system) measurements the range exceeds 60-70 m.

A number of significant reflexions which have been identified in the radar reflection maps from borehole C1 are listed in Table 3.1. The strongest reflex is caused by the access drift to the 3D-migration drift. The drift appears as two reflectors; one which is perpendicular to the hole and intersects the hole at 0 m and one which makes an angle of 50° to the hole and has an apparent intersection 10 m behind the start of the hole. The latter reflex is caused by the access drift to the 3D-migration area which changes direction approximately 15 m from C1 (cf. Figure 1.1). The hyperbola reflexion 25 m from the borehole at the borehole depth of 10 m is caused by the access drift at the 385 m level.

At about 35-40 m depth three hyperbolie reflexions close to the borehole can be seen in the 60 MHz data but not as clear in the 22 MHz data. These are the reflexions from the D-holes drilled from the 385 m level. The borehole C1 is just passing the 6 D-holes causing the reflexions to look like hyperbola (point) reflexions. The intersection angle is 40° which corresponds well with the real angle, 38°. Unfortunately, the zone called RH is mixed with these reflexions in C1. The reflexions from the D-holes are

not visible in the 22 MHz data due to the small size of the holes (76 mm). The 22 MHz data contains one very clear reflex intersecting the hole at 0 m, having an intersection angle of 35°. This reflex is from the borehole W1 which at the time of the measurement contained packers and aluminum rods used for head monitoring. The aluminum rods were removed at the time of the 60 MHz measurement, making that reflex weak even at the higher frequency.

The most significant reflexions of geological origin intersect the borehole at 95, 120 and 140 m. One strong reflex can also be observed which intersect a linear extrapolation of the borehole intersecting 75 m behind the start of the borehole. The location of this intersection is found from extrapolation of the reflection patterns and are hence not as accurate as the other intersection depths given in the table. It is difficult to determine whether it is from a point or a plane source, but it was also clearly visible in the W1 measurement in Stage I, intersecting W1 at 80 m behind the start of the borehole.

Table 3.1 Reflectors identified from single hole radar reflection measurements in C1.

Zone	Borehole inter-section	Intersection angle α lower 22 MHz	60 MHz	upper 22 MHz	60 MHz	Azimuth angle ß	Strength 22	60
	-75	30	30			165	3	3
drift	-10	50	50			0	3	3
drift	0	90	90			75	1	1
W1	0	35	30			30	3	2
RC	30				55	30		1
D-holes	36			44	42			3
D-holes	40	37	42					3
RH	50		40			75		2
RH	61	39					1	
RH	64		37					2
	70				40	165		3
RB	91				60	45-90		2
RB	94			48	60	60	2	2
	107			42			2	
RA	120			53	42	-	2	2
	136				37	-		2
	141			53			2	
	143				48	-		2

3.3.3 Borehole C2

The significant reflexions identified in the radar reflection maps from borehole C2 are listed in Table 3.2. The 3-D migration drift and the access drift at the 385 m level causes a complex pattern in the radar map at the beginning of the borehole. The curved shape of the reflexes is caused by the end of the access drift which constitutes the western part of the drift (cf. Figure 1.1) and the D-holes. The other reflexes in this part of the hole are most likely caused by waves propagating back and forth in the drift.

The most significant reflexions intersect the borehole at the approximate depths of 30, 56, 64, 73 and 110 m. These reflexions are essentially linear and can thus be expected to be caused by planar features such as fracture zones. Two lower reflexions intersecting at 64 and 73 m are clearly seen in both the 22 MHz and the 60 MHz measurement, creating a rather complex set of reflexions with intersection angles between 25° and 60° in the same region. The zone GH are predicted to cross C2 between 56 and 66 m depth respectively having and intersection angle of 56°.

There are three moderately strong reflexions visible in the 60 MHz data which intersect the borehole at 74, 80 and 102 m. These reflexions are very weak in the 22 MHz data probably due to the thickness of the fractures. It is possible that these three reflectors belong to a parallel set of fractures having the same angle of intersection i.e. $\alpha \approx 40\text{-}45^\circ$ and $ß \approx 90^\circ$.

The reflexions intersecting the borehole at 127-159 m do not belong to the dominating group of reflectors as it intersects the borehole at a relatively large depth, i.e. outside the investigation volume. Two reflexions which intersects the borehole at relatively small angle 15° at 35 m depth and 10-15° at a depth around 120-130 m have also been found. These two reflexions, could however be part of only one and thus the same reflex. In that case it comes from something which is almost parallel to the borehole and passing 15 m from the borehole (i.e. not intersecting the borehole) at a closest point (distance), which should be around the depth of 70 m. The complex set of reflexions close to that area makes it very difficult to determine whether it really intersect the borehole or not.

There is also a major reflex intersecting the linear extension of the borehole at a depth of 192 m.

Table 3.2 Reflectors identified from single hole radar reflection measurements in C2.

Zone	Borehole inter-section	Intersection angle α lower 22 MHz	60 MHz	upper 22 MHz	60 MHz	Azimuth angle ß	Strength 22	60
360 Drift	0	65	65			105	3	3
385 Drift	25					120		3
RC	32				60	105	1	1
	35		15			120		3
	42	15					3	
	56				39	105		2
RH	64				60	120		3
	73	51	45			105	3	3
	74		40			90		2
	80		40			90		2
	102				45	90		2
	106			48			1	
RA	110		70		70	100		3
	127				42			1
	130			37			1	
	140				37			2
	144			28	25	0	2	3
	149				32			2
	150				8	90		1
	159			48			2	
	191				45	135		3
	192			55			3	

3.3.4 Borehole C3

The significant reflexions identified in the radar reflection maps from borehole C3 are listed in Table 3.3.

The reflex from the access drift at the 385 m level as well as the D-holes are clearly seen in all reflection maps from C3. The D-holes looks like a plane reflector intersecting the line of the borehole at about 120-125 m depth with an angle of approximately 10°. In the 22 MHz measurement the reflexions from the D-holes are so prominent in the region close to the borehole that many other reflexions from fractures becomes invisible. The reflex from the end of the drift (where the D-holes start) is seen as a hyperbolic reflex with the closest point at a borehole depth of approximately 20 m and a distance from the borehole of about 25 m i.e. the distance between the 360 m level and the 385 m level.

The most significant reflexions associated with fracture zones and geology can be identified at borehole depths of 54-67 and 110-115 m.

There is also a major reflex intersecting the line of the borehole at a depth of 265 m. The intersection angle is 20°.

Table 3.3 Reflectors identified from single hole radar reflection measurements in C3.

Zone	Borehole intersection	Intersection angle α lower 22 MHz	lower 60 MHz	upper 22 MHz	upper 60 MHz	Azimuth angle ß	Strength 22	Strength 60
	-5		30			90		2
	10		30			15		2
	20-26		20			90		2
RC	38	30					2	
	44		20					1
RH	54	-		-	70	120		2
point	60				-	105		2
	67	-		-	60	0		1
	85				55	120		2
	98				42			1
	100			48			2	
	102			65			2	
	104				64			2
RB	110				50	30		3
	113			42			2	
	118				37			2
D-holes	≈125			10	10	15-30	3	3
	265			21			3	
	293				16	120		3

3.3.5 Boreholes D1-D6

The significant reflexions identified in the radar reflection maps from borehole D1 are listed in Table 3.4. The single hole reflection measurements in D2, D3, D4, D5 and D6 are almost exactly the same as in D1. Thus, the depths and intersection angles in Table 3.4 are representative of all D boreholes.

The strongest reflexions are caused by the borehole C3 intersecting with an angle of 10° at a depth of 95 m and zone RB at 81 m depth. The zone RH is also prominent at about 25 m depth.

Two nearly parallel reflectors which are located at a distance of 25-30 m and 35-40 m from the borehole can be followed for almost the entire length of the

borehole. The one at the largest distance from the borehole is very strong in the beginning of the borehole, diminishing in strength with depth in the borehole. These reflectors are most prominent in D1, D3 and D5. Point reflectors have also been identified at distances of about 20 m from the borehole which appear to be associated with the fracture zone which intersect the borehole at 62 m. The point reflexions in that area could also be caused by faults within the fracture.

There is also a major reflex intersecting the line of the borehole at a depth of 274 m. The intersection angle is 15°. This reflector seems to be the same reflector as the reflex observed in C3 at a depth of about 265-290 m and the intersection angle 15-20°. The reflexions are both clearly seen at a large distance, i.e. 60 m.

Table 3.4 Reflectors identified from single hole radar reflection measurements in D1-D6.

Zone	Borehole inter-section	Intersection angle α lower 60 MHz	upper 60 MHz	Azimuth angle ß	Strength 60
	-10	80		60	1
	0	90		90	1
	10	35		165	2
RH	21	60		165	2
	25	60	60	120	1
	30	60		120	2
	33		30	30	3
	62		60	30	3
RB	80		35	15	3
	85		35	15	3
C3-hole	95		10	30	3
	95		60	120	3
RA	105		50	30	3
	115		50	0	2
	274		15	120	2

3.3.6 Borehole W1

The borehole W1 was actually part of the Stage I measurements and the 22 MHz and 45 MHz data are presented and described in Olsson, Eriksson, Falk and Sandberg, 1988. The directional antenna system was not available at that time and an extra measurement of W1 was therefore made in order to compare the result from Stage I and to get a good check of the orientation from the fractures obtained earlier in W1.

The significant reflectors which have been identified in the directional radar reflection maps from borehole W1 are listed in Table 3.5. The strongest reflexions are caused by the access drift to the 3D-migration drift and the access drift to the evaluation drift at the 385 m level. The 3D-migration drift appears as two reflectors; one which is perpendicular to the hole and intersects the hole at 0 m and one which makes an angle of 55° to the hole and has an apparent intersection 9 m behind the start of the hole. The latter reflex is caused by the access drift to the 3D-migration area which changes direction approximately 15 m from W1 (cf. Figure 1.1). The hyperbola reflex from the drift at 385 m can be seen as a hyperbola shaped reflex at the very beginning of the measurement. The distance is 24-25 m at the closest point. The D-holes can also be seen as

prominent reflections. The azimuthal direction were they have their minimum is around 30° which corresponds to right under or above W1 (i.e. 25°).

Another strong reflex which was not present in the Stage I measurement is a reflex with 20° intersection angle (lower angle) intersects the hole at 17 m. That is the reflex from borehole C3.

The most significant reflex of geological origin are the same as before. They intersect the borehole at 48-49 and 132-140 m. The reflex pattern close to these intersections is quite complex and the approximation of the geological structures as planes appears to be an oversimplification.

The two strong reflexions intersecting the line of the borehole are not as prominent in this directional measurement, but they still exist; one intersecting about 80 m behind the start of the borehole and one at a depth of approximately 202 m. The reason for this discrepancy is probably the different radiation pattern between the omni-directional antenna and the directional antenna. The location of these intersections are found from extrapolation of the reflex patterns and are hence not as accurate as the other intersection depths given in the table.

Table 3.5 Reflectors identified from single hole radar reflection measurements in W1.

Zone	Borehole inter-section	Intersection angle α lower 60 MHz	upper 60 MHz	Azimuth angle ß	Strength 60
	-80	≈20		≈0	3
	-9	55		105	3
	0	34		0	2
	0	90		90	1
C3-hole	17	20		45	3
D-holes	20-120	parallel		30	3
	35		40	90	2
RC	49		35	90	2
RH	56	70		165	2
	61		40	90	1
	88		45	60	1
	98		45	60	2
	109		70	30	2
	120		55	?	1
	130		30	0	3
RB	140		35	40	3
	147		40	0	2
RA	≈202		≈20	40	2

4 RESULTS FROM CROSSHOLE REFLECTION MEASUREMENTS

4.1 INTERPRETATION PROCEDURE

When the transmitter and receiver are positioned in different boreholes, reflected pulses are observed some time after the directly propagated pulse has arrived. Only the direct pulse is used in the tomographic analysis, so the crosshole reflections provide additional independent information about the fracture zones.

It is particularly convenient that crosshole reflections in principle can determine a complete orientation of a fracture zone. This is due to the additional freedom provided by a bistatic radar configuration. The analysis is however more complicated than for single hole measurements.

Figure 4.2 shows a typical result from a crosshole reflection scan performed between borehole C1 and C2. During this measurement the receiver was moved along borehole C1 while the transmitter was kept fixed at a depth of 31.5 m in borehole C2. As the receiver is moved the direct pulse registered by the receiver traces a hyperbola. After the direct pulse several reflected pulses arrive. If the reflections are caused by fracture planes these curves will also be hyperbolas of similar shape. It is however difficult to use this geometrical information directly to extract information from the radar maps. A different method of analysis has therefore been used.

The bistatic radar configuration is defined in Figure 4.1. The receiver and transmitter are in known positions described by the vectors $\mathbf{x}_0$ and $\mathbf{x}_1$. The distance l propagated by the direct pulse and the distance l′ propagated by the reflected pulse are then conveniently combined into the expression

$$l'^2 = l^2 + 4(\mathbf{x}_0\ \mathbf{n})(\mathbf{x}_1\ \mathbf{n}) \qquad (4.1)$$

where $\mathbf{n}$ is the unit normal vector of a plane causing the reflection. The formula is valid as long as the origin is in the reflecting plane. One such point can be determined from the radar picture, since l=l′ when the antenna passes that point where the fracture plane intersects the borehole. Using this point as an origin one can then proceed to analyze the reflection. A detailed derivation of the formula is

found in Olsson, Falk, Forslund, Lundmark, and Sandberg, 1987.

The reflection curves are digitized and analyzed in a special program. In principle all quantities in the formula can be obtained from the measured data, so the two independent components of the unit vector **n** can be determined from a minimum of two separate measurements. This should be compared with the special case of a single hole measurement where the receiver and the transmitter are moved along the same borehole. The angle between the fracture plane and the borehole can then be determined immediately but no more information about the orientation of the plane is available due to the axial symmetry of the single hole configuration.

The crosshole configuration in principle provides complete information about **n**, but the results can not be directly interpreted as orientation angles. Instead we obtain a "slope", the quantity $(\mathbf{x}_0\ \mathbf{n})(\mathbf{n}\ \mathbf{t})$ appearing in the formula 4.1 (**t** is here the unit vector along the borehole).

The formula 4.1 can be used to plot the possible orientations of a zone for every reflection identified with it. The normal of the possible orientations are preferably plotted in a Wulff diagram in the same way as is done during the analysis of the single hole reflection data. Performing the same procedure for several different crosshole measurements one obtains a number of curves all intersecting each other near some point corresponding to the correct orientation.

There are obviously uncertainties involved in this method as well as any other. For instance the selected reflections must really correspond to the same fracture zone. It is also an idealization to describe the fracture zones as planes. On a large scale they are often remarkably plane but there are always slow undulations in a zone and since the point of reflection varies during the different measurements there will inevitably be some variation in the direction of the normal **n**.

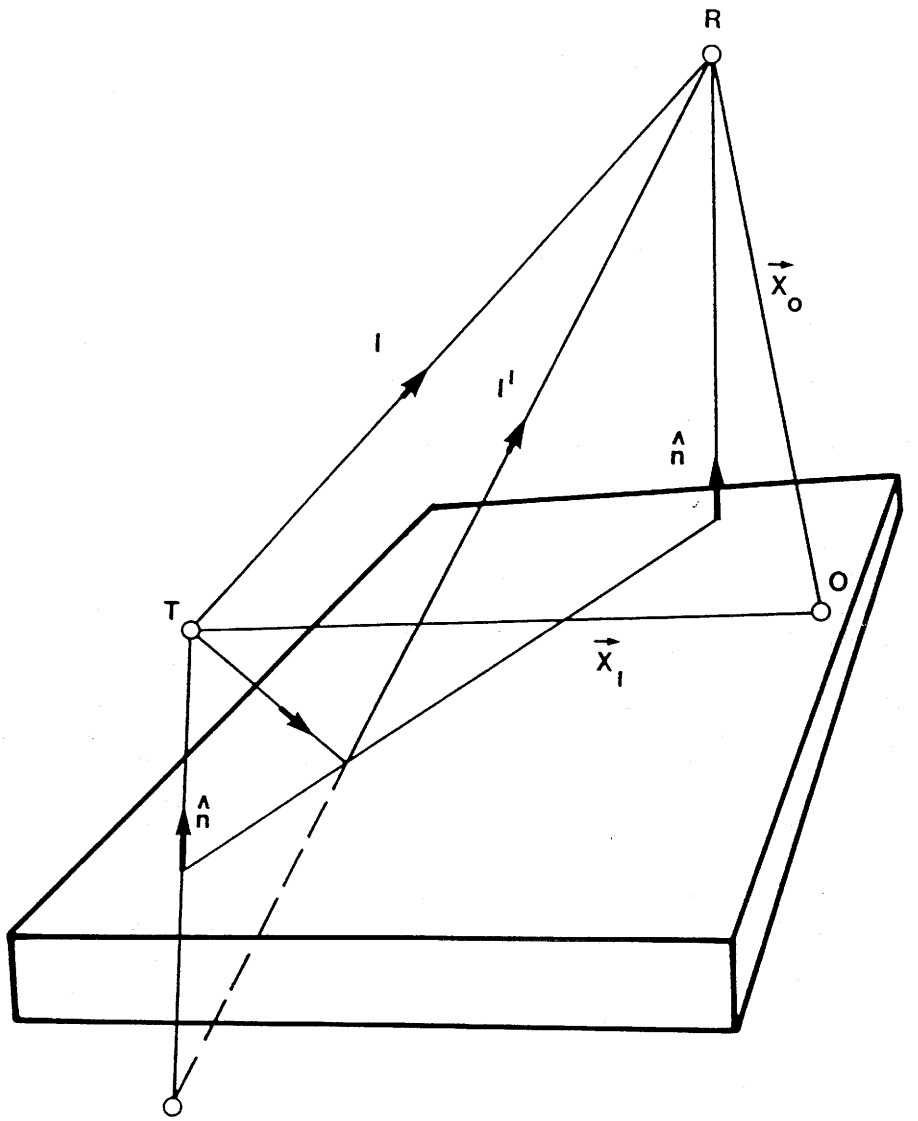

Figure 4.1 Principal ray paths in a bistatic radar configuration where the ray is reflected in a plane. T = transmitter, R = receiver, l = direct wave, l′ = reflected ray, $\mathbf{x}_0$ = location vector of receiver, $\mathbf{x}_1$ = location vector of transmitter, $\mathbf{n}$ = normal vector to plane.

4.2 DATA PROCESSING

The signal processing performed on the crosshole reflection measurements have been limited to a removal of the DC-level offset. An example of a grey scale radar map from a crosshole reflection scan is shown in Figure 4.2. The reflections identified in the grey scale maps have been digitized and the data used to obtain values for the "slope" (the quantity $(\mathbf{x}_0\ \mathbf{n})(\mathbf{n}\ \mathbf{t})$ in the equation 4.1).

4.3 RESULTS FROM CROSSHOLE REFLECTION SURVEYS

The radar reflection maps from the crosshole reflection measurements are not shown in this report. A representative example of the results is shown in Figure 4.2. The most significant reflectors identified from the radar maps and which have been used in the integrated analysis of all radar data described in Chapter 6 are listed in Tables 4.1-4.5.

Table 4.1 Reflectors identified from crosshole reflection measurements with the moving probe in C1.

Zone	Fix position of receiver (m)	Depth in C1 (m)	Slope	Regression coefficient
	C2: 30	-9	107	0.9996
	140	6	87	0.9992
	C2: 140	37	288	0.9994
	C2: 30	117	-48	-0.9996
	30	120	-235	-0.9989
RA	30	123	-141	-1.0000
	C2: 30	143	-380	-1.0000
	C2: 140	172	-156	-0.9998

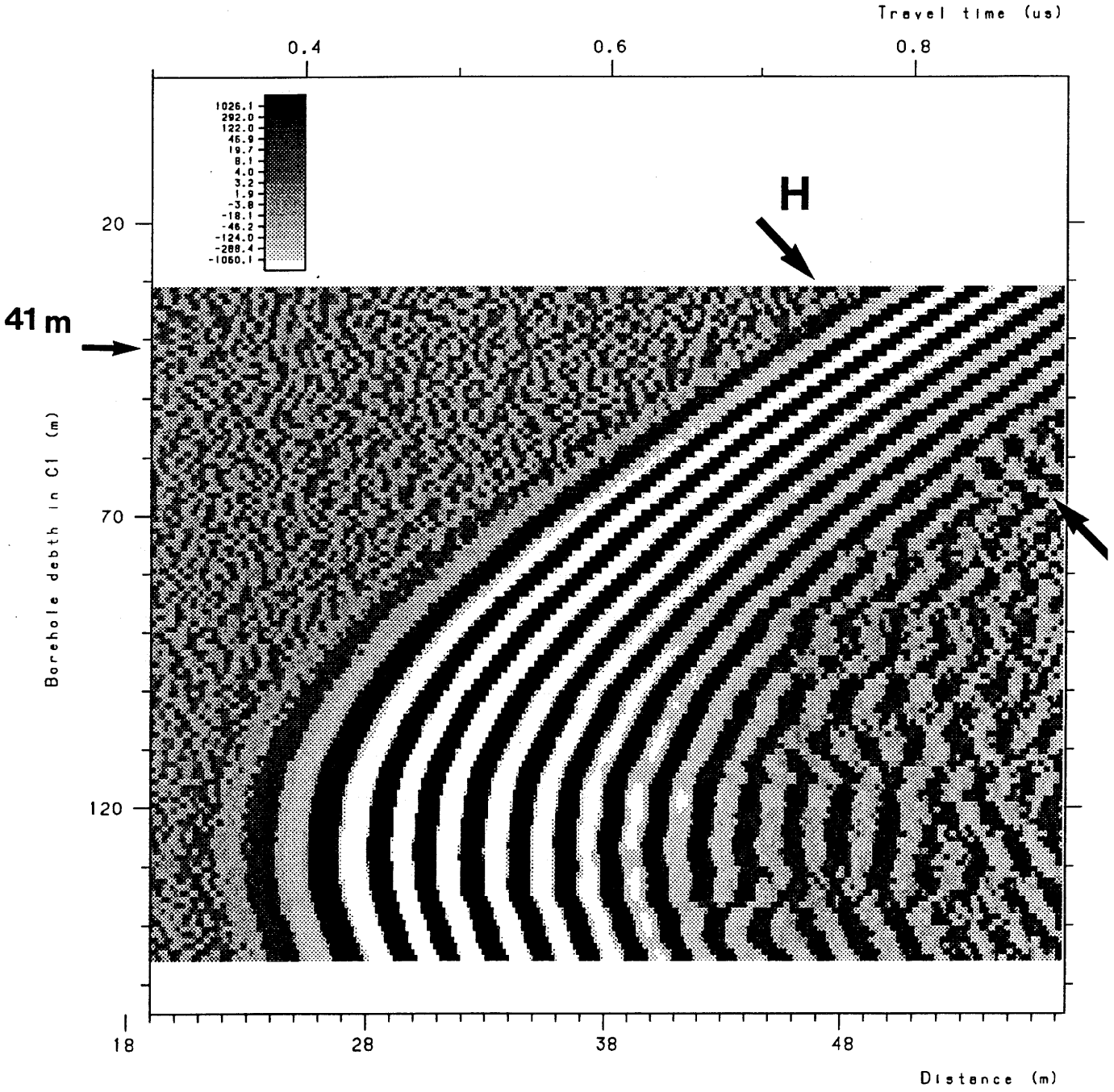

Figure 4.2 Radar map from crosshole reflection measurement between C1 and C2. Transmitter fixed in C2 at 30 m while receiver is moved in C1. Centre frequency 60 MHz.

Table 4.2 Reflectors identified from crosshole reflection measurements with the moving probe in C2.

Zone	Fix position of receiver (m)	Depth in C2 (m)	Slope	Regression coefficient
	C1: 30	-16	135	0.9996
	W1: 30	0	60	0.9900
	C1: 144	57	157	0.9999
	C1: 30	95	-75	-0.9995
	30	102	-238	-0.9999
RA	30	110	-320	-1.0000
	30	123	-258	-0.9999
	W1: 30	132	-409	-0.9994
	C1: 30	140	-56	-0.9952
	C1: 144	163	-185	-0.9999

Table 4.3 Reflectors identified from crosshole reflection measurements with the moving probe in W1.

Zone	Fix position of receiver (m)	Depth in W1 (m)	Slope	Regression coefficient
	C2: 30	-15	127	0.9998
	30	-3	146	0.9975
	C2: 30	94	-137	-0.9997
RB	C2: 30	140	-363	-0.9997
	C2: 30	185	-73	-0.9969
	30	194	-21	-0.9945

5 RESULTS FROM TOMOGRAPHY SURVEYS

5.1 INTERPRETATION PROCEDURE

5.1.1 Definition of the problem

The general idea behind tomographic reconstruction is that information about the properties of the interior of a region can be obtained through measurements at the boundary. In general the transmitter and receiver probes are located at the boundary of the area and each ray connecting transmitter and receiver can in principle be considered to represent the average of a measured property of the rock along the ray. In order to obtain an estimate of this property at a given point it is necessary that several rays pass close to the same point and that the rays have different directions and hence different information content. The requirement that several rays should intersect the same point puts some severe constraints on the borehole geometry. The main one being that the source and receiver positions and hence the boreholes have to be confined to the same plane.

In mathematical terms the tomographic problem can be formulated in the following way

$$d_i = \int_{T_i(m)} m(x) \cdot ds \qquad (5.1)$$

where d_i is the measured data for ray number i. The objective of the tomographic inversion is to estimate the spatial distribution of some property, $m(x)$, characteristic of the medium (x denotes the spatial location). The data is thought of as being a sum (line integral) of this property along the ray path, $T_i(m)$, from the transmitter to the receiver. The actual ray path is dependant on the properties of the medium, $m(x)$, and is normally the curve which gives the least possible travel time. The complex dependance of the ray paths, T_i, on the properties of the medium, $m(x)$, makes the problem nonlinear. The problem can be linearized by replacing the curves T_i with straight line segments, L_i, connecting sources and receivers.

In a borehole radar crosshole measurement data on the travel time and the amplitude of the direct wave between transmitter and receiver, i.e. the first arrival, can be extracted. It is assumed that the

travel time can be constructed as the line integral of the slowness, s(x), along each ray.

The amplitudes can not be obtained from a line integral directly but the problem can be linearized by taking the logarithm of the data. The logarithm of the amplitudes can then be subject to tomographic inversion. The data used in the tomographic analysis are obtained from the measured amplitudes, E_m, according to the following equation

$$d_i = \int_{L_i} \alpha(x) \cdot ds = \ln \frac{c\, a(\theta_1) a(\theta_2)}{r\, E_m} \qquad (5.2)$$

where $a(\theta)$ is the antenna radiation pattern and 'c' represents a normalization constant describing the combined effect of transmitter power and receiver gain.

A discretization is made of the problem. The plane between the boreholes is divided into a number of cells and the line integral is calculated as a sum where the contribution from each cell is considered in proportion to the length of the ray within each cell, cf. Figure 5.1. A discretization of (5.1) transforms the equation into the following form

$$d_i = \sum_{j=1}^{M} G_{ij}\, b_j \qquad (5.3)$$

where G_{ij} represents the length of ray 'i' in cell 'j' and b_j the attenuation or slowness of cell 'j'.

The problem has now been transformed into a system of linear equations, where the number of equations correspond to the number of rays, N, and the number of unknowns, b_i, to the number of cells, M. Hence, we may write

$$\mathbf{d} = \underline{\mathbf{G}} \cdot \mathbf{b} \qquad (5.4)$$

This equation system can be both overdetermined and underdetermined at the same time and errors in the data may cause some equations to be in conflict. The most common solution concept for this type of equation is through minimization of the functional $|\mathbf{d}-\underline{\mathbf{G}}\cdot\mathbf{b}|^2$.

Experience shows that the equation system is often unstable and it is necessary to introduce some form of damping. An effective and natural way of introducing damping is to assume that the slowness (or attenuation) of adjacent cells are equal. Introducing equations constraining the solution in

this way gives that a minimization should be made of the functional

$$|\mathbf{d} - \underline{\mathbf{G}}\cdot\mathbf{b}|^2 + \lambda^2 \, |\underline{\mathbf{C}}.\mathbf{b}|^2 \qquad (5.5)$$

where the parameter λ is a measure of the strength of the damping and $\underline{C}$ is a matrix containing the equations for equal slowness (or attenuation) in adjacent cells. λ determines the weight of the constraining equations and the practical consequence is that the differences in slowness between adjacent cells are limited to a certain extent. This type of damping gives a smoothed tomographic image without creating serious artifacts.

Normally the number of unknowns in the equation system is very large and iterative procedures will have to be used to obtain the solution. The conjugate gradient (CG) method which was developed as a part of the Stripa Project is considered to be an efficient inversion procedure. The convergence is fast and hence few iterations are needed to arrive at the final solution. The CG-method has been shown to give smaller computing times and better reconstructions of model examples than the other iterative methods (Ivansson, 1984).

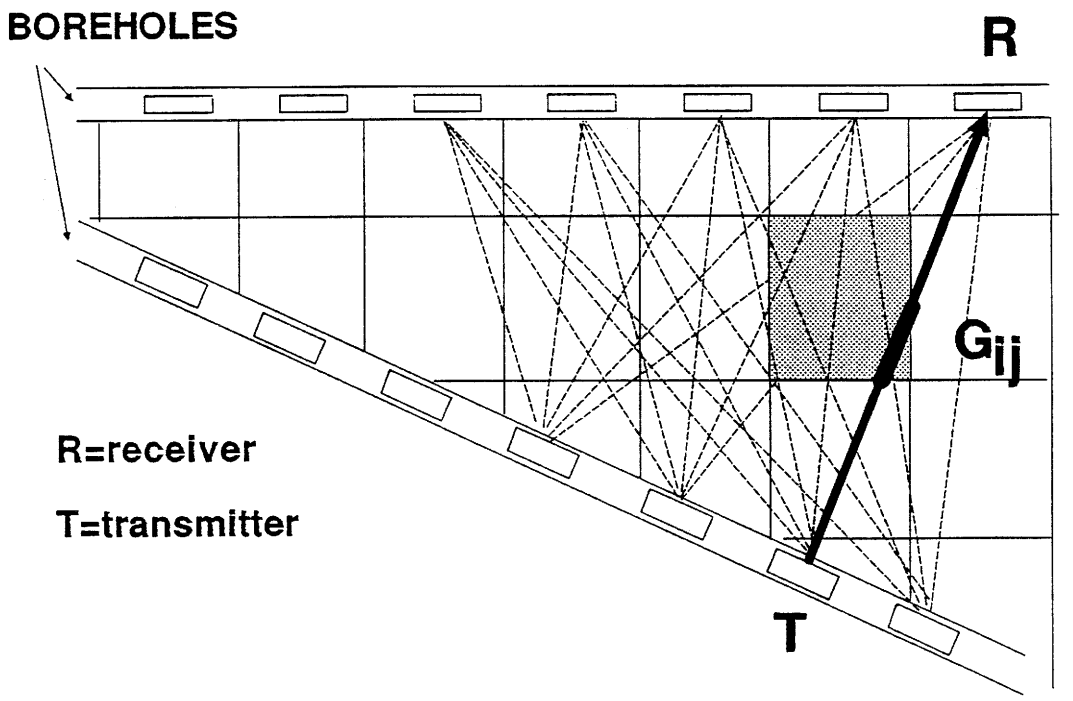

Figure 5.1 Generalized crosshole tomography geometry with a decomposition into cells and an example of a ray pattern.

5.1.2 Residual attenuation and velocity

The radar velocity (or slowness) has small variations around a certain average value. We have found it useful to put the crosshole data in such a form that these variations are studied rather than the absolute values of these properties. The concept has also been adopted for the amplitude data. In this context we define the terms 'residual travel time' and 'residual amplitude'. These residual data correspond to the measured data after subtraction of the expected data value which would have been obtained in a homogeneous medium with properties close to those of the investigated rock.

The residual travel time, t_r, is defined as the measured travel time, t_m, minus the estimated travel time for a homogeneous medium with a constant velocity, v_0. The residual travel time then becomes

$$t_r = t_m - r/v_0 \qquad (5.6)$$

where r is the distance between transmitter and receiver.

The residual amplitude is defined as the quotient (expressed in dB) of the received amplitude, E_m, and the estimated amplitude in a homogeneous medium with constant attenuation α_0. The residual amplitude, d_r, thus becomes

$$d_r = -20 \log_{10}\left(\frac{E_0}{E_m} \; \frac{\exp(-\alpha_0 r)\; a(\theta_1)\; a(\theta_2)}{r}\right) \qquad (5.7)$$

where E_0 represents a reference level corresponding to the ratio of transmitted power to receiver sensitivity. Through the use of the base 10 logarithm and the multiplication by 20, the residual amplitudes become represented in dB.

With this conversion into residual data it is possible to look at small variations from large average values. The residual data are also suitable for detecting systematic errors in the data and can be used for calibration of some system parameters.

5.2 DATA PROCESSING

5.2.1 Travel time and amplitude picking

A typical example of a radar signal recorded from a crosshole measurement is shown in Figure 5.2. From

this signal trace we want to obtain the time of first arrival and the magnitude of the signal.

A tomographic survey normally includes a large number of rays. It is therefore of utmost importance to arrive at some automatic procedure which can pick the data from the recorded traces, especially as a manual treatment of each ray would be extremely time consuming and hence costly. For the radar data we have adopted a simple approach which has in a number of cases proven to be reasonably efficient. An algorithm has been devised which picks out the maximum and the minimum for each trace and the time instances at which these events occur. The travel time is then defined as the time to the maximum or minimum of the pulse and the amplitude is defined as the difference between the maximum and the minimum, i.e. peak-to-peak amplitude. In two sections the peak amplitude of the envelop of the radar signal have been used for the analysis, which in theory should be more representative of the pulse energy than the peak-to-peak amplitude. However, no significant difference were obtained between the two methods.

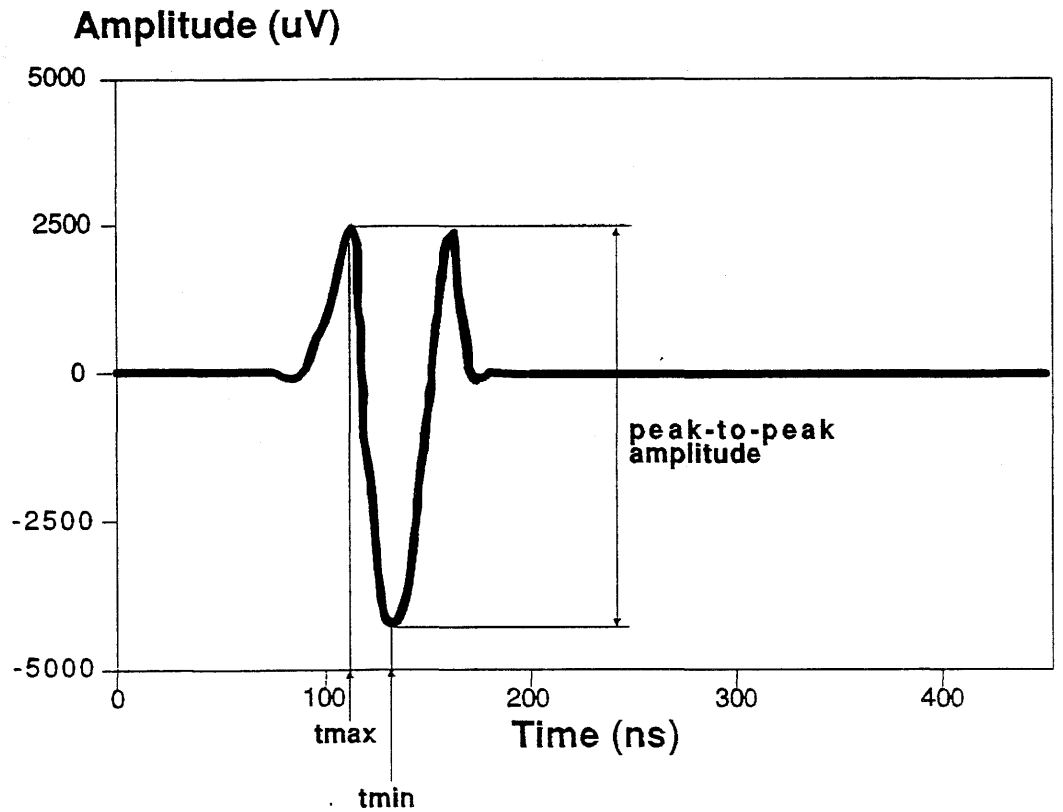

Figure 5.2 Radar signal obtained from a crosshole measurement. The data identified by the automatic routine for extraction of travel times and amplitudes are indicated.

5.2.2 Attachment of coordinates to data

The basic step in preparing data for tomographic inversion is the attachment of coordinates to the picked travel times and amplitudes. The accuracy required in source and receiver coordinates is of the same order as the propagation distance during a sampling interval. The sampling interval normally corresponds to a propagation distance of 0.2-0.5 m. The borehole coordinate measurements are described in the report on the results of the geophysical logging in the boreholes at the SCV-site by Fridh, 1988.

After the travel time and amplitude data have been combined with the coordinates of the source and receiver points the residual data are calculated according to (5.6) and (5.7).

The tomographic inversion software requires the source and receiver points to be in the plane spanned by the two boreholes and in order to accomplish this the coordinate system is rotated.

5.2.3 Data quality checks and corrections - general remarks

The tomographic data is subject to a number of errors such as; errors in time and amplitude picking, constant offset errors in time and gain, and coordinate errors. It is essential to get a grasp of both the stochastic and systematic errors which may exist in the data set. The errors must be understood, quantified and corrected before a tomographic inversion is attempted. A good way to reveal errors is to plot the residual data as a function of the length of the rays. From these plots an offset and a slowness or attenuation correction is determined. A grey scale plot (or ray check plot) is then made of the average slowness or attenuation for all rays. In this plot individual rays containing errors (e.g. due to errors in time and amplitude picking) can be identified. Rays containing errors are removed from the data set before tomographic inversion.

The data correction and quality checking procedure is described in detail by Olsson, Falk, Forslund, Lundmark, and Sandberg, 1987.

5.2.4 Tomographic inversion procedure

Tomographic inversions were performed of the residual travel times and the residual amplitudes after corrections and removal of erroneous rays as described in the previous section. The inversion was made with the Conjugated Gradient (CG) method described by Ivansson (1984).

The inversion was made with rectangular basis functions, i.e. the velocity of each cell is assumed to be constant within that cell. This means that no interpolation is made of the values between adjacent cells. In the tomographic inversion of a data set the following parameters may be varied:

- the cell size
- the number of iterations
- the damping constant (λ).

For this project cell sizes of approximately 3 m have been used. The damping constant is a measure of the length over which the slowness or attenuation is averaged. The definition of the damping constant used in this Stage has been changed since the Stage I tomographic inversion procedure. This is described later in this section.

The tomographic inversion of the slowness and attenuation data was carried out in two steps. The first step consisted of inversion of the data sets where rays assumed to contain errors had been removed manually. The rays to be removed were identified on the ray check plots.

The general strategy of the two step inversion procedure is first to make a tomographic inversion with a large damping constant in order to identify any remaining rays containing errors. The large damping constant will give a smoothed solution and rays inconsistent with this solution will be identified and removed. The criteria for removal of rays has been that the error should be greater than 2 times the RMS-error of all rays compared to the solution obtained by the tomographic inversion. In the second step a small damping constant is used to obtain a high resolution image. The cell size is the same for both inversions.

The damping constant used during the first inversion has had a value of 50. Previous experience has shown that it is essential to have a large damping constant during the first inversions in order to assure that the correct rays are removed (Niva and Olsson, 1988). If the damping constant is too small it may well happen that a ray containing a large error will distort the solution with the consequence that rays adjacent to the erratic one are removed

incorrectly. The number of iterations used in all inversions has been 11.

Ivansson, Hammarström, and Pihl (1987) has shown that the conjugated gradient method tends to concentrate errors into regions of low ray density when the number of iterations is large. They also showed that the CG-method converges to the correct solution. If the iterative process is interrupted after a small number of iterations the least square solution to (5.5) has not been obtained, but in practice this means that errors are more evenly distributed over the tomographic section.

It has been found that the accumulation of errors in certain parts of the section must be due to the applied damping procedure (Andersson, Andersson, Gustavsson and Olsson, 1989). The damping is defined by the matrix $\underline{C}$ which contains equations for equal attenuation or slowness in adjacent cells. In the original algorithm $\underline{C}$ only included equations for adjacent cells along the same row or column (a quadratic cell mesh is used). Hence, no equations constrained the velocities of diagonally located cells. This at times generated anomalies along the cell diagonals, especially when low damping constants were used. In the attempt to improve the tomographic inversion algorithm constraining equations for diagonal cells were added to the matrix $\underline{C}$.

Another feature of the old damping algorithm was that the weight (λ) of all constraining equations was the same. This actually means that the relative damping is less for cells intersected by few rays compared to cells with many rays. A consequence of this is that anomalies appear in parts of the tomograms where there actually no information to define the location of the anomalies. The most common example are circular type anomalies at the edges of the tomographic sections where there are essentially only parallel rays. If a region is covered only by parallel rays it is not possible to define the location of the anomaly and a proper representation of the data should give an anomaly of roughly the equal magnitude along the rays which extends all the way between the boreholes. To accomplish this we introduced a weight on the constraining equations which was dependant on the ray density in each cell. The weights were defined by the following equation

$$\lambda_j = \frac{\lambda_0}{1 + \rho_j/\rho_0} \qquad (5.8)$$

where λ_j is the damping constant for cell j
ρ_j the ray density for cell j

λ_0 a parameter defining the magnitude of the damping

ρ_0 a parameter determining the sensitivity of the damping constant to the ray density.

The best results is obtained with small values for the parameter ρ_0, i.e. a strong dependance on the ray density (Andersson, Andersson, Gustavsson and Olsson, 1989). For the tomograms presented in this report the following values have been used; λ_0=100 m, ρ_0=1. The average ray density for the sections measured at the SCV site has been in the range 25 to 30, this implies that the damping effectively has been inversely proportional to the ray density. In some cells the number of rays are down to 10 and in other up to 70 rays. The corresponding damping in these cells are 10 and 1.4 m, respectively.

The ray density dependent damping algorithm has been used for all tomograms within the SCV Stage III programme. The SCV Stage I tomograms were made with the old damping algorithm i.e. independently of the ray density.

5.3 RESULTS FROM THE BOREHOLE SECTIONS

5.3.1 General comments

Tomographic surveys have been made of three borehole sections and for each of these sections two tomograms have been produced. When analyzing the tomograms it is essential to be aware of some general characteristics of the tomographic inversion procedure which has consequences for the interpretation of the tomograms in geological terms.

Tomographic inversion may be considered as a two stage mapping process or transform. First the geologic structure is transformed into a data set of travel times and amplitudes. Secondly this data set is transformed into maps of slowness and attenuation through the tomographic inversion procedure described in the previous Sections. These maps thus constitute a representation of the geologic structure in terms of the physical properties measured.

The tomographic maps may not give a correct representation of the geologic structures due to different types of random and systematic errors and limitations in the information content of the data collected (limited coverage of rays). Errors in the data will appear in the tomograms as anomalies which might be misinterpreted as geologic structures. Anomalies due to errors are termed artifacts and a

discussion on how different types of errors are represented in the tomograms can be found in Ivansson, 1984.

In this case six different tomograms have been produced for the three borehole sections i.e. attenuation and slowness on each section. Attenuation and slowness are two different properties where the attenuation essentially corresponds to the electric conductivity of the rock and the slowness to the dielectric constant. Both of these parameters are to a first approximation related to the fracturing of the rock, but other characteristics of the rock might influence the value of these parameters as well. In Stage I tomographic inversion was made with different centre frequencies, 25 and 60 MHz (Olsson, Eriksson, Falk and Sandberg, 1988). The results from Stage I showed that the resolution with the 60 MHz antennas is better even if the attenuation is increasing with frequency, i.e. decreasing range. All tomograms in Stage III are made with a centre frequency of 60 MHz.

One consequence of errors and limitations in the data is that the tomograms should not be overinterpreted, i.e. every little enhancement or spot in attenuation or slowness should not be considered as an indication of a significant geological structure. Instead most confidence should be put in larger structures which appear similar in most of the tomograms.

5.3.2 Borehole section C1-C2

The attenuation tomograms from the plane between boreholes C1 and C2 are shown in Figures 5.3 and 5.4. The dominating feature in both tomograms is the feature which extends from 40-50 m in C1 to 50-60 m in C2 (RH), i.e. the feature strikes North-South. The slowness tomogram gives a more clear indication of the structure RH than the attenuation tomogram.

The feature at about 90 m in C1 shows the same behaviour as the feature RQ found in the Stage I tomograms from the section N3-N4. In the slowness tomogram it is a spot with increasing slowness but in the attenuation tomogram it is more like a black ring with very low attenuation (white area) within the ring. As a matter of fact, the feature is according to the Stage I predictions a part of the same zone, i.e. GB (RB in this report). The zone RB seems to end or diminish in the plane between C1 and C2. As we also have seen in the Stage I results the slowness anomaly is located within the attenuation anomaly which appears at approximately the same location. It appears as if the slowness anomaly is enclosed by a

highly attenuating region. An interesting characteristic of this anomaly complex is that the attenuation in the region of increased slowness is comparatively low. The relative displacement of the slowness and attenuation anomalies is considered to be related to the properties of the rock and not an artifact caused by errors in the data or the tomographic inversion procedure. A more detailed discussion of this problem were made in the Stage I report, see Olsson, Eriksson, Falk and Sandberg, 1988 (chapter 6 page 66).

The last feature of interest seen in this section is the one at the bottom of the section, i.e. 140 m in C1 and 110 m in C2. In the slowness tomogram the part close to C1 is not prominent while the part close to C2 is very prominent but spreads out between 100 and 120 m. In the attenuation tomogram the same feature is clearly seen all the way between C1 and C2.

Another feature may also be interpreted from the tomograms e.g. a black area close to RB in C1 at a depth of about 100 m. It is however very difficult to determine if it is a part of RB or if it is crossing both RB and RH and intersecting C2 at about 50 m depth.

A white thin line crossing the attenuation tomogram between the start of C1 and the end of C2 is considered to be an artifact due to a bad ray.

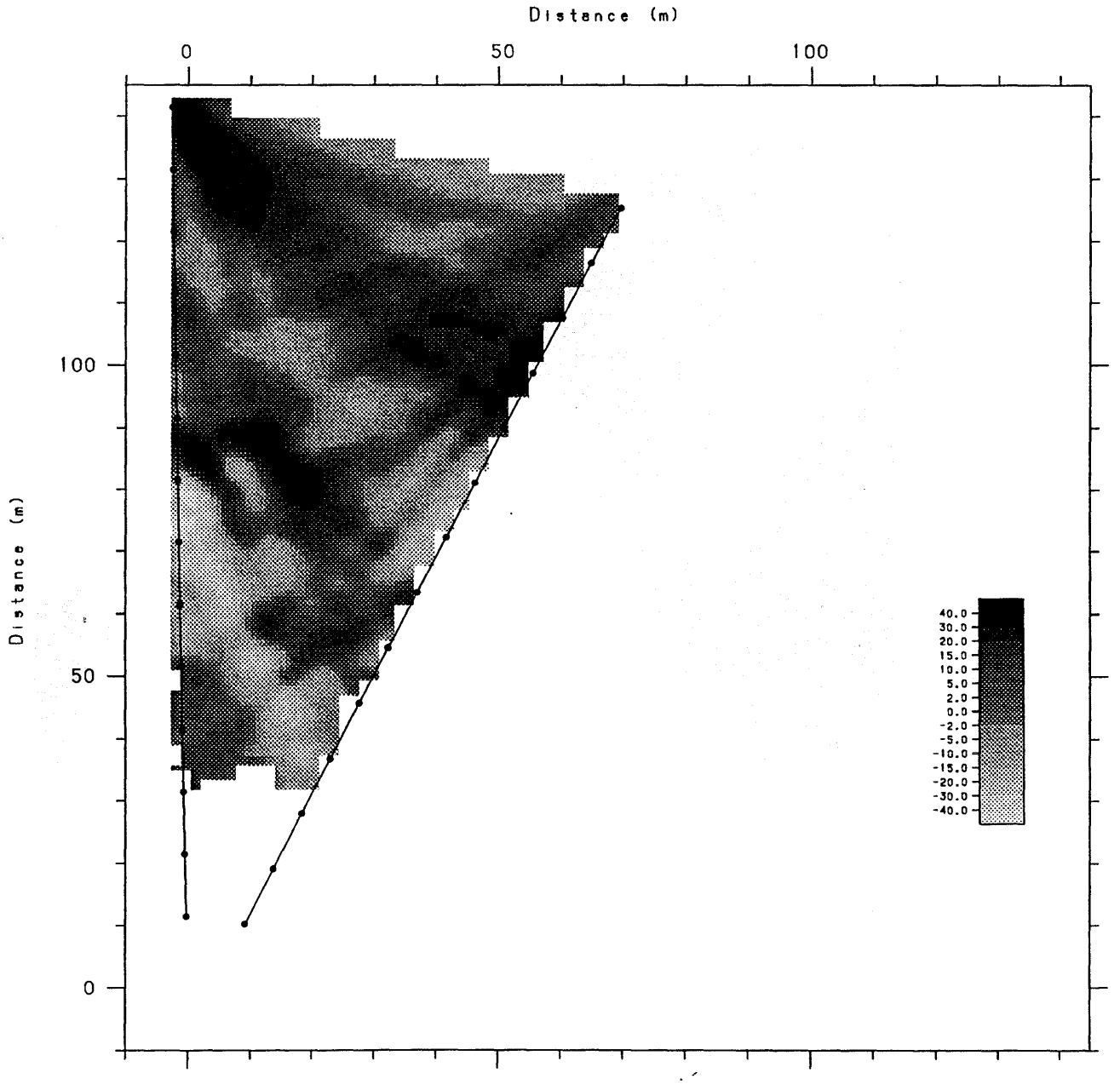

Figure 5.3 Residual attenuation tomogram for the borehole section C1-C2 made with a centre frequency of 60 MHz.

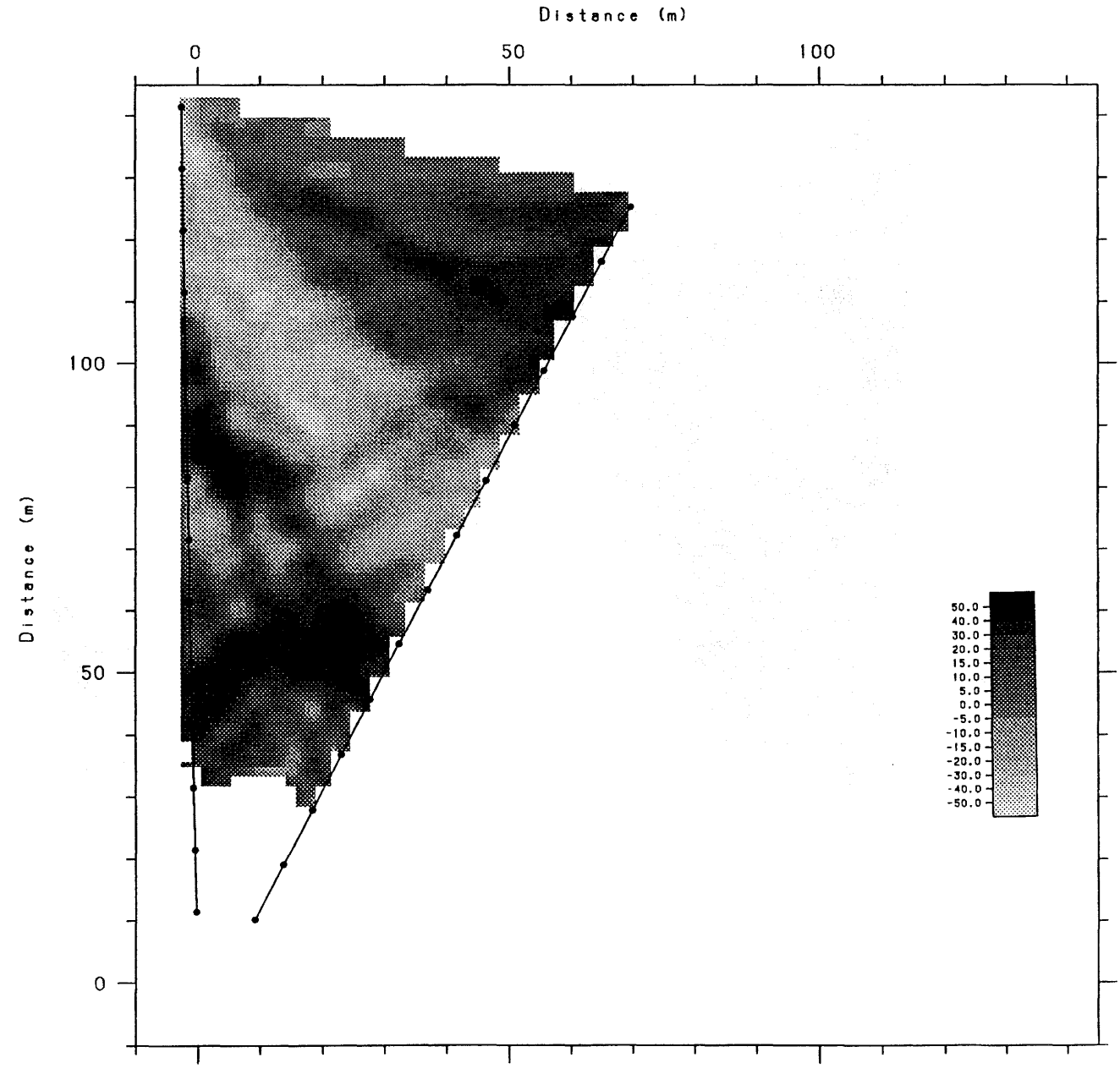

Figure 5.4 Residual slowness tomogram for the borehole section C1-C2 made with a centre frequency of 60 MHz.

5.3.3 Borehole section W1-C2

The attenuation and slowness tomograms from the borehole section W1-C2 are shown in Figures 5.5 and 5.6.

There are three features of interest in the tomograms. The two most marked anomalies extend from 50-60 m in W1 to 50-60 m in C2 (RH) and from the bottom of W1 at 140 m to 110 m in C2 (RA).

The feature RQ is clearly seen in the attenuation tomogram. It fits perfectly with anomaly RQ seen in the N3-N4 tomogram obtained during the Stage I. In this section GB (RB in this report) should intersect W1 at the very end of the borehole, at 140 m. It is passing very close to the anomaly RQ which could be a part of the zone RB and again ending or diminishing close to C2 (cf. borehole section C1-C2 above). The results from the C1-C2 and N3-N4 sections are similar also in the respect that a well defined slowness anomaly is surrounded by an attenuation anomaly.

There is also an indication of a large local anomaly at about 100 m in W1 which is not extending more than approximately 20 m from W1 towards C2. It is clearly seen in both the attenuation and slowness tomograms.

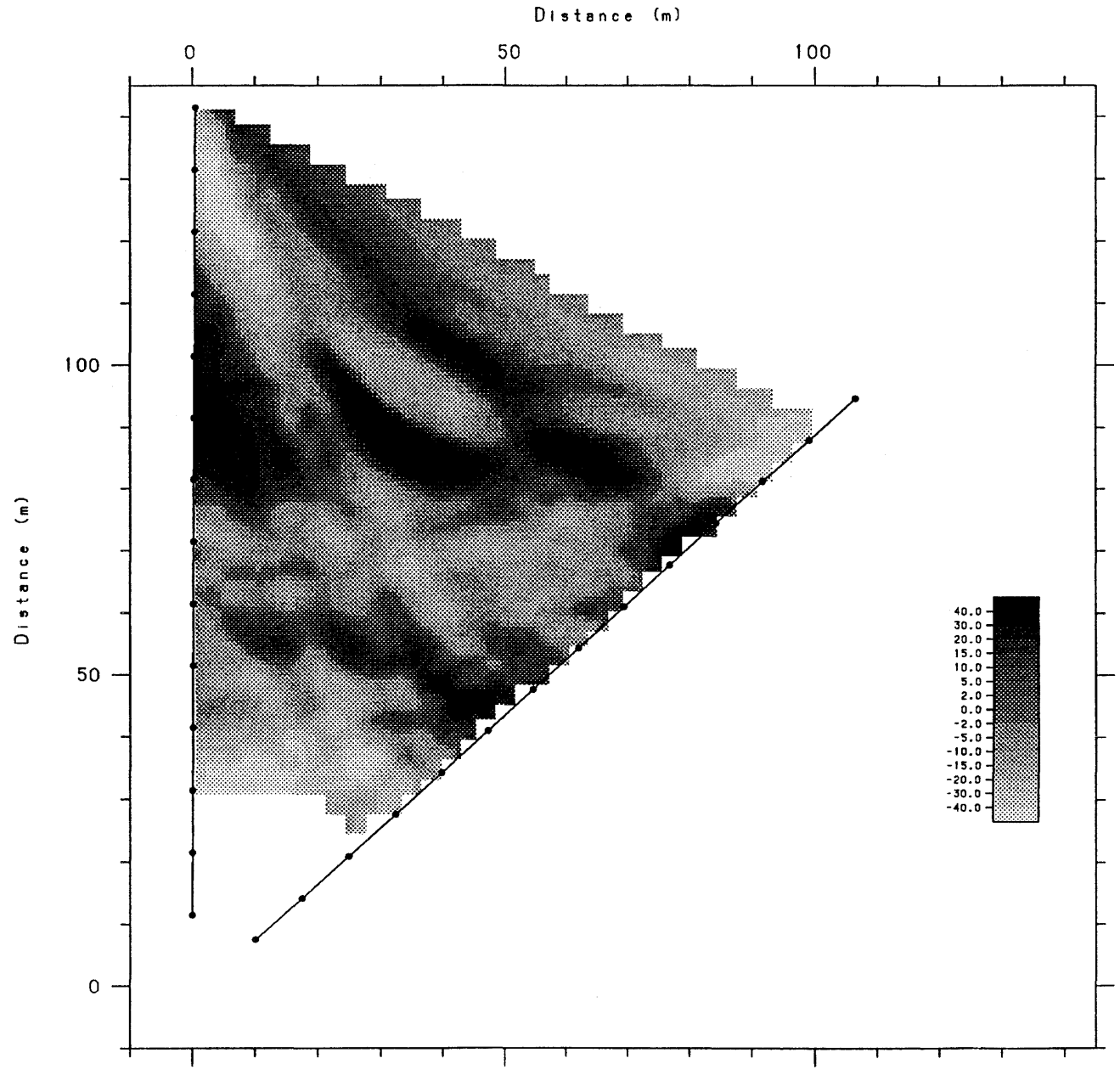

Figure 5.5 Residual attenuation tomogram for the borehole section W1-C2 made with a centre frequency of 60 MHz.

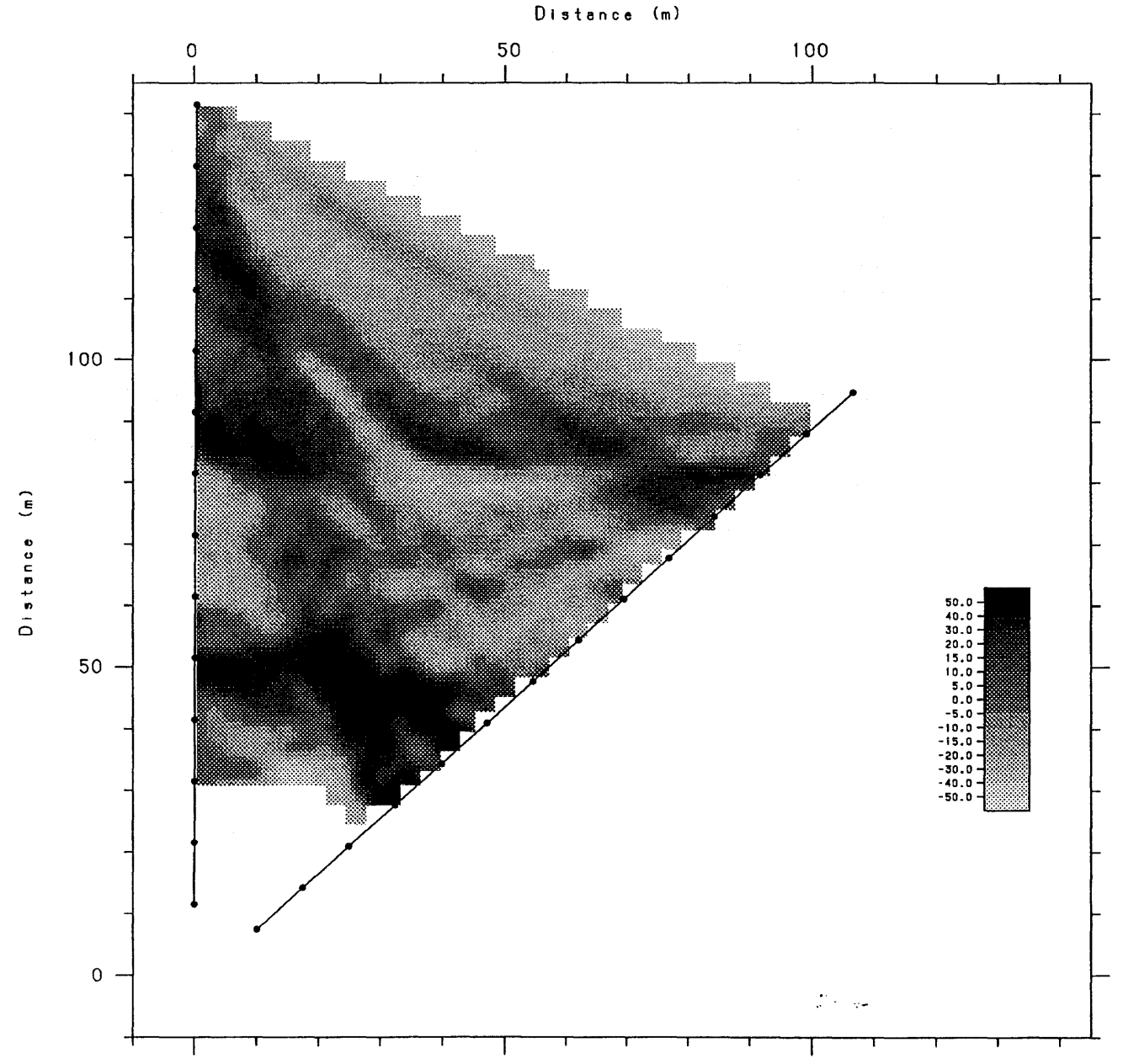

Figure 5.6 Residual slowness tomogram for the borehole section W1-C2 made with a centre frequency of 60 MHz.

5.3.4 Borehole section W1-C1

The attenuation and slowness tomograms from the borehole section W1-C1 are shown in Figures 5.7 and 5.8. As for the previous sections the dominating features obtained in the tomograms are very similar.

Especially the attenuation tomogram shows very clearly zone GH (RH in this report) around 40-50 m in W1 and 50 m in C1. The travel time data from this section contained considerable errors which were difficult to correct for.

In Figure 5.8 white stripes, due to bad rays, can be seen. They go from shallow depth in one borehole to the bottom of the other borehole. One reason for this might be that the zone RA is intersecting W1 and C1 almost at the end of the measured section affecting the most attenuated rays (time dispersion of the pulse) at the boundary, in an area where the errors of the tomographic inversion method already are large and the ray coverage is poor.

In the attenuation tomogram the feature at 140 m in W1 and at 140 m in C1 (RA) is very big due to the boundary effect described above and the feature at about 100 m in C1 (RB) crossing RA and intersecting W1 at a depth of 150-160 m.

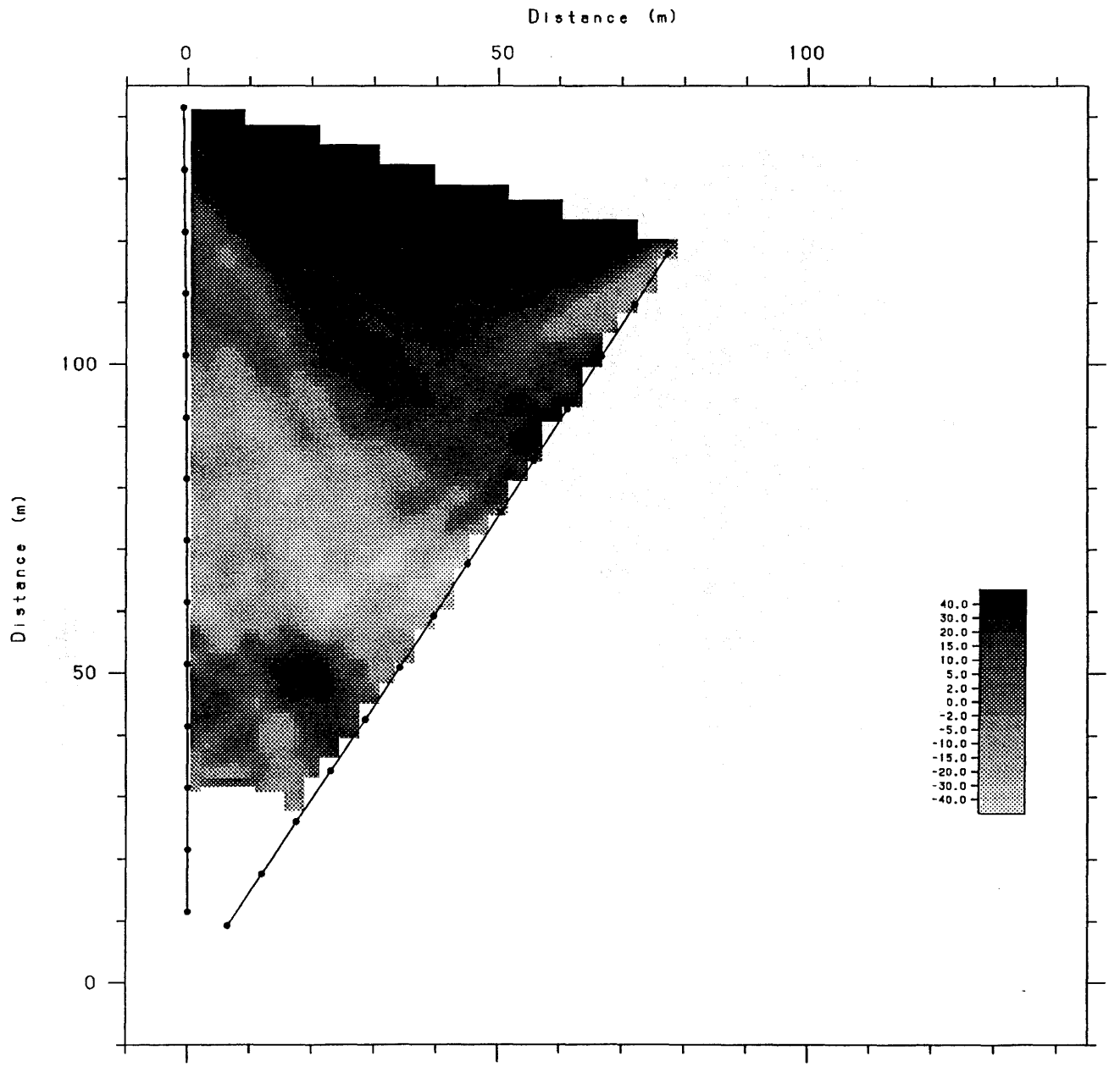

Figure 5.7 Residual attenuation tomogram for the borehole section W1-C1 made with a centre frequency of 60 MHz.

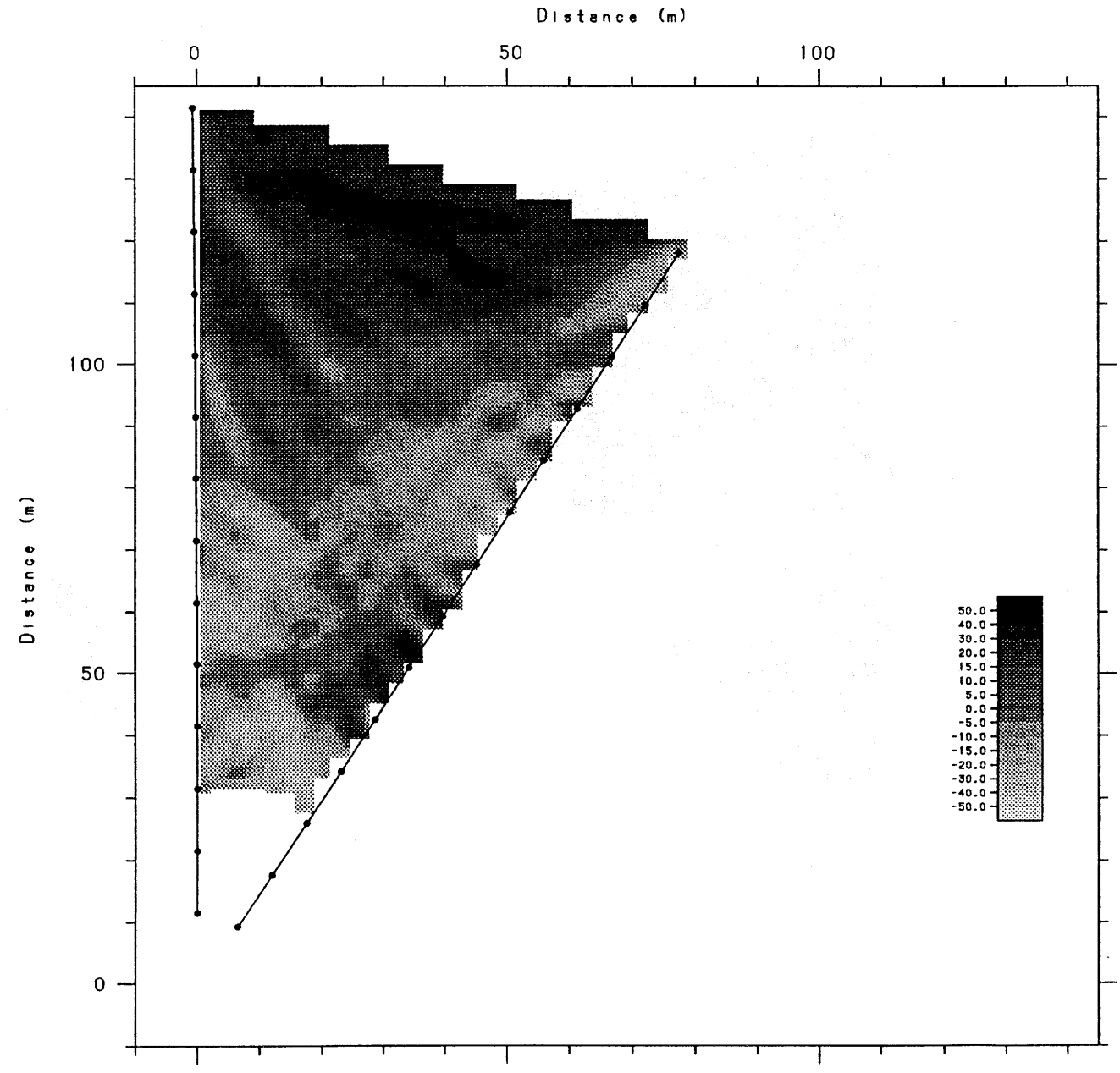

Figure 5.8 Residual slowness tomogram for the borehole section W1-C1 made with a centre frequency of 60 MHz.

6 INTEGRATED ANALYSIS OF RADAR DATA

6.1 PROCEDURE

This chapter describes the integrated analysis of all radar data collected at the SCV-site. The analysis has been performed with the objective to provide a three dimensional model of the major features at the SCV-site with respect to their geometry and electric properties.

During Stage I of the SCV Project the borehole radar has been applied in three different measurement configurations; single hole reflection, crosshole reflection, and tomography. Each configuration has provided a data set which gives independent information with respect to the other sets.

During Stage III of the SCV Project the borehole radar has been applied in one more measurement method; the directional antenna system which has given additional information about the location of the fracture zones. It has proved to be a valuable tool in determining the exact location of the zones. The uncertainty in the interpretation of the integrated analysis has been much reduced by using the directional antenna.

The data sets, which are described in the previous chapters, contain enormous amounts of data (about 3 million data points within Stage III and 10 million within Stage I) which can not be used directly for the definition of a model of the site. Instead basic information concerning the major features has to be extracted from the data and used in the description of the site. In a more detailed study of specific features than the one performed here it will be necessary to go back to the original data again. It will then be possible to make a more detailed description of the geometry and properties of larger features and to identify and characterize also smaller features.

From each measurement mode the following information has been extracted from the processed radar data;

The grey scale radar maps from single hole reflection measurements have provided data on where features intersect the boreholes (or their linear extension) and the angle with which the structures intersect the boreholes. The directional antenna system has been a

very useful tool in determining the azimuth angle and hence leading to a more accurate interpretation. The data is listed in Tables 3.1-3.5.

The crosshole reflection grey scale radar maps have given data on where features intersect the boreholes (or their extensions) and a value of the "slope" defined in equation 4.1. The slope and the intersection data for the most significant reflectors are listed in Tables 4.1-4.3.

The tomography surveys have provided a description of the features in the plane defined by the two boreholes between which the measurements were preformed. From the tomographic inversion we get a map of the variation of electric properties in the plane. This gives a possibility of studying variations in the properties of the feature along its lateral extent and to study details of its geometry (undulations, faulting, etc.). In the three dimensional geometric analysis of the structures the location of the feature in the plane is used (or actually the intersection of the feature with the two boreholes).

The first step in Stage I of the integrated analysis was to identify the major features in the three data sets and to make certain that each feature was identified correctly in all three data sets. Normally a feature was first identified in one of the tomographic maps. The intersection of the feature with two of the boreholes was then readily identified. If the feature (fracture zone) is assumed to be planar then the definition of two points on that plane defines a normal of the plane perpendicular to the line connecting the two points. The possible orientations of the normal can then be displayed as a line in a Wulff diagram (cf. Figure 6.1a). The corresponding details from the Stage I integrated analysis is described in Olsson, Eriksson, Falk and Sandberg, 1988.

When the intersection of a feature with two boreholes is known the single hole reflection data from these boreholes are studied. Reflections can normally be found at the intersection points and the angle of intersection between the borehole and the feature gave another constraint on the possible orientation of the fracture plane. The curve describing the possible orientations of the normal defined by the single hole reflection data are also plotted in a Wulff diagram (e.g. Figure 6.1b). The intersection of the curves obtained from the tomography data and the single hole reflection data normally define two points, i.e. there are two possible orientations. This ambiguity was a consequence of the fact that up

to this point only data collected in one plane has been considered. Due to the omnidirectionality of the radar antennas such data will always show a mirror symmetry with respect to the plane of measurement. Using the directional antenna system this ambiguity has been resolved. The minimum (or maximum) of a reflection gives the azimuth angle. The azimuth angle together with the intersection angle and the phase of the reflection from the dipole antenna can in theory give one single solution and thus the absolute orientation of a fracture plane. However, this is not always possible. It is often a difficult and time consuming procedure to determine the right phase of the reflections. During Stage III the minimum azimuth angle has been used in the same way as for the single hole omni-directional data and the intersection point data, i.e. by plotting the possible orientation in a Wulff diagram (cf Figure 6.1c).

The following step in the analysis is to identify the same feature in the other plane defined by the "boundary boreholes". Suitable candidate features are sought in the tomographic maps and the single hole reflection data belonging to the "other" plane. The values on borehole intersections, angles of intersections and azimuth angles are compared with the previously obtained data and checked for consistency. Finally crosshole reflection data is also included in the analysis and checked for consistency (cf. Figure 6.1d).

If all the data included in the analysis is consistent it may be assumed that a major feature with significant lateral extent has been identified, i.e. a zone at least comparable to the dimensions of the site. In this case the location of the feature and its orientation can also be considered to be defined with a high degree of confidence.

During the interpretation of borehole radar data there will be varying degrees of consistency between the data sets for different features. The reliability in the various aspects of the description of the zones will thus vary between the zones. Smaller features which may exist but which are only defined with a low degree of confidence have not been included in the present description of the site.

The analysis of the radar reflection data has been performed under the assumption that the reflectors (fracture zones) are essentially planar features. This assumption is of course a generalization which appears to be relevant at the scale of the site. If the zones are studied in detail we observe that the zones are not exactly planar; instead they tend to

undulate somewhat and their thickness and contrast in properties with respect to the background varies along their extent. These small scale variations are particularly visible in the tomograms.

The integrated analysis within the Stage III was preformed in the same way as Stage I. A detailed comparison was made between these two radar models of the site. It was found that the major zones (GH, GB and GA) fit well together with the predicted intersections. However, the accuracy of the predicted locations of the minor zones (GC and GI) in the boreholes was bad. The minor zones found in the N-holes and W-holes are probably of limited extent or undulating too much from the assumed planes.

6.2 DESCRIPTION OF MAJOR FEATURES

A description of the major features GA, GB and GH will be given in this report. The Stage I radar measurement report (Olsson, Eriksson, Falk and Sandberg, 1988) contains a preliminary description of these zones and their orientation. The minor features; RC, RD, RK and RL were of smaller magnitude and are not considered here. The description in this report sometimes also refer to the Stage I boreholes W1, W2, N2, N3 and N4 and the complete description of the radar measurements made in these boreholes is found in the Stage I radar measurement report.

A brief interpretation of where the zones intersected other boreholes in the Stripa mine e.g. N1, V1, SBH1, SBH2, SBH3 and SBH4 can also be found in Olsson, Eriksson, Falk and Sandberg, 1988.

The preliminary predictions (Olsson, Black, Gale and Holmes, 1988) based on measuring geology, fracture characteristics, stress, single borehole geophysical logging, radar, seismics and hydrogeology resulted in four major zones GA, GB, GH and GI and one minor zone GC. These predictions have been used in this report to verify the orientation and extent of the zones. The zones identified in radar measurements are named RA, RB, RH, RC and RI.

6.2.1 Zone RA

Zone RA was clearly seen in the attenuation tomograms from the borehole sections N2-N3-N4 where it constituted one of the major anomalies. The zone appeared during Stage I to be irregular and the tomograms indicated that it consisted of patches of increased fracturing. The zone RA intersects the line of borehole W1 at about 200 m. It is therefore not prominent in the W1-C1 and W1-C2 tomograms. It is very prominent in the C1-C2 tomograms, but in the C1-C2 tomograms zone RA seems to intersect C1 at about 140 m instead of the predicted, 120 m. This should correspond to a zone with the same strike as before (40°) but dipping 70° instead of 35-40°. During the interpretation many attempts were made to confirm this location of RA but in that case zone RA should appear at the same location as RB in the W1-W2 plane. RA and RB should also cross each other in that plane which seems unlikely from the tomograms from W1-W2. The crosshole reflection measurement from C1 and C2 also indicated that a steep dipping zone was unlikely.

In the reflection data zone RA is seen as one of the prominent reflectors but not as prominent as RH and RB. However, it seems to undulate and the reflection data do not fit perfectly to the prediction.

The data on the geometry obtained from the analysis of the three measurement modes is tabulated in Table 6.1 and shown in a graphical representation in Figure 6.1. As can be seen from the figure the data from all configurations is consistent and the orientation of the zone can be considered to be well defined. The average orientation of zone RA, as obtained from the radar data is given in Table 6.1. The predicted zone RA was found to have an average strike of N40°E and dipping 40° towards SE. The zone intersects the plane C1-C2, at 120 m and 110 m, and increased attenuation and slowness can be observed at this location in the C1-C2 tomograms.

RA is considered to be a prominent zone at the SCV-site and its existence and strike are considered to be well established. An ambiguity in the dip of the zone gives two possible solution; 40° and 70° towards SE. The 40° dip (5° more than the predicted) has been favored mainly depending on the intersection in C1 and the crosshole reflection data from C1-C2.

Table 6.1 Data used in the interpretation of Zone RA. The possible orientations of the normal of Zone RA given by the restrictions defined by each data value is plotted in Figure 6.1.

Intersections with the "boundary boreholes" based on radar data:

Intersection with:	C1 120 m
	C2 110 m
	C3 -
	D1 105 m

Figure 6.1a:
Intersections:

C1 120 m -- C2 110 m	(a)
C1 120 m -- D1 105 m	(b)
C2 110 m -- D1 105 m	(c)

Figure 6.1b:
Radar intersection angles:

C1 45°	(a)
C2 70°	(b)
C3 -	
D1 50°	(c)

Figure 6.1c:
Radar azimuth angles:

C1 -	
C2 100°	(a)
C3 -	
D1 30°	(b)
W1 40°	(c)

Figure 6.1d:
Crosshole reflection data:

Moving position	Fix position	Slope	
C1 119 m	C2 31.4	-235	(a)
C2 110 m	C1 31.4	-320	(b)

Orientation of Zone GA: N040°E/40°S

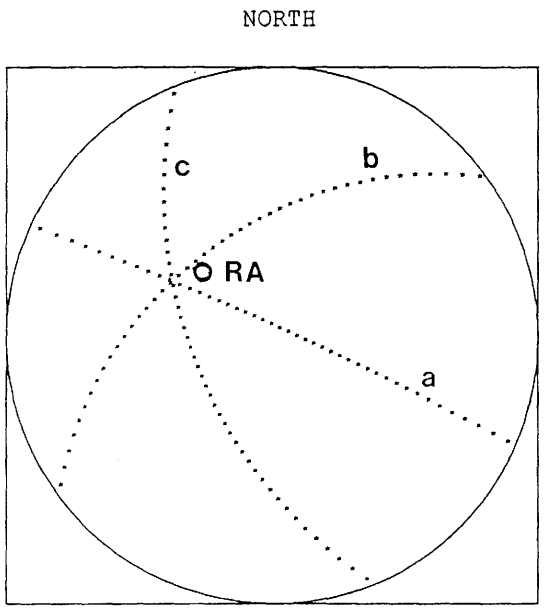

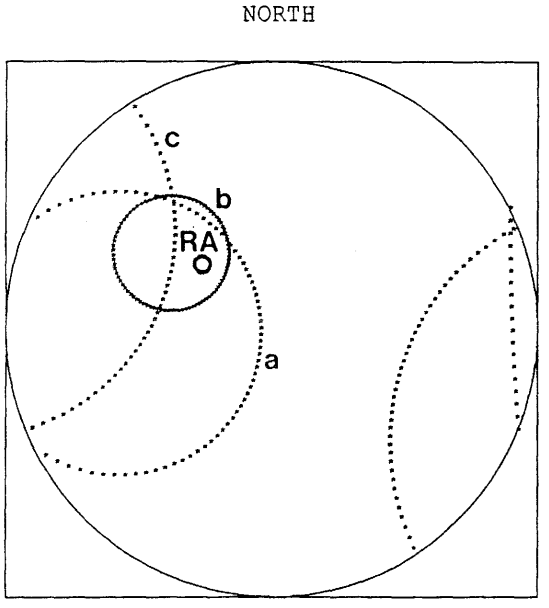

Figure 6.1 Possible orientations of the normal of Zone RA based on the data listed in Table 6.1. The data are presented in a Wulff projection. The predicted Zone GA is plotted as a single point in all diagrams.

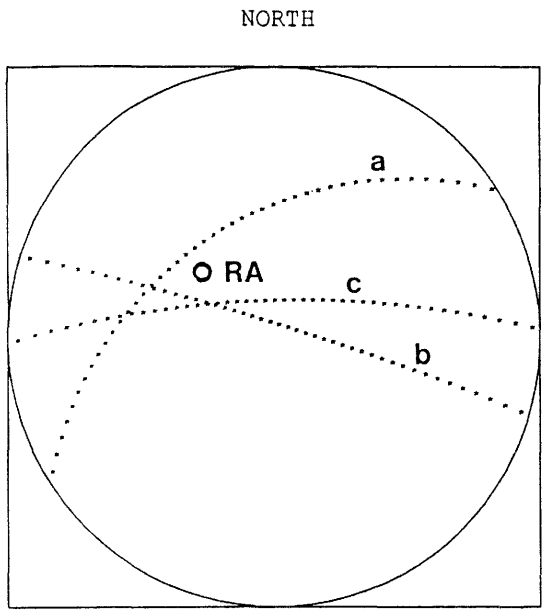

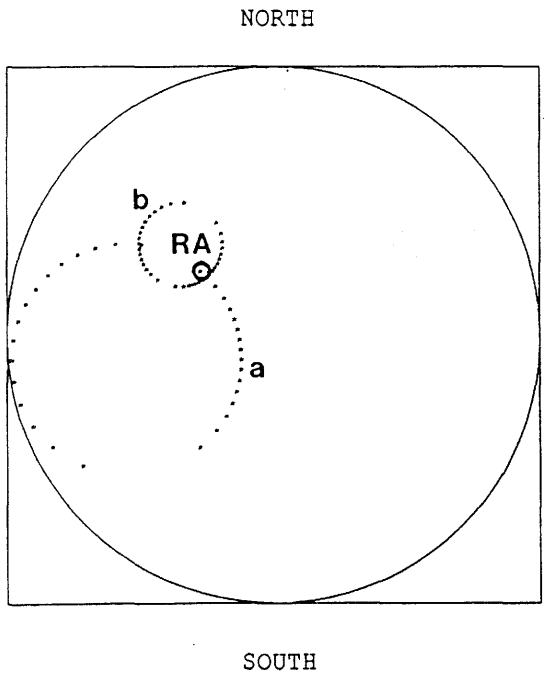

Figure 6.1 (continued) Possible orientations of the normal of Zone RA based on the data listed in Table 6.1. The data are presented in a Wulff projection. The predicted Zone GA is plotted as a single point in all diagrams.

6.2.2 Zone RB

Zone RB is nearly parallel to RA but located about 50 m SE of RA. RB was clearly seen in the attenuation tomograms for the sections N2-N3-N4 and N2-N4 during Stage I. In this region between N3 and N4 and close to RB a complex ringshaped structure (RQ) could be observed in the attenuation tomograms. The appearance of the structure is identical in the tomograms from W1-C2 and C1-C2. Actually, the one in W1-C2 fits perfectly with the feature RQ as the plane W1-C2 intersects the N3-N4 plane in that region.

The reason for the displacement between the slowness and attenuation anomalies is currently not well understood. The slowness anomaly directly corresponds to the variations in dielectric constant, which is expected to depend on the water content (porosity). Increased attenuation can be expected both from increased water content and the presence of conductive minerals. One possible explanation could be that the slowness anomaly represents regions of increased fracturing leading to significant increases in porosity. The attenuation anomaly can possibly be caused by alteration and formation of clay minerals at the sides of the fracture zone. If this explanation is correct high permeabilities would be expected near the slowness anomaly (in the centre of the ring). This structure was also discussed in Olsson, Eriksson, Falk and Sandberg, 1988, Chapter 8. The D-holes were drilled to intersect this structure and it is characterized as a vuggy granite with high porosity i.e. 5-10% (Stripa Quarterly Report, Jan-March, 1989).

The single hole reflections observed from zone RB belonged to the most prominent ones in boreholes N2 and N3 without being particularly strong. The reflection observed in N4 was relatively weak and it might be considered uncertain whether zone RB continues all the way to N4. It is likely that the zone ends or changes character significantly in connection with the ringshaped structure (RQ) described above. The reflections associated with RB are prominent in C1 and C3. In C2 the intersection angle should be about 80° which is difficult to detect in single hole reflection mode. C2 has therefore not been used for the interpretation of RB.

In the reflection measurements RB is most prominent in the D-holes at a depth of 80-85 m where at least two parallel and very strong reflexions of equal angle, strength and extent intersect the borehole. They are strong also at larger distances from the

borehole but end fairly abruptly at a distance of about 25 m.

In the W1-W2 tomograms RB was seen as a series of connected patches during Stage I. This behaviour of RB is also obtained in the W1-C2 and the C1-C2 tomograms. RB is very hard to follow, especially close to borehole C2. In the attenuation tomogram from W1-C2 RB seems to end with the RQ feature and does not intersect C2. In the attenuation tomogram from C1-C2 RB again seems to end after the circular feature close to C1 without intersecting C2.

The spread in the data is quite small and the orientation of the zone is determined with a high degree of confidence. The strike of the zone is N40°E and it is dipping 40° to SE. When determining the average orientation of the zone more weight has been given to intersection data than to reflection data.

RB was considered as one of the more prominent zones at the SCV-site. The interpretation made in the Stage III together with the predictions made in the Stage I confirms the existence and orientation of zone RB.

Table 6.2 Data used in the interpretation of Zone RB. The possible orientations of the normal of Zone RB given by the restrictions defined by each data value is plotted in Figure 6.2.

Intersections with the "boundary boreholes" based on radar data:

Intersection with:	
	C1 94 m
	C2 -
	C3 110 m
	D1 80 m
	W1 140 m

Figure 6.2a:
Intersections:

C1 94 m -- C3 110 m	(a)
C3 110 m -- D1 80 m	(b)
C1 94 m -- D1 80 m	(c)
W1 140 m -- C3 110 m	(d)
W1 140 m -- D1 80 m	(e)
W1 140 m -- C1 94 m	(f)

Figure 6.2b:
Radar intersection angles:

C1 60°	(a)
C2 -	
C3 50°	(b)
D1 35°	(c)
W1 35°	(d)

Figure 6.2c:
Radar azimuth angles:

C1 60°	(a)
C2 -	
C3 30°	(b)
D1 30°	(c)
W1 40°	(d)

Orientation of Zone GB: N040°E/40°S

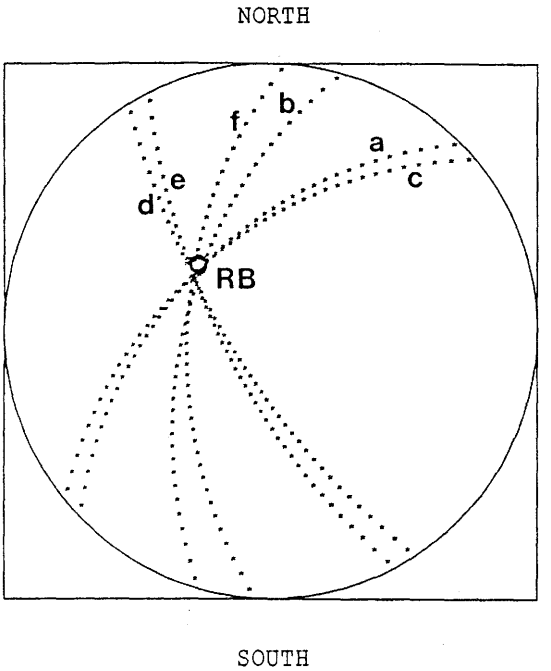

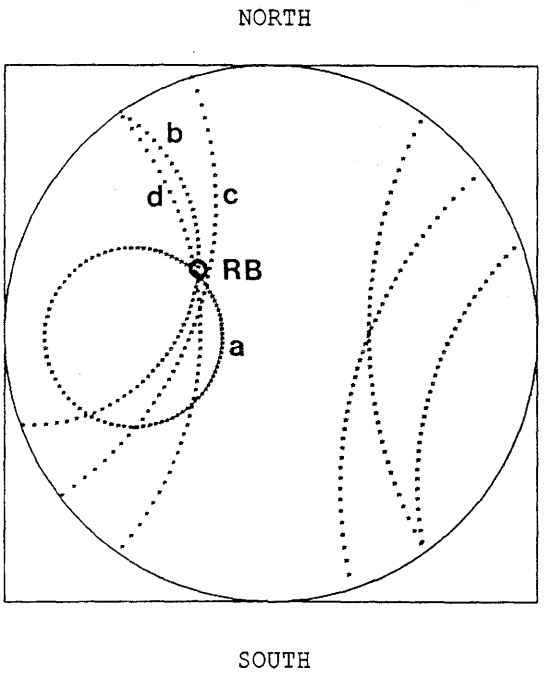

Figure 6.2 Possible orientations of the normal of Zone RB based on the data listed in Table 6.2. The data are presented in a Wulff projection. The predicted Zone GB is plotted as a single point in all diagrams.

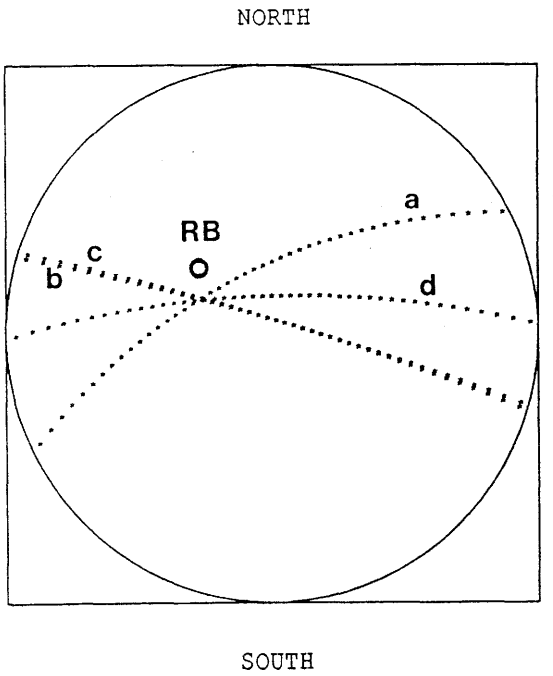

Figure 6.2 (continued) Possible orientations of the normal of Zone RB based on the data listed in Table 6.2. The data are presented in a Wulff projection. The predicted Zone GB is plotted as a single point in all diagrams.

6.2.3 Zone RH

Zone RH was clearly seen in all W1-W2 tomograms where it extends in a northerly direction almost perpendicular to the boreholes. This zone was during Stage I characterized by a spatial displacement of the attenuation and slowness anomalies. This indication of a displacement is only obtained in the W1-C2 section close to W1 where the zone seems to be separated into two parts. The reason is probably that RH is separated in the W1-W2 plane, but seems to change with the depth into one major zone containing a set of parallel fractures.

Zone RH is clearly seen in all Stage III tomograms and boreholes as major zone. The tomograms show that the zone is about 10-15 m wide, it is undulating and not quite plane. There is a relative displacement of the slowness and amplitude anomalies in the tomograms which is considered to represent true variations of physical properties in this part of the rock.

The reflexions associated with zone RH in the single hole measurements are generally strong. The zone was clearly seen during Stage I as a reflector nearly parallel to boreholes N2 and N3. In the C and D-holes clear reflexions are obtained from the zone RH, often as several parallel reflexions.

The intersection of the zone with boreholes W1 and W2 suggested a strike which was essentially N-S. The dip was more difficult to determine from the Stage I reflection data, but the intersection with the C and D-holes gives an accurate dip of 60° which was in very good agreement with the predicted dip. The zone also intersects the access drift to the 3D-migration site and the access drift to the 385 m level validation drift where it can be observed directly.

Zone RH is considered to be a major feature and its existence very well established. The zone was during Stage I associated with a slowness anomaly surrounded by an attenuation anomaly, which indicated that the boundaries of the zone had different character compared to the center of the zone. This behaviour is not seen in the deeper part below the W-holes i.e. W1-C1, W1-C2 and C1-C2 sections and it is therefore likely that the zone is separated into two zones at shallower depths in the mine, i.e. in the W1-W2 plane.

Table 6.3 Data used in the interpretation of Zone RH. The possible orientations of the normal of Zone RH given by the restrictions defined by each data value is plotted in Figure 6.3.

Intersections with the "boundary boreholes" based on radar data:

Intersection with:		
	C1	50 m
	C2	64 m
	C3	54 m
	D1	21 m
	W1	51 m

Figure 6.3a:
Intersections:

C1	50 m	--	C2	64 m	(a)
C2	64 m	--	C3	54 m	(b)
C3	54 m	--	D1	21 m	(c)
C2	64 m	--	D1	21 m	(d)
W1	51 m	--	C3	54 m	(e)
W1	51 m	--	D1	21 m	(f)
W1	51 m	--	C2	64 m	(g)

Figure 6.3b:
Radar intersection angles:

C1	-	
C2	60°	(a)
C3	70°	(b)
D1	60°	(c)
W1	70°	(d)

Figure 6.3c:
Radar azimuth angles:

C1	-	
C2	120°	(a)
C3	130°	(b)
D1	165°	(c)
W1	165°	(d)

Figure 6.3d:
Crosshole reflection data:

Moving position	Fix position	Slope	
C1 41 m	C2 141.4	270	(a)
C2 62.5 m	C1 144.4	241	(b)

Orientation of Zone GH: N355°E/60°E

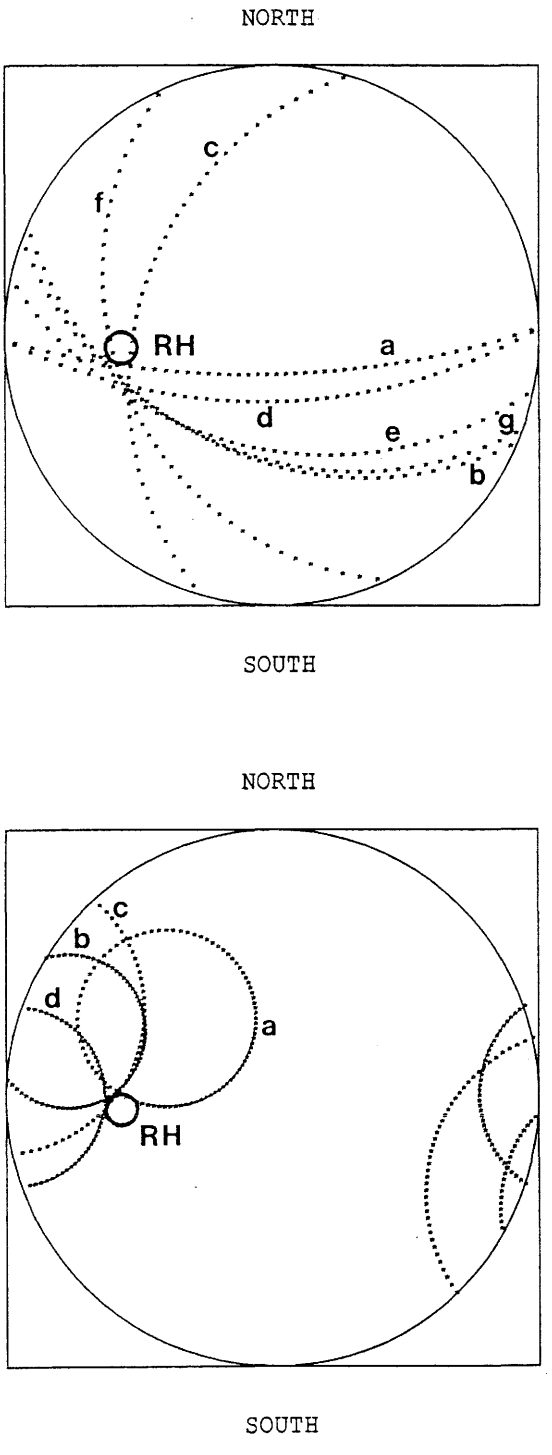

Figure 6.3 Possible orientations of the normal of Zone RH based on the data listed in Table 6.3. The data are presented in a Wulff projection. The predicted Zone GB is plotted as a single point in all diagrams.

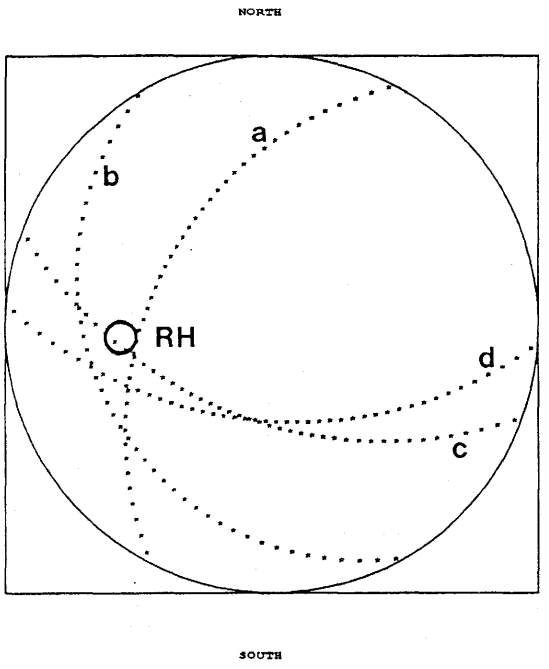

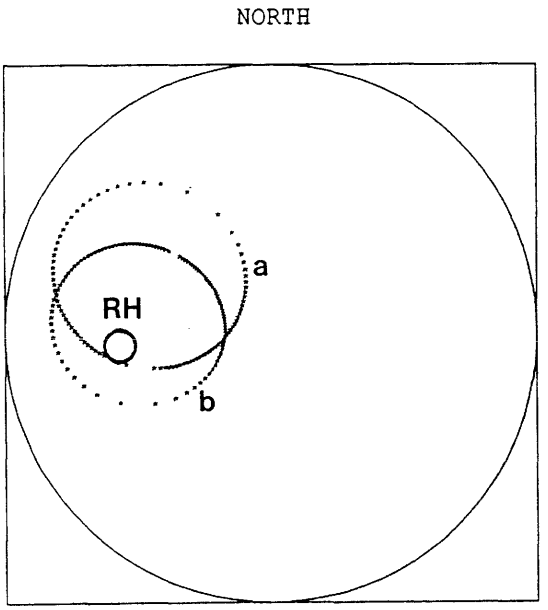

Figure 6.3 (continued) Possible orientations of the normal of Zone RH based on the data listed in Table 6.3. The data are presented in a Wulff projection. The predicted Zone GB is plotted as a single point in all diagrams.

6.2.4 Zone RC

The clearest identification of Zone RC was obtained in the attenuation tomogram of the borehole section N2-N3-N4. The feature appeared to be essentially straight with a few patches of increased attenuation (fracturing). The zone is associated with relatively weak reflexions except in borehole N4, where the reflexion is somewhat stronger. In the W1-W2 attenuation tomograms there is a weak indication of the zone which partly coincides with the artifact caused by a part of the 3-D migration drift.

The zone is orientated essentially parallel to RA and RB. The single hole reflection and intersection data are fairly consistent and suggest that the zone is striking 40° and dipping 35° as predicted (Figure 6.4). The location in C2 (32 m) differs by 7 m from the predicted position (25 m) which changes the dip. The directional antenna data give a large scatter in orientation. Considering this discrepancy in the data set and that the location is poorly defined in both Stage I and Stage III the existence of this zone must be considered uncertain.

Table 6.4 Data used in the interpretation of Zone RC. The possible orientations of the normal of Zone RC given by the restrictions defined by each data value is plotted in Figure 6.4.

Intersections with the "boundary boreholes" based on radar data:

Intersection with:		
	C1	30 m
	C2	32 m
	C3	38 m
	D1	- m
	W1	49 m

Figure 6.4a:
Intersections:

C1	30 m	C2	32 m	(a)
C1	30 m	C3	38 m	(b)
C2	32 m	C3	38 m	(c)
W1	49 m	C1	30 m	(d)
W1	49 m	C2	32 m	(e)
W1	49 m	C3	38 m	(f)

Figure 6.4b:
Radar intersection angles:

C1	55°	(a)
C2	60°	(b)
C3	30°	(c)
D1	-	
W1	35°	(d)

Figure 6.4c:
Radar azimuth angles:

C1	30°	(a)
C2	105°	(b)
C3	-	
D1	-	
W1	90°	(c)

Figure 6.4d:
Crosshole reflection data:

Moving position	Fix position	Slope	
C1 37 m	C2 141.4	287	(a)

Orientation of Zone GC: N040°E/35°E

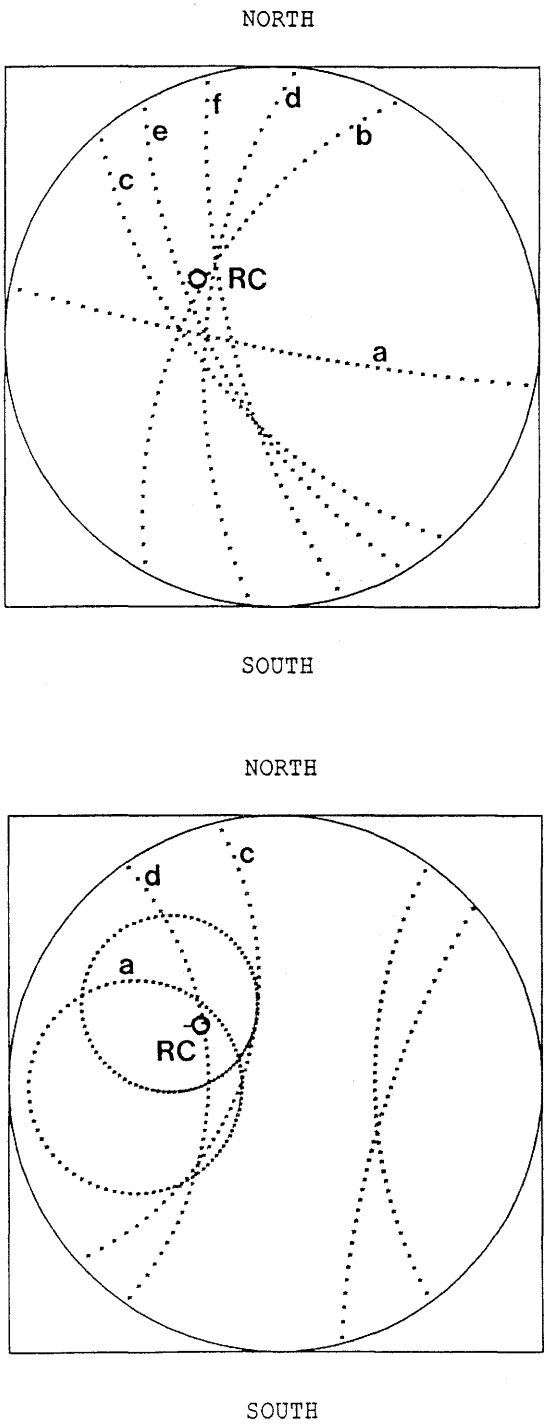

Figure 6.4 Possible orientations of the normal of Zone RC based on the data listed in Table 6.4. The data are presented in a Wulff projection. The predicted Zone GC is plotted as a single point in all diagrams.

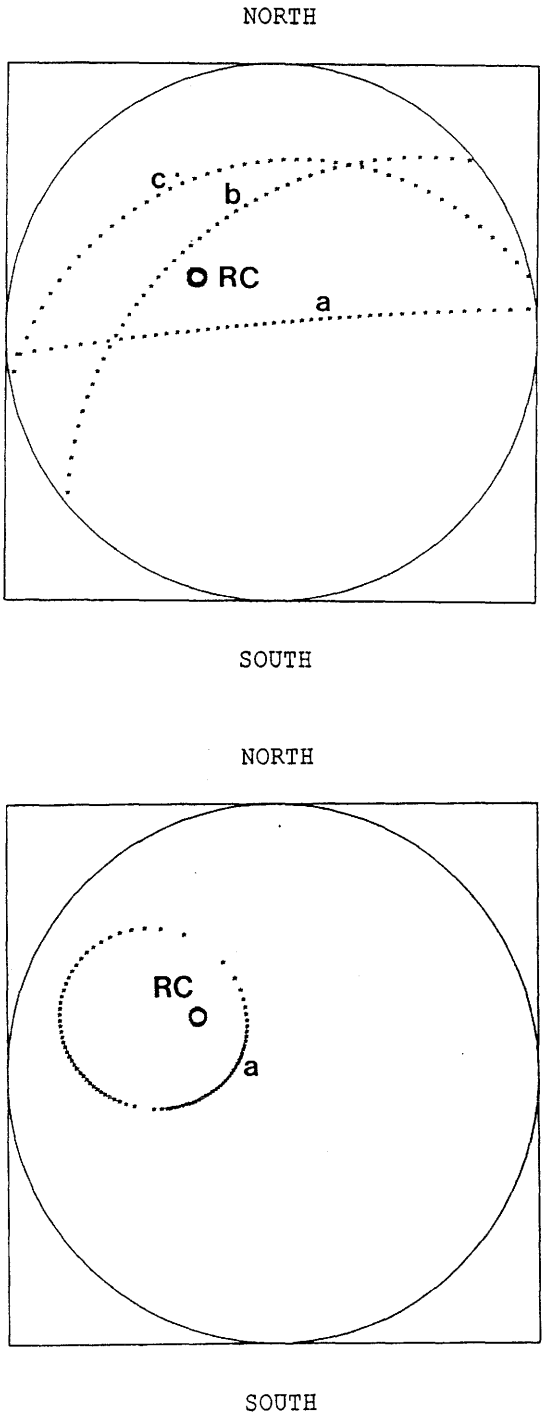

Figure 6.4 (continued) Possible orientations of the normal of Zone RC based on the data listed in Table 6.4. The data are presented in a Wulff projection. The predicted Zone GC is plotted as a single point in all diagrams.

6.2.5 Zone RI

The preliminary results from N2, N3, and N4 indicated in addition to RH several reflectors with an orientation nearly parallel to the boreholes. These reflectors may indicate that there are additional features with an orientation similar to RH. One such reflector was identified and associated with data from the W1-W2 plane. It is seen weakly in the radar tomograms from the W1-W2 section. This feature was termed GI (RI in this report) and it was not included in the original interpretations of the radar and seismic data. The lateral extent of GI was estimated from the N4 radar reflection data. A parallel reflection was observed in the borehole interval 50 to 200 m and the extent in the north-south direction was estimated to be at least 150 m.

RI is also observed as a fairly strong radar reflex from all C-holes and also the D-holes (particularly strong in D3 and D4). The intersections with the C and D-holes give a well defined orientation striking 345° and dipping 10° steeper than RH, i.e. 70°. The radar intersection angles indicate a strike which may be essentially the same but a steeper dip (≈80-90°) and the directional antenna azimuth angle indicate both solutions. The steep dip is mainly determined from D1.

In the tomograms one can observe anomalies close to the boreholes at the locations where RI is predicted but in all tomograms e.g. C1-C2, W1-C1 and W1-C2, there are no continuous anomalies extending between the boreholes.

Considering the discrepancies between the intersection and azimuth angles and that the accuracy is poor both in Stage I and Stage III, the existence of this zone must be considered uncertain. However, the intersections in the C and D-holes is in good agreement with the predictions.

Table 6.5 Data used in the interpretation of Zone RI. The possible orientations of the normal of Zone RI given by the restrictions defined by each data value is plotted in Figure 6.5.

Intersections with the "boundary boreholes" based on radar data:

Intersection with:		
	C1	107 m
	C2	149 m
	C3	113 m
	D1	95 m
	W1	109 m

Figure 6.5a:
Intersections:

C1 107 m -- C2 149 m	(a)
C1 107 m -- C3 113 m	(b)
C1 107 m -- D1 95 m	(c)
C2 149 m -- C3 113 m	(d)
C2 149 m -- D1 95 m	(e)

Figure 6.5b:
Intersections with W1:

W1 109 m -- C1 107 m	(a)
W1 109 m -- C2 149 m	(b)
W1 109 m -- C3 113 m	(c)
W1 109 m -- D1 95 m	(d)

Figure 6.5c:
Radar intersection angles:

C1 48°	(a)
C2 32°	(b)
C3 42°	(c)
D1 60°	(d)
W1 70°	(e)

Figure 6.5d:
Radar azimuth angles:

C1 -	
C2 120°	(a)
C3 30°	(b)
D1 120°	(c)
W1 30°	(d)

Orientation of Zone GI: N345°E/70°E

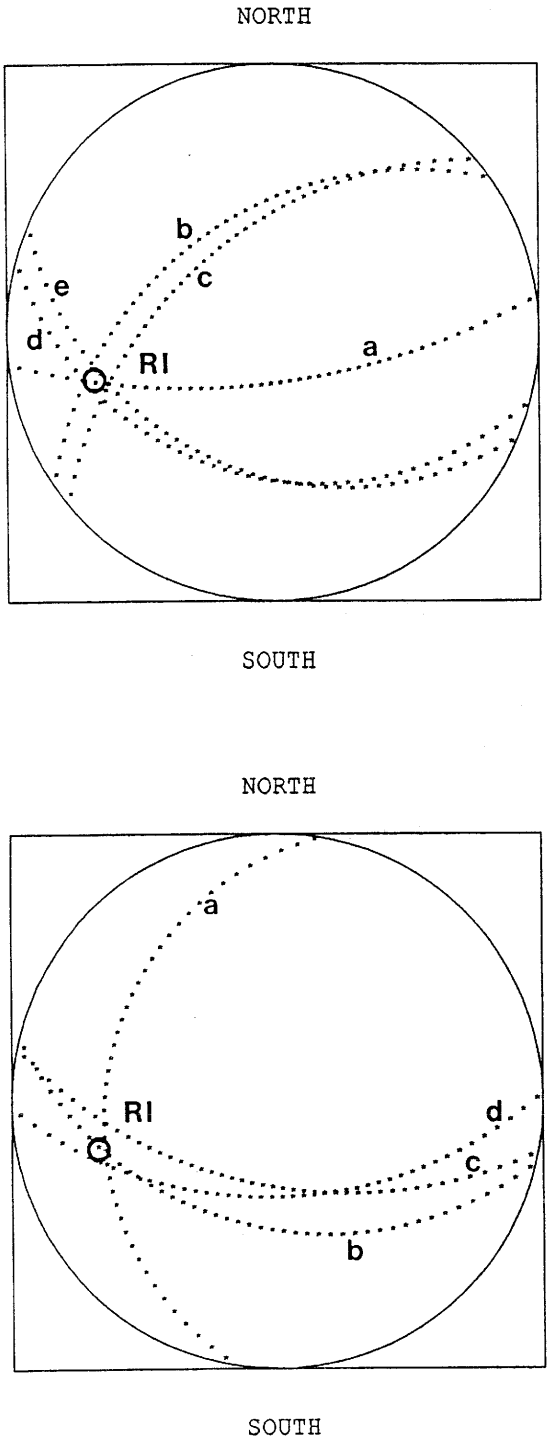

Figure 6.5 Possible orientations of the normal of Zone RI based on the data listed in Table 6.5. The data are presented in a Wulff projection. The predicted Zone GI is plotted as a single point in all diagrams.

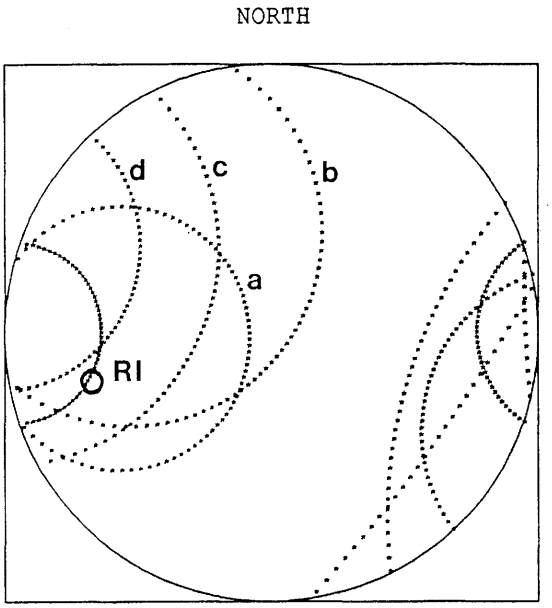

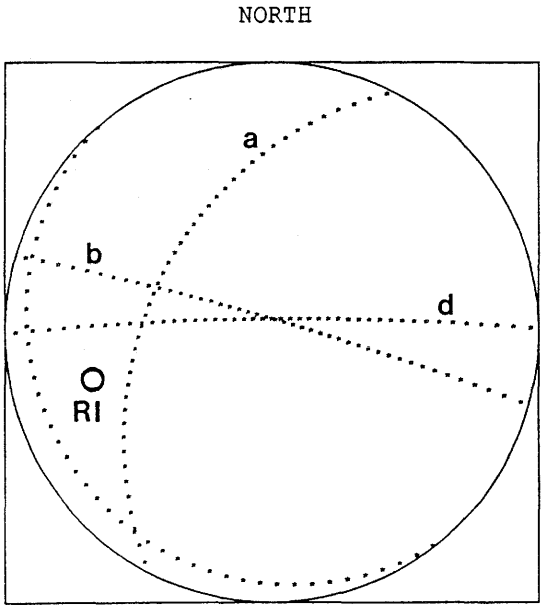

Figure 6.5 (continued) Possible orientations of the normal of Zone RI based on the data listed in Table 6.5. The data are presented in a Wulff projection. The predicted Zone GI is plotted as a single point in all diagrams.

7 DISCUSSION

In this discussion we compare the results from the Stage III investigations with the conceptual model. In the conceptual model the zones are named GA, GB, GC, GH and GI. In this report, the names used are RA, RB, RC, RH and RI to emphasize that the interpretation is based on radar data. The feature RQ is not found by any other method and exists only with the name RQ.

The location of the features identified from the radar data is displayed in three different planes; the plane defined by boreholes W1-C1 (Figure 7.1), by boreholes W1-C2 (Figure 7.2) and by boreholes C1-C2 (Figure 7.3).

The interpretation within the SCV-project, Stage III, is in good agreement with predictions. The zones GA, GB, and GH are considered to be major features while the existence of zones GC and GI is considered uncertain and if they exist they are of smaller magnitude. The zones can also be grouped according to their orientation. Three zones have a northeasterly strike (≈N40°E) and a dip of approximately 40° to the South, namely GA, GB and GC. The zones GH and GI strike NNW and have a steep dip (60°) to the East. The angle between planes in the two sets is thus about 50°. This is in fair agreement with theoretical prediction. The orientation of the major zones is different compared to the results found at the Crosshole Site where there were two sets of features with the orientations N225°E/75°N and N010°E/65°E.

At the SCV-site the magnitude of the reflections and anomalies is generally very small and there are many relatively small reflections and weak anomalies. This is an indication that the structure of the rock at the SCV-site is complex. The features observed in the tomograms are more complex and they appear to be "patchy".

Zone GA and GB have been found to be almost parallel and of equal magnitude. Their existence and orientations are considered to be well established even if they sometimes seem to vary in different areas. GA and GB also extend over a relatively large distance i.e. 100-150 m. The orientations of GA and GB are not as accurately determined as one would expect, in particular GA suffers because it is located at the corner of the SCV-site and does not intersect all boreholes. The orientation of GH which is the most prominent zone within the SCV-site, is determined with fairly high accuracy. In the

tomograms GH is clearly seen both in the attenuation and slowness tomograms. The reflections from the zone are prominent as well as the anomalies in the tomograms.

The minor zones GI and GC did not fully agree with the predictions. The intersection and azimuth angles and the accuracy is poor both in Stage I and Stage III. The orientation and also the existence of these zones must be considered uncertain. If one only considers the intersections of GI in the C and D-holes and of GC in the N-holes, they are in good agreement with the Stage I predictions.

An extraordinary feature found in the attenuation tomograms is the circular structure, RQ, located between boreholes N3 and N4. This feature was found in the two attenuation tomograms from the borehole section N3-N4 and in the borehole section N2-N4. RQ has also been found in the W1-C2 tomogram at exactly the same place as between N3 and N4. These two planes intersect in the interesting area and RQ is clearly seen as a circle in the W1-C2 attenuation tomogram and as a single black anomaly in the slowness tomogram.

The D-holes were later drilled through this region. It was then discovered that the structure consists of an extremely porous granite (5-10% porosity) probably created by gas inclusion at the formation of the granite. Similar porous structures have previously been observed at the Crosshole Site (zone B in borehole F1 and F2) (Olsson, Falk, Forslund, Lundmark and Sandberg, 1987; Olsson, Black, Cosma and Pihl, 1987).

The circular feature, RQ, is located close to GB and it is anticipated that the zone GB at least partly consists of the same type of porous rock. This idea is supported by the fact that a circular feature is also found in the C1-C2 tomogram close to the predicted position of GB. The feature RQ is remarkable because the circular shape is only evident in the attenuation tomograms, while the slowness tomograms show an anomaly in the center of the structure.

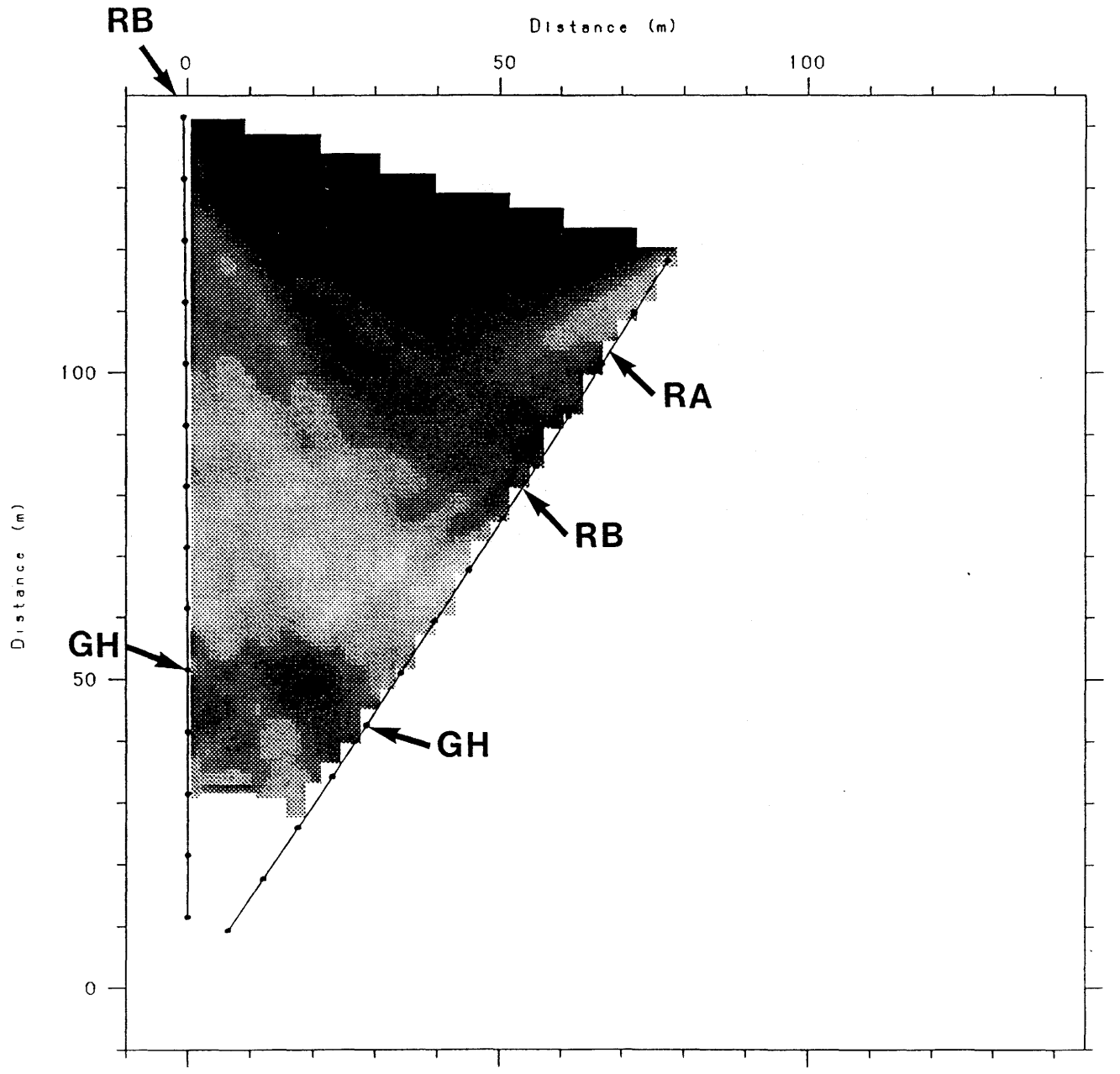

Figure 7.1 Residual attenuation tomogram (60 MHz) for the plane defined by the boreholes W1-C1. The location of the major features included in the radar model of the SCV-site are indicated.

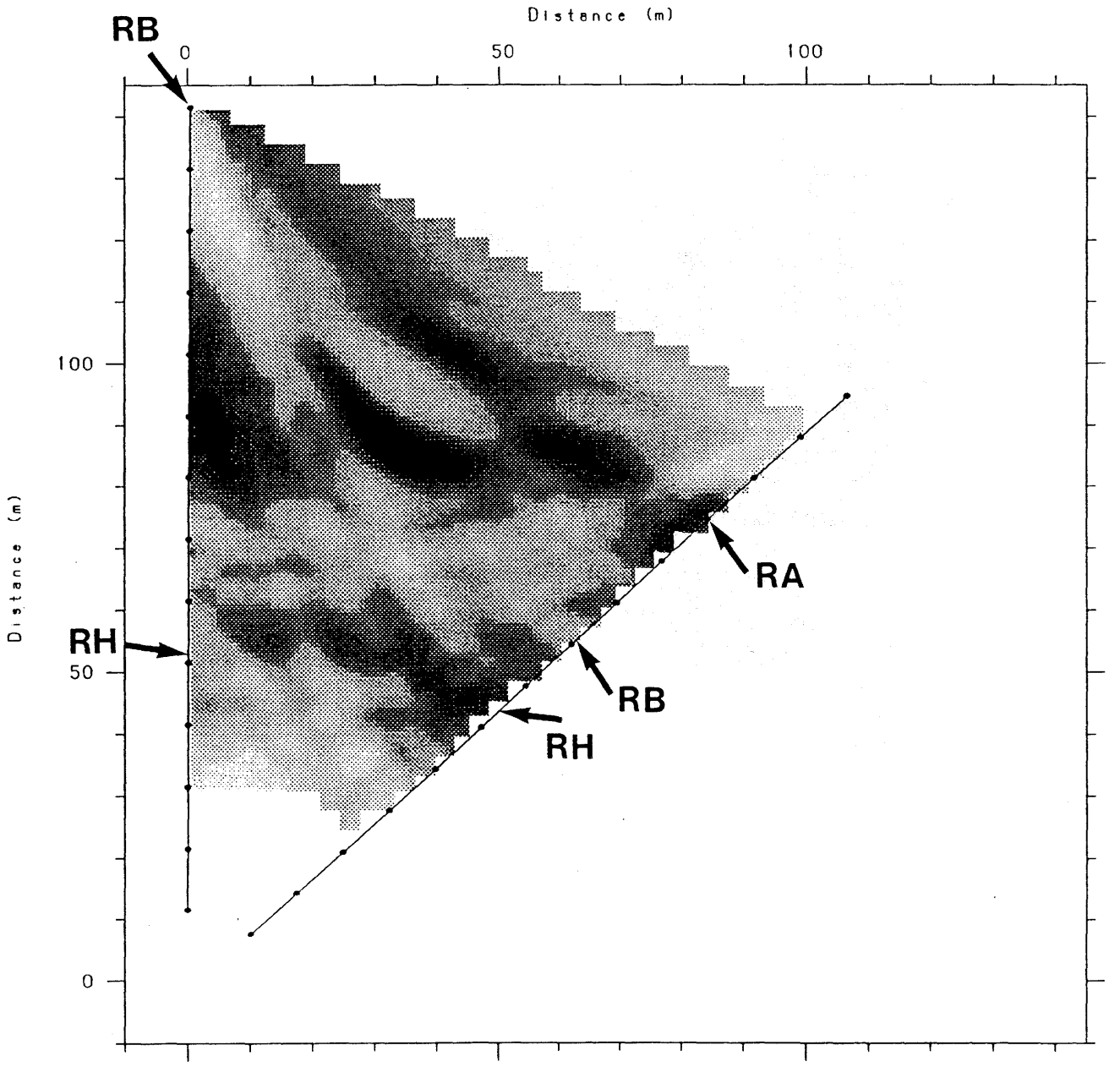

Figure 7.2 Residual attenuation tomogram (60 MHz) for the plane defined by the boreholes W1-C2. The location of the major features included in the radar model of the SCV-site are indicated.

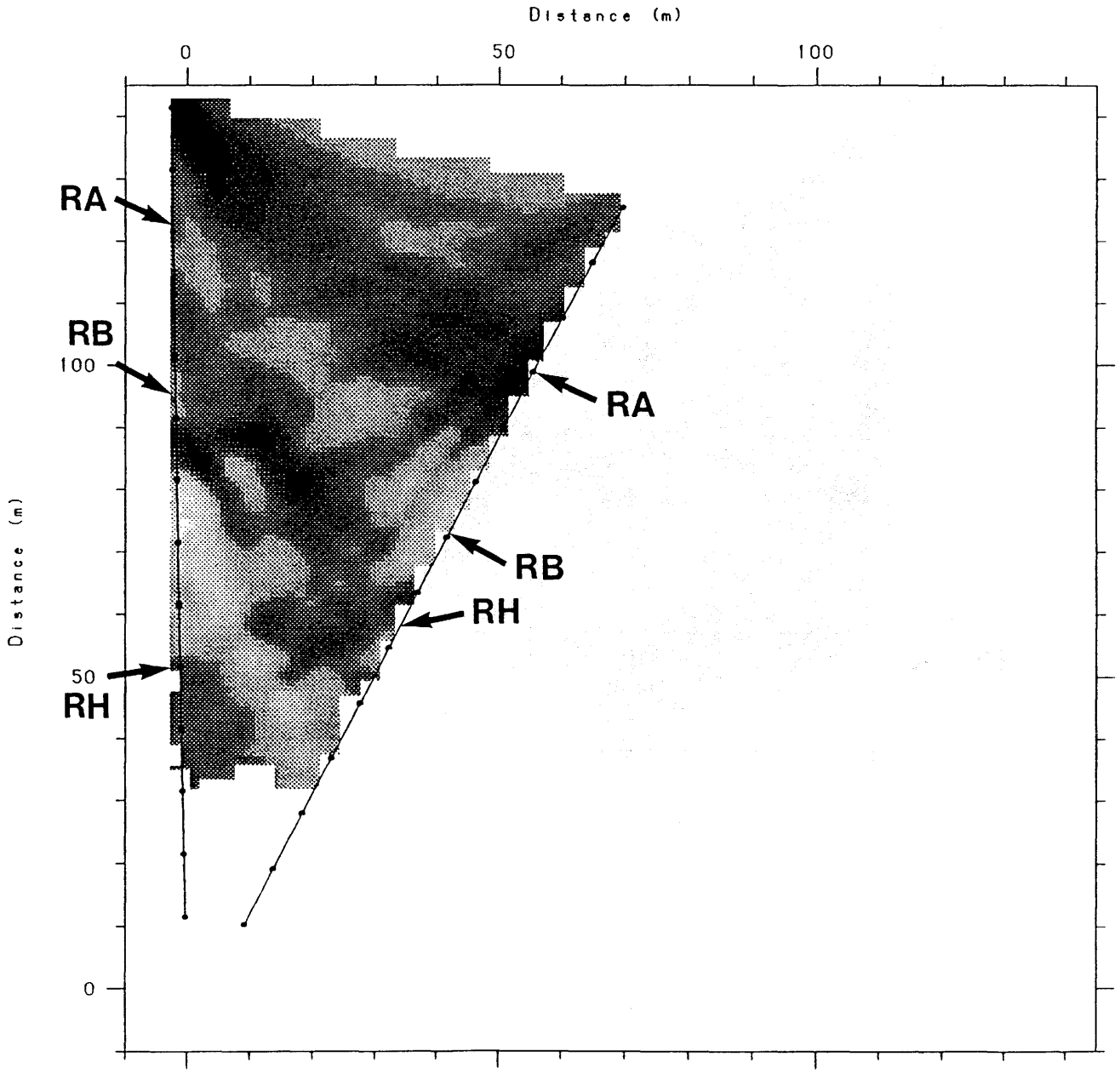

Figure 7.3 Residual attenuation tomogram (60 MHz) for the plane defined by the boreholes C1-C2. The location of the major features included in the radar model of the SCV-site are indicated.

8 ACKNOWLEDGEMENT

Ove Persson participated in making the bulk of the field measurements. Ove Persson and Georg Gabriel made the processing of the reflection data and prepared the radar reflection maps.

The assistance given by the personnel at the Stripa Mine during the field work has been of great value to the project.

9 REFERENCES

Andersson, P., Andersson, P., Gustavsson, E., Olsson, O., 1989. Investigation of Flow Distribution in a Fracture Zone, using the Radar Method, Results and Interpretation. SKB-report TR 89-xx (in press), SKB, Stockholm, Sweden.

Fridh, B., 1988. Site Characterization and Validation - Geophysical single hole logging. Stripa Project IR 88-17, SKB, Stockholm, Sweden.

Ivansson, S., 1984. Crosshole investigations - Tomography and its application to crosshole seismic measurements. Stripa Project IR 84-08, SKB, Stockholm, Sweden.

Ivansson, S., Hammarström, M., Pihl, J., 1987. Tomographic calculations for synthetic data. NAGRA, Baden, Switzerland.

Niva, B., Olsson, O., 1988. Radar Crosshole Tomography at the Grimsel Test Site - Results from phase 3. NAGRA, Baden, Switzerland.

Olsson, O., Black, J., Cosma, C., Pihl, J., 1987. Crosshole Investigations - Final Report. Stripa Project TR 87-16, SKB, Stockholm, Sweden.

Olsson, O., Falk, L., Forslund, O., Lundmark, L., Sandberg, E., 1987. Crosshole investigations - Results from borehole radar investigations. Stripa Project TR 87-11, SKB, Stockholm, Sweden.

Olsson, O., Eriksson, J., Falk, L., Sandberg, E., 1988. Site Characterization and Validation - Borehole Radar Investigations, Stage I. Stripa Project TR 88-03, SKB, Stockholm, Sweden.

Olsson, O., Black, J. H., Gale, J. E., Holmes, D. C., 1988. Site Characterization and Validation Stage 2 - Preliminary Predictions. Stripa Project TR 89-03, SKB, Stockholm, Sweden.

Olsson, O., Gale, J., Barton, N., Holmes, D., Sehlstedt, M., Ramqvist, G., 1989. Site Characterization and Validation. Stripa Project Quarterly Report July-Sept 88, SKB, Stockholm, Sweden.

Olsson, O., Holmes, D., Barton, N., Black, J., 1989. Site Characterization and Validation. Stripa Project Quarterly Report Jan-March 89, SKB, Stockholm, Sweden.

Pihl, J., Hammarström, M., Ivansson, S., Morén, P., 1987. Crosshole Investigations -Results from Seismic Borehole Tomography. Stripa Report IR 87-06, SKB, Stockholm, Sweden.

10 APPENDIX A

LIST OF RADAR REFLECTION MEASUREMENTS

Figure A.1 Radar reflection map from the borehole C1 measured with a centre frequency of 22 MHz. Dipole antenna and bandpass filter.

Figure A.2 Radar reflection map from the borehole C2 measured with a centre frequency of 22 MHz. Dipole antenna and bandpass filter.

Figure A.3 Radar reflection map from the borehole C3 measured with a centre frequency of 22 MHz. Dipole antenna and bandpass filter.

Figure A.4 Radar reflection map from the borehole C1 measured with a centre frequency of 60 MHz. Directional antenna and bandpass filter. Dipole component.

Figure A.5 Radar reflection map from the borehole C2 measured with a centre frequency of 60 MHz. Directional antenna and bandpass filter. Dipole component.

Figure A.5 Radar reflection map from the borehole C2 measured with a centre frequency of 60 MHz. Directional antenna and bandpass filter. Direction 0°.

Figure A.6 Radar reflection map from the borehole C2 measured with a centre frequency of 60 MHz. Directional antenna and bandpass filter. Direction 30°.

Figure A.7 Radar reflection map from the borehole C2 measured with a centre frequency of 60 MHz. Directional antenna and bandpass filter. Direction 60°.

Figure A.8 Radar reflection map from the borehole C2 measured with a centre frequency of 60 MHz. Directional antenna and bandpass filter. Direction 90°.

Figure A.9 Radar reflection map from the borehole C2 measured with a centre frequency of 60 MHz. Directional antenna and bandpass filter. Direction 120°.

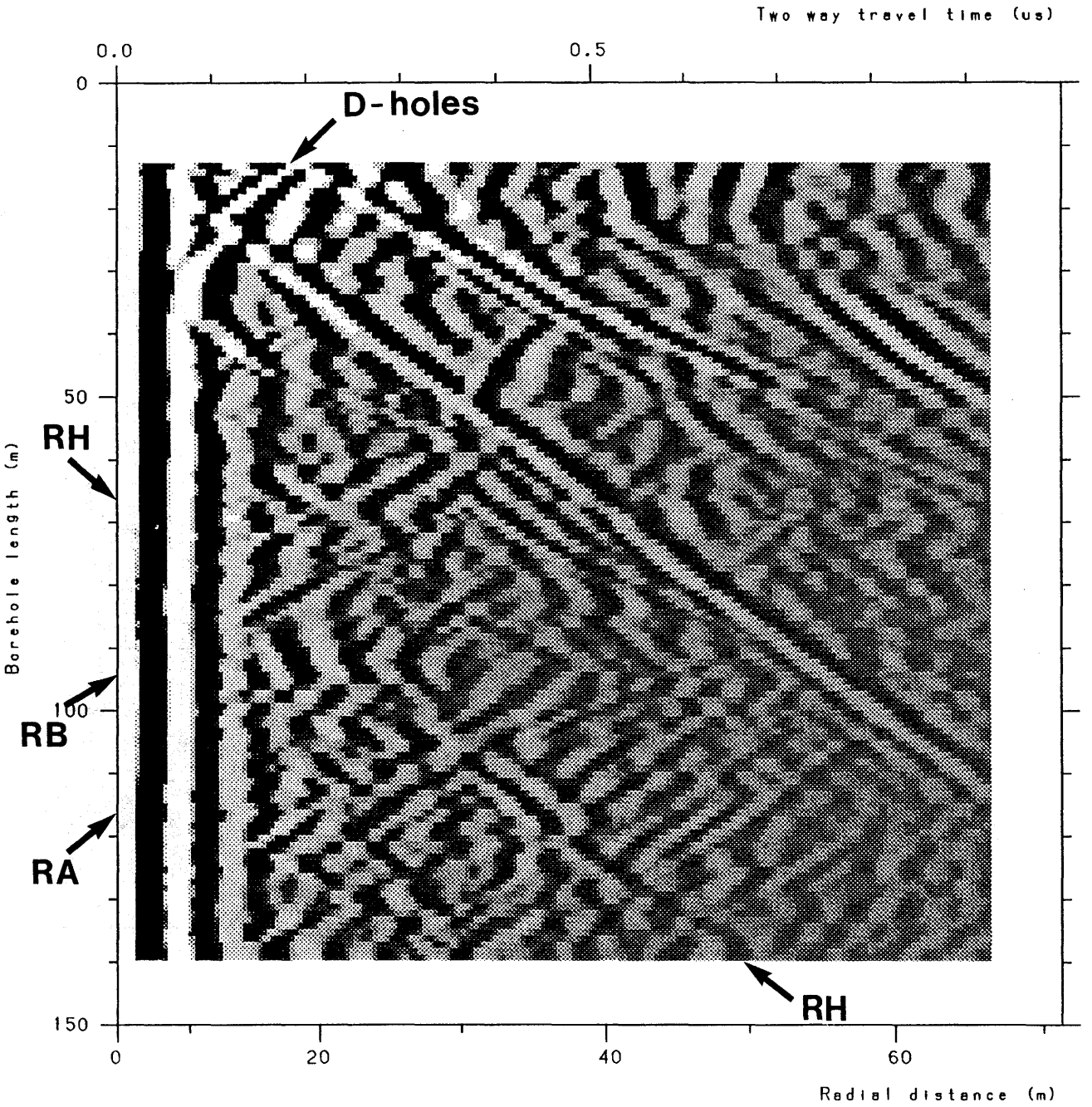

Figure A.1 Radar reflection map from the borehole C1 measured with a centre frequency of 22 MHz. Dipole antenna and bandpass filter.

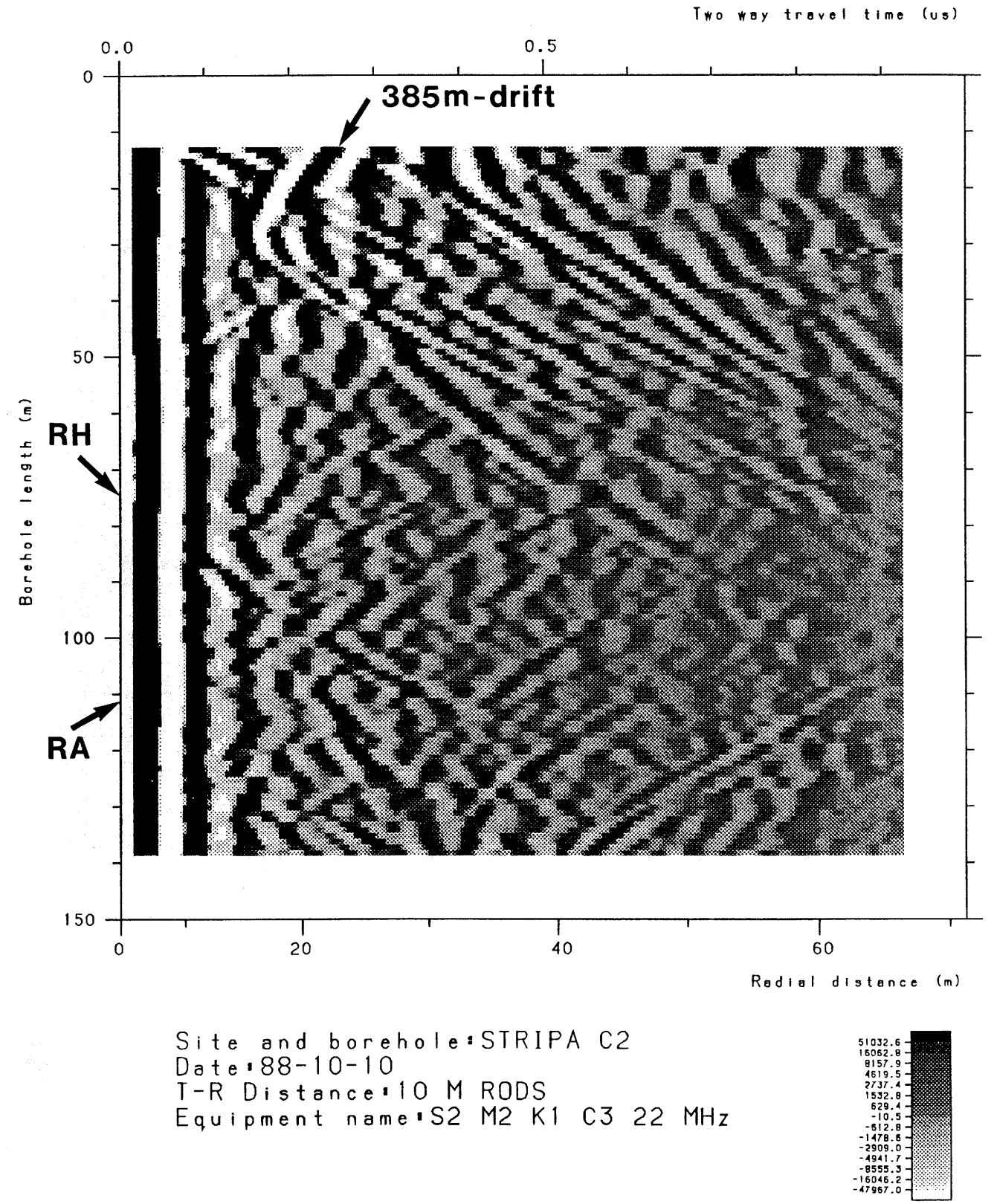

Figure A.2 Radar reflection map from the borehole C2 measured with a centre frequency of 22 MHz. Dipole antenna and bandpass filter.

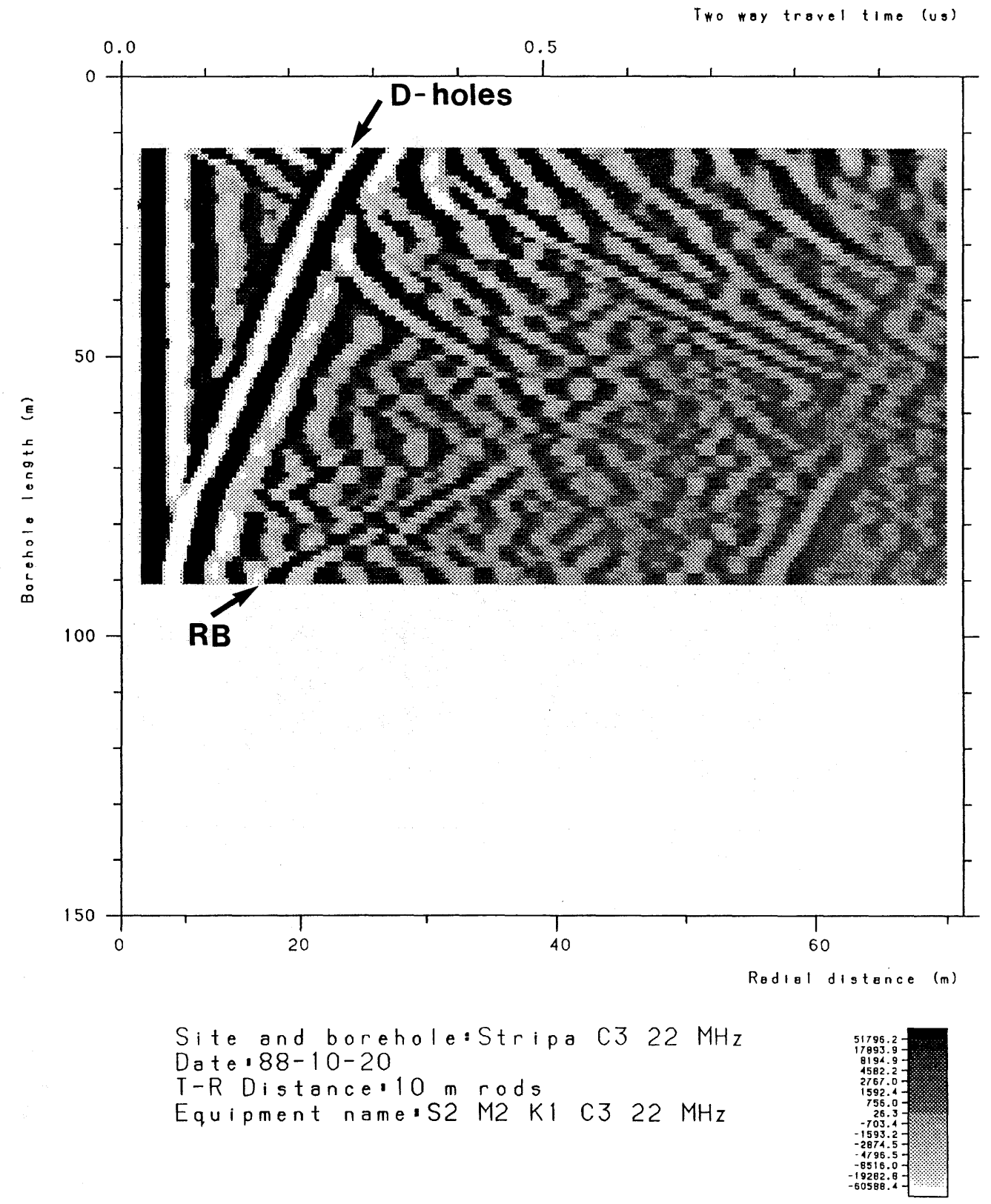

Figure A.3 Radar reflection map from the borehole C3 measured with a centre frequency of 22 MHz. Dipole antenna and bandpass filter.

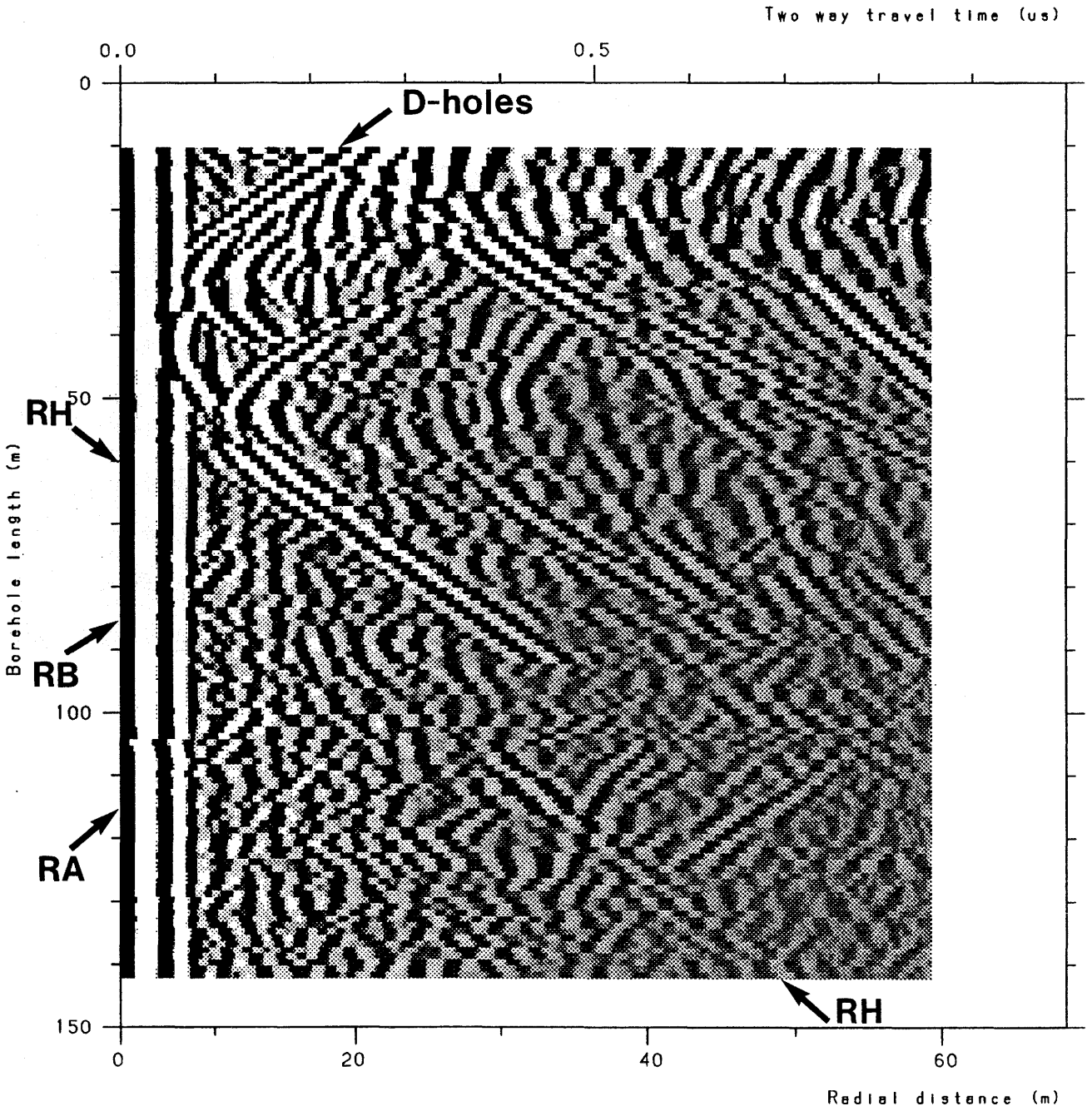

Figure A.4 Radar reflection map from the borehole C1 measured with a centre frequency of 60 MHz. Directional antenna and bandpass filter. Dipole component.

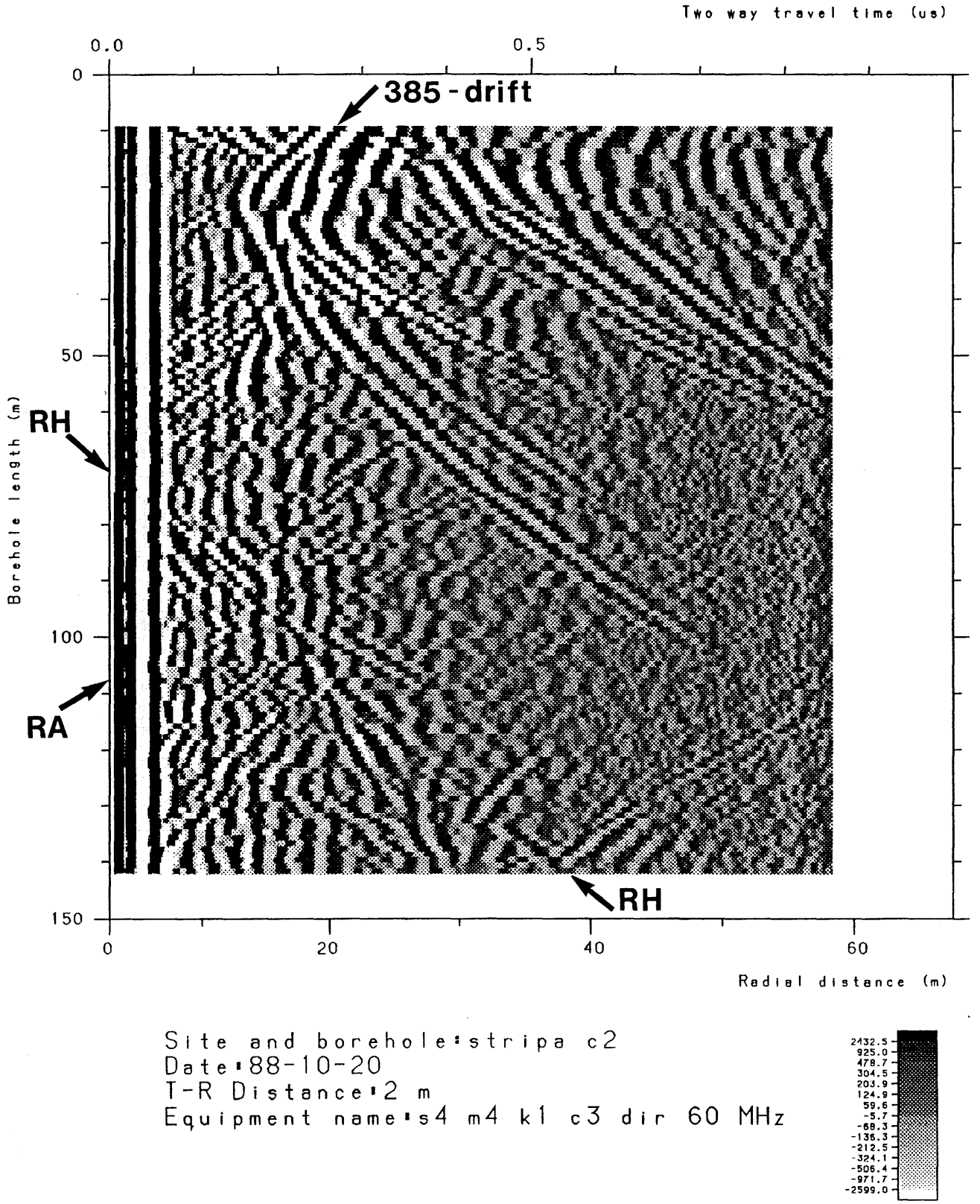

Figure A.5 Radar reflection map from the borehole C2 measured with a centre frequency of 60 MHz. Directional antenna and bandpass filter. Dipole component.

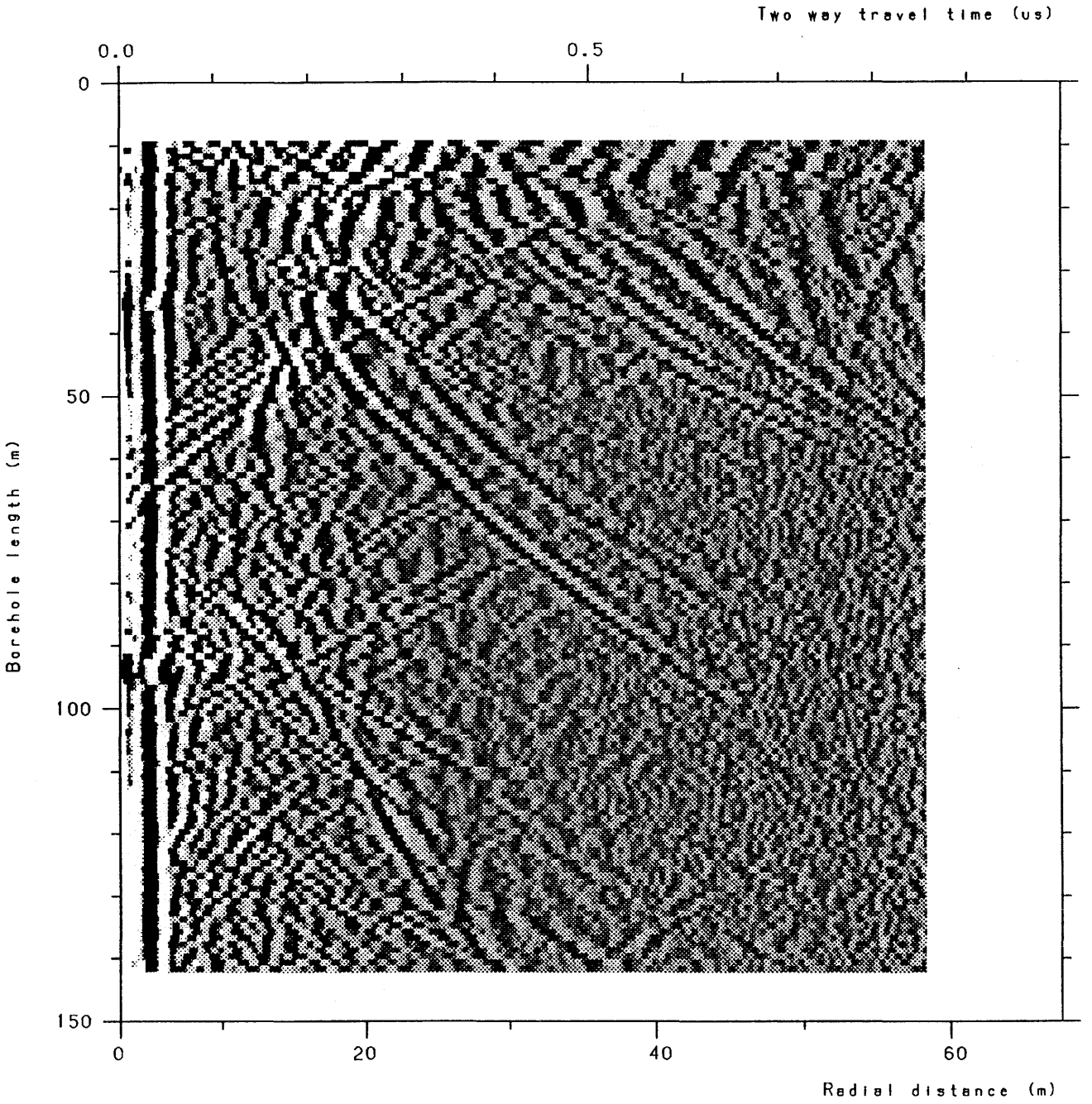

Figure A.5 Radar reflection map from the borehole C2 measured with a centre frequency of 60 MHz. Directional antenna and bandpass filter. Direction 0°.

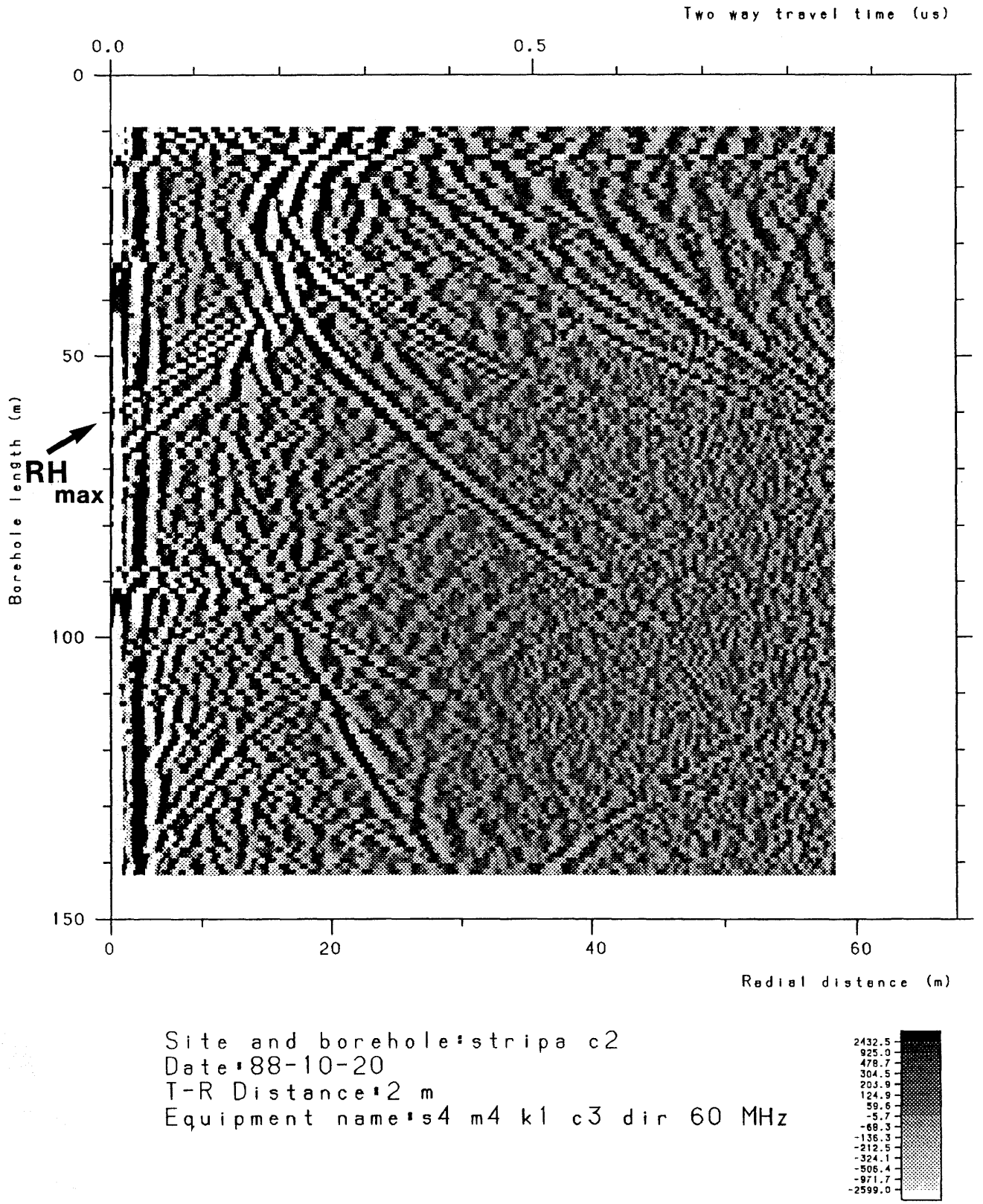

Figure A.6 Radar reflection map from the borehole C2 measured with a centre frequency of 60 MHz. Directional antenna and bandpass filter. Direction 30°.

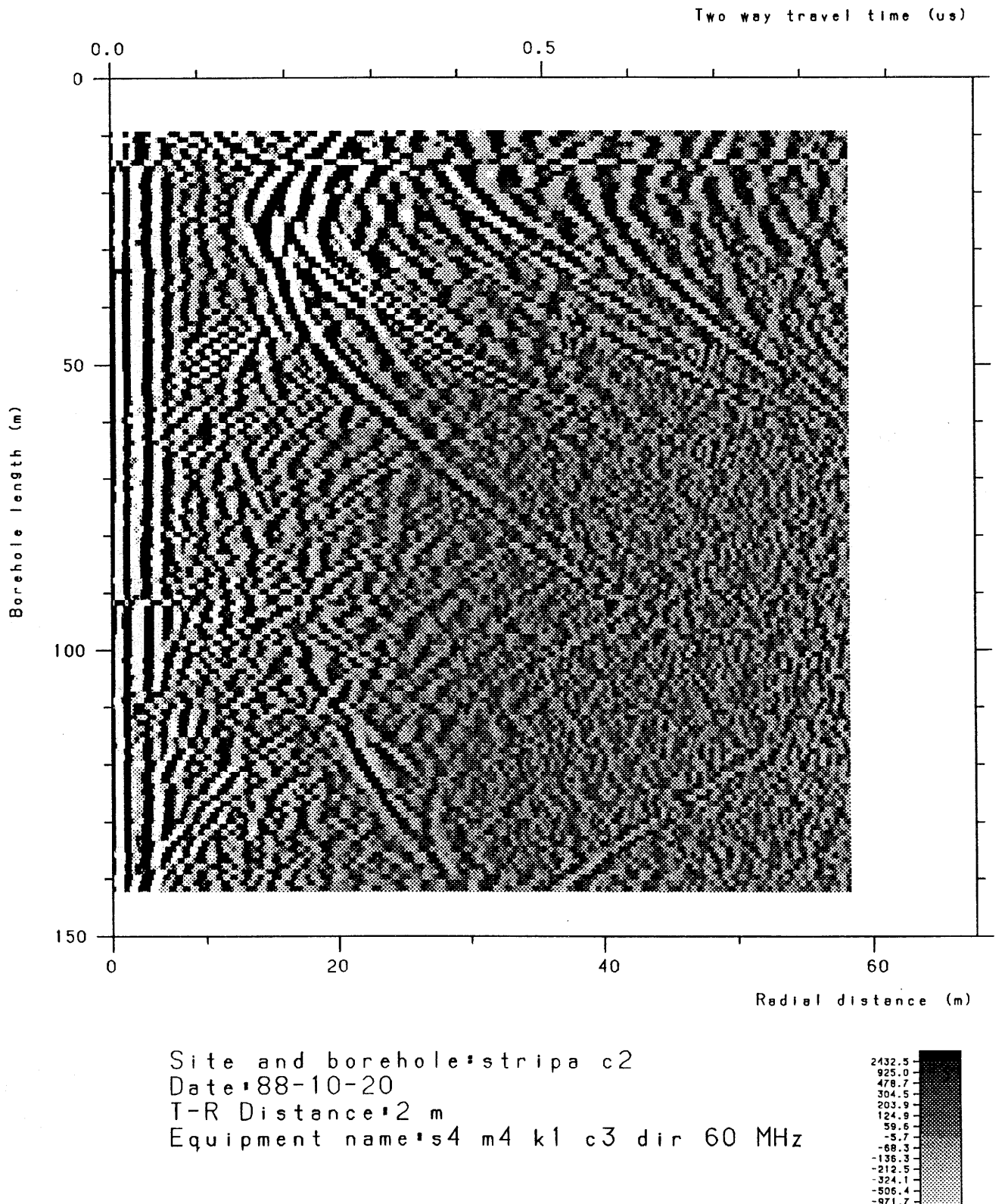

Figure A.7 Radar reflection map from the borehole C2 measured with a centre frequency of 60 MHz. Directional antenna and bandpass filter. Direction 60°.

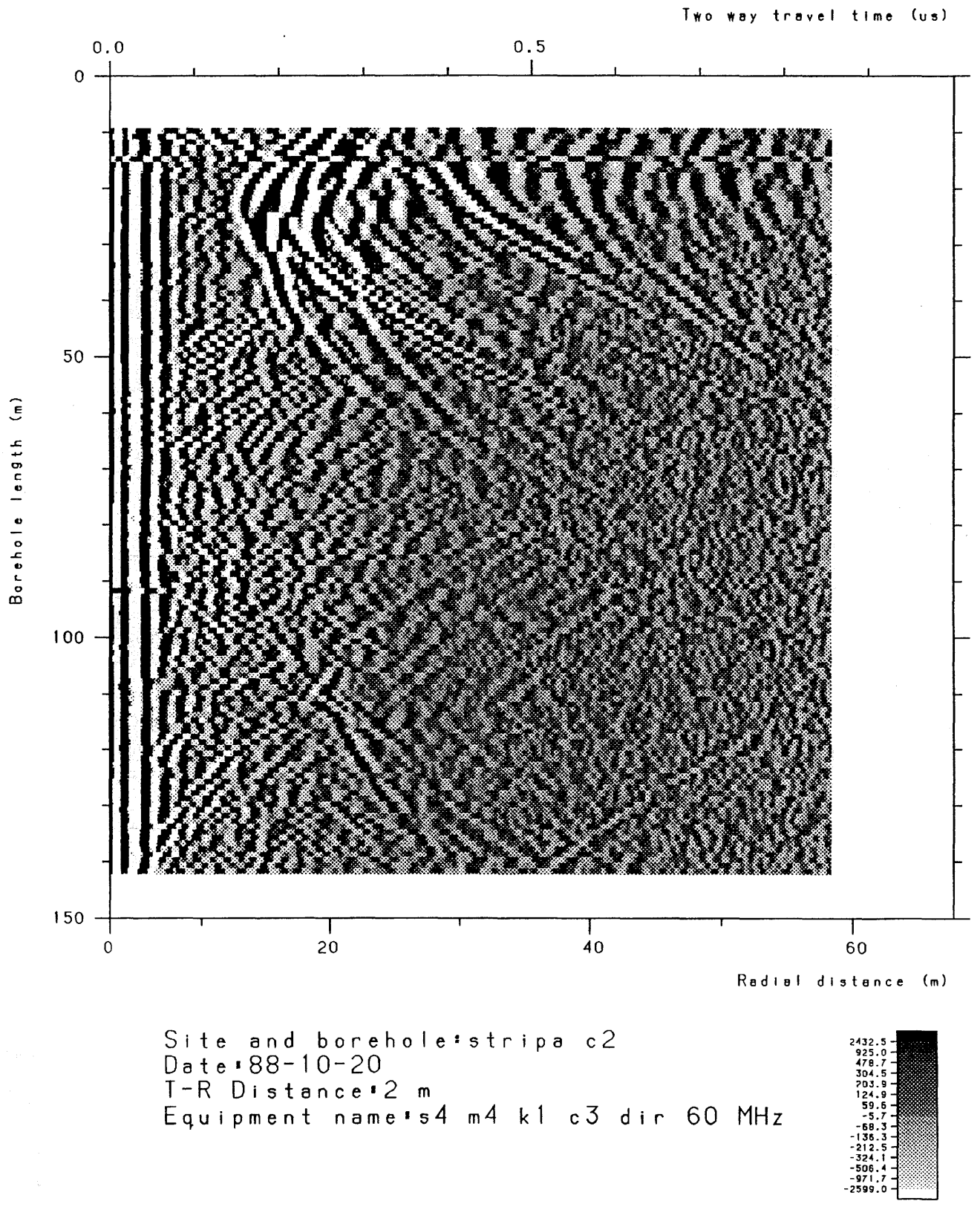

Figure A.8 Radar reflection map from the borehole C2 measured with a centre frequency of 60 MHz. Directional antenna and bandpass filter. Direction 90°.

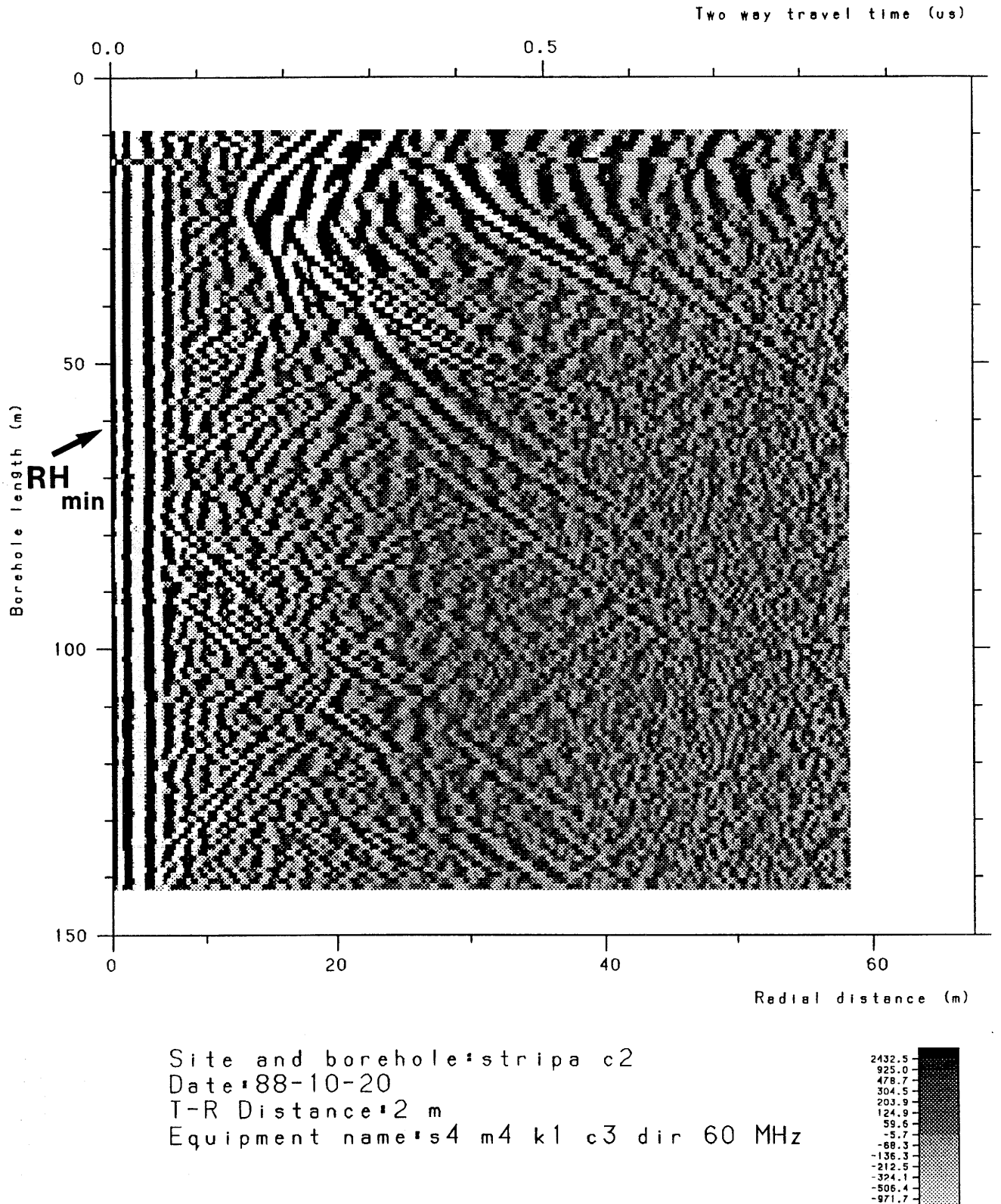

Figure A.9 Radar reflection map from the borehole C2 measured with a centre frequency of 60 MHz. Directional antenna and bandpass filter. Direction 120°.

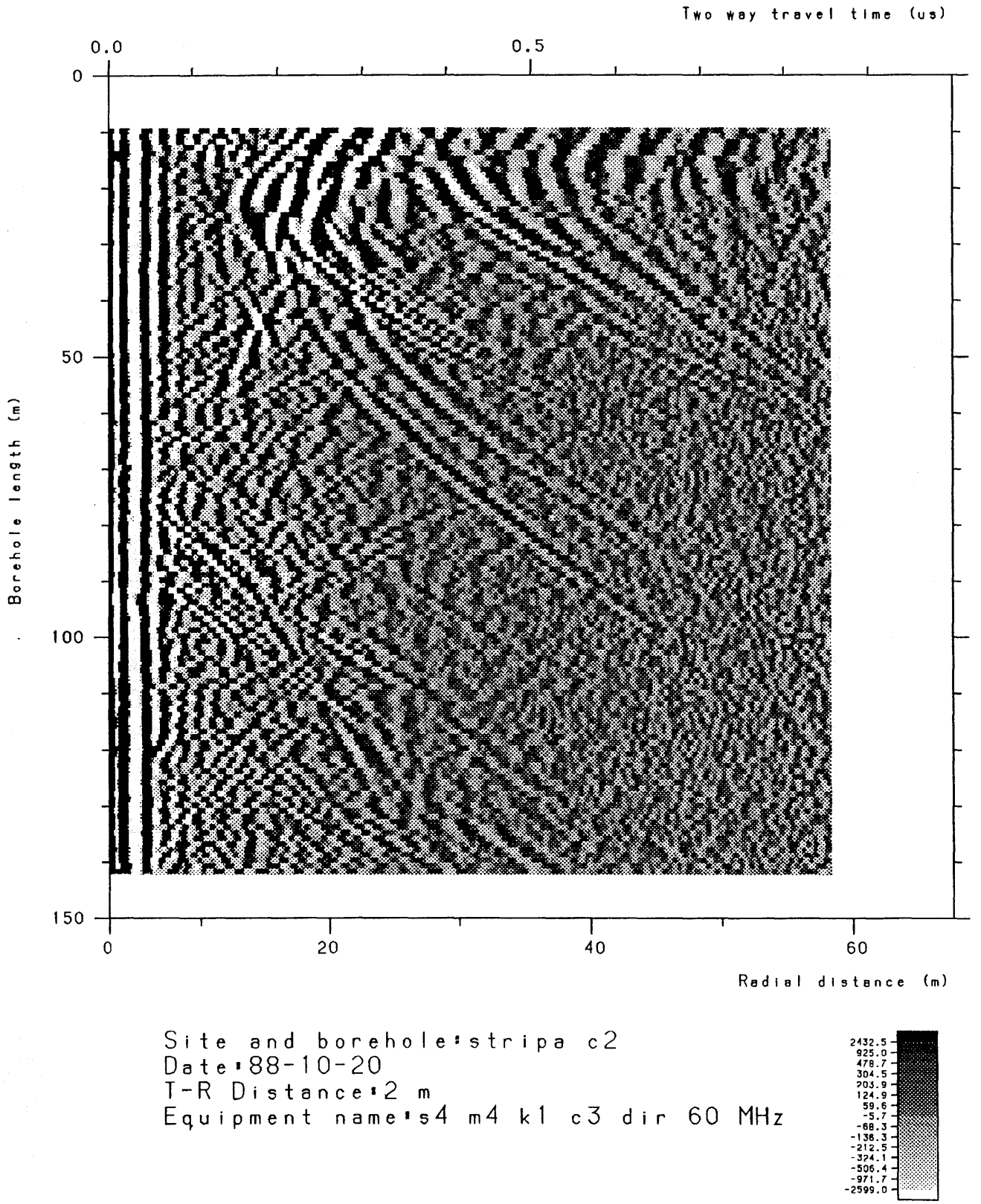

Figure A.10 Radar reflection map from the borehole C2 measured with a centre frequency of 60 MHz. Directional antenna and bandpass filter. Direction 150°.

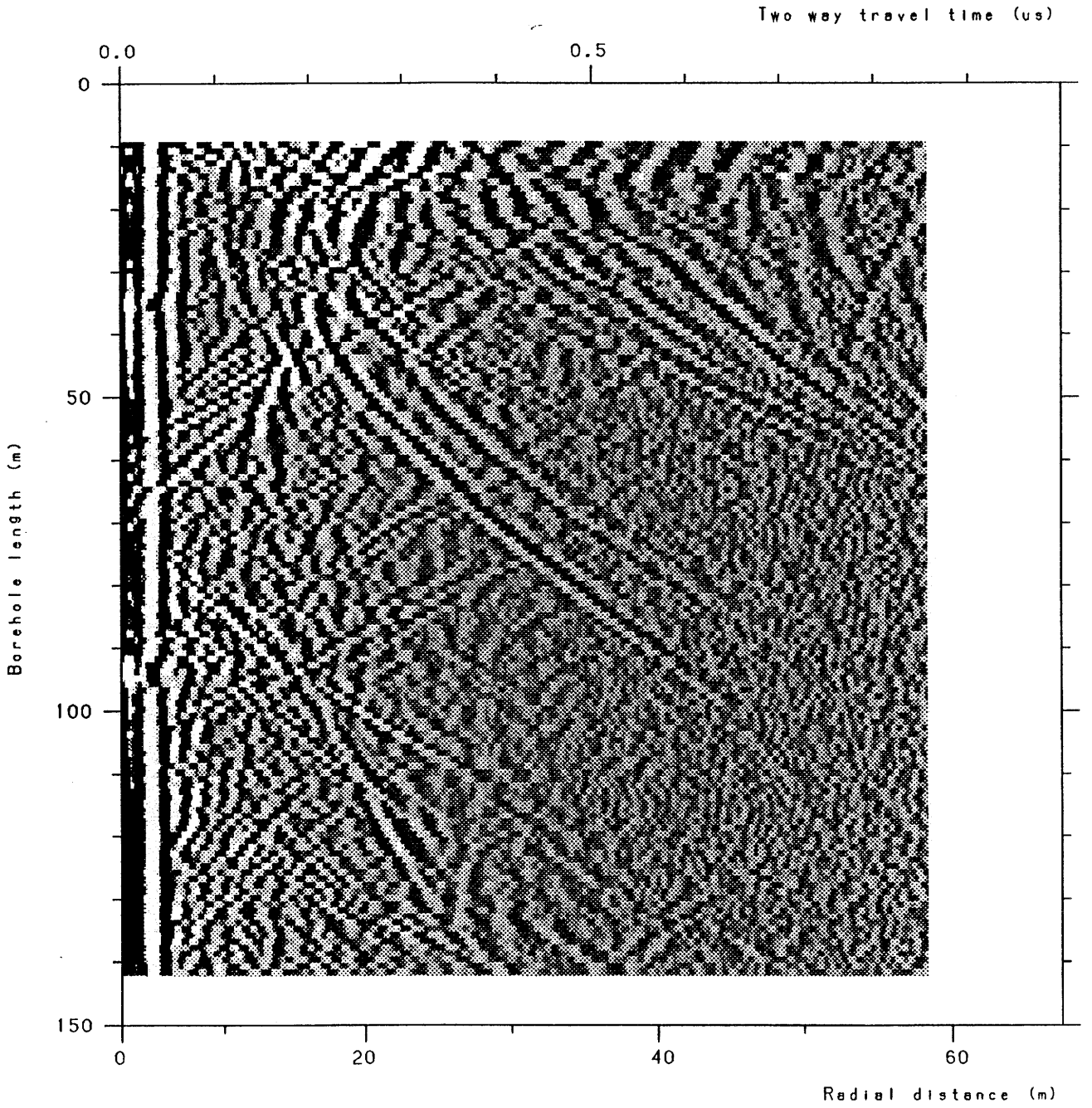

Figure A.11 Radar reflection map from the borehole C2 measured with a centre frequency of 60 MHz. Directional antenna and bandpass filter. Direction 180°.

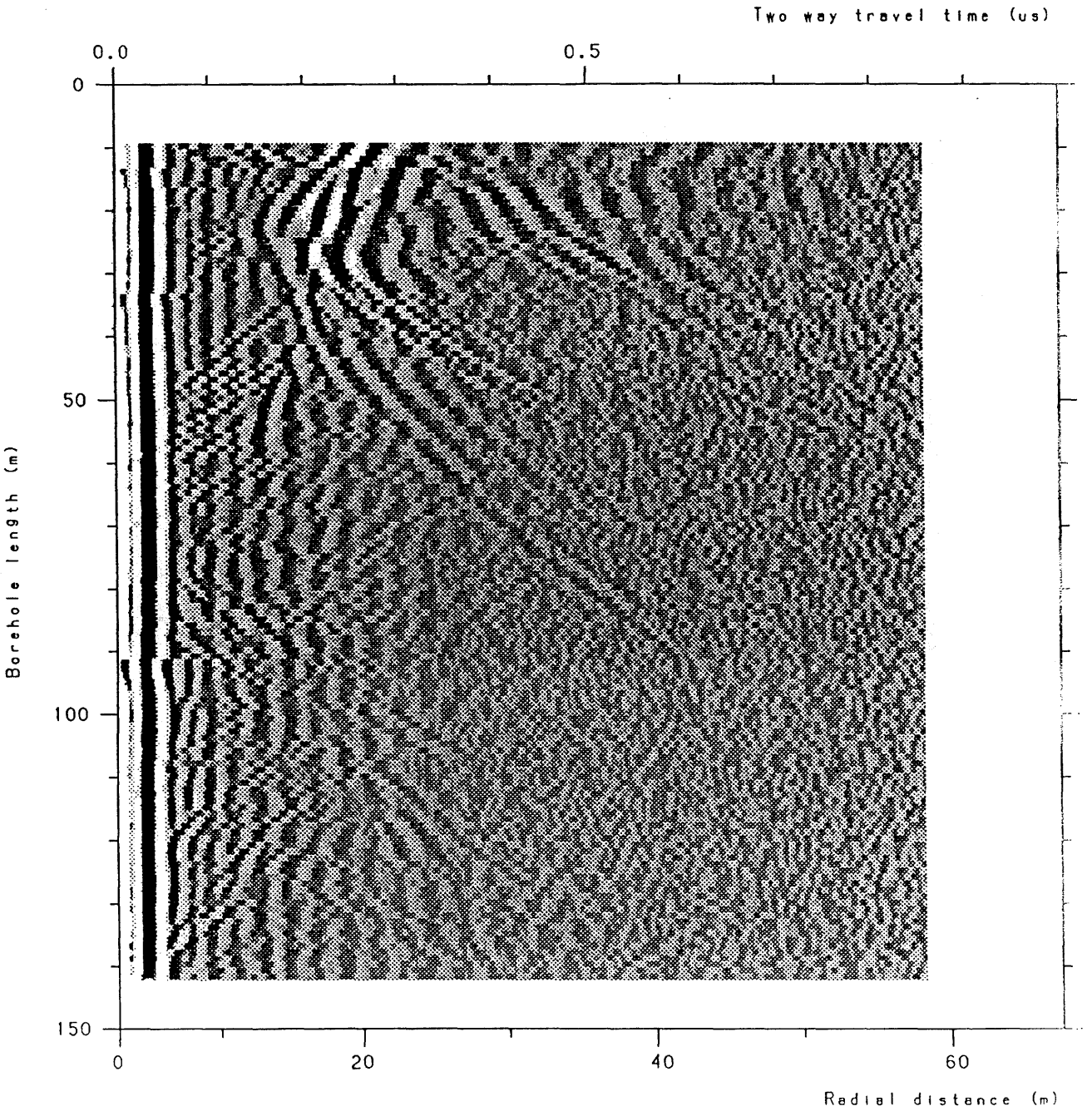

Figure A.12 Radar reflection map from the borehole C2 measured with a centre frequency of 60 MHz. Directional antenna and bandpass filter. Checksum which should give a zero signal proving that the antennas are working properly.

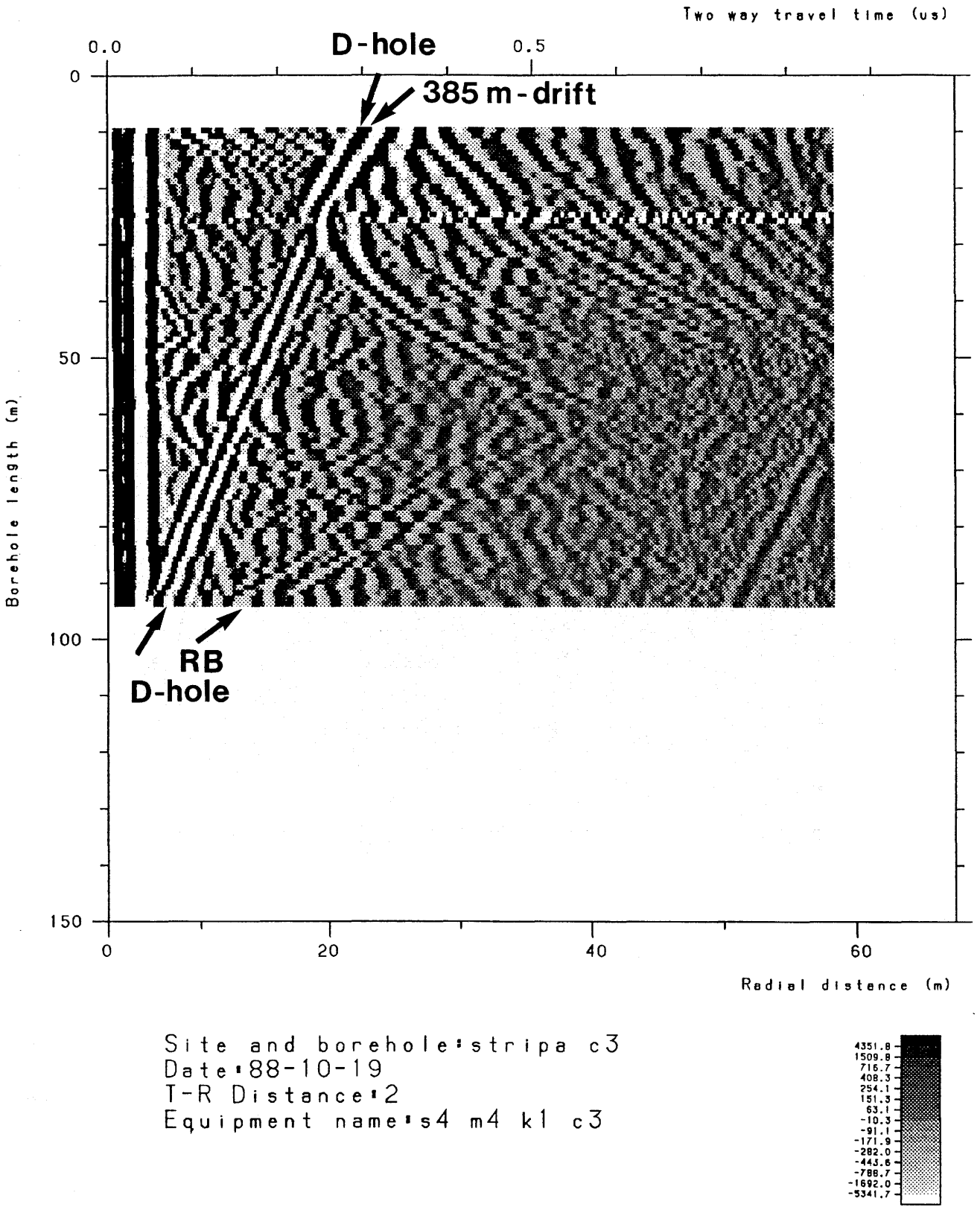

Figure A.13 Radar reflection map from the borehole C3 measured with a centre frequency of 60 MHz. Directional antenna and bandpass filter. Dipole component.

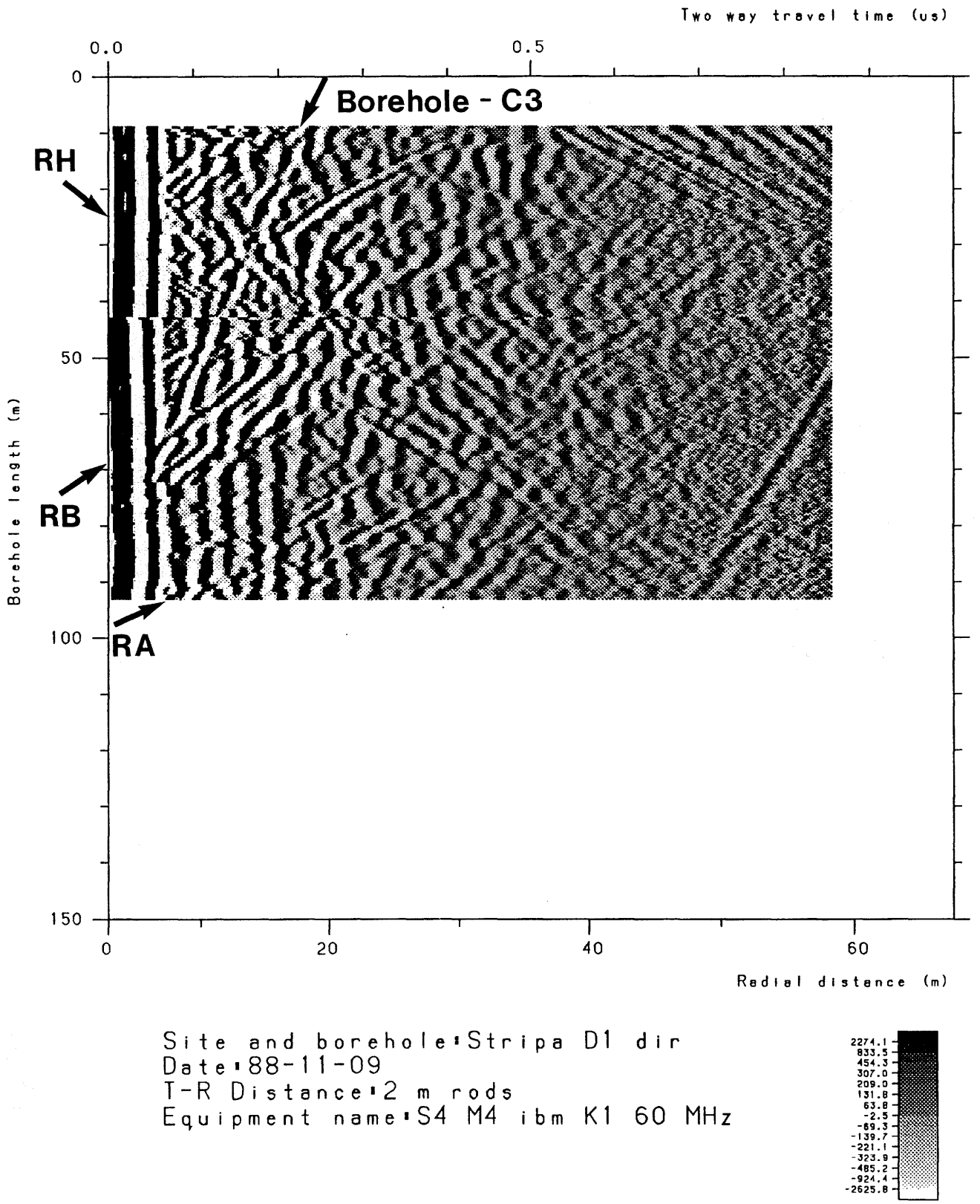

Figure A.14 Radar reflection map from the borehole D1 measured with a centre frequency of 60 MHz. Directional antenna and bandpass filter. Dipole component.

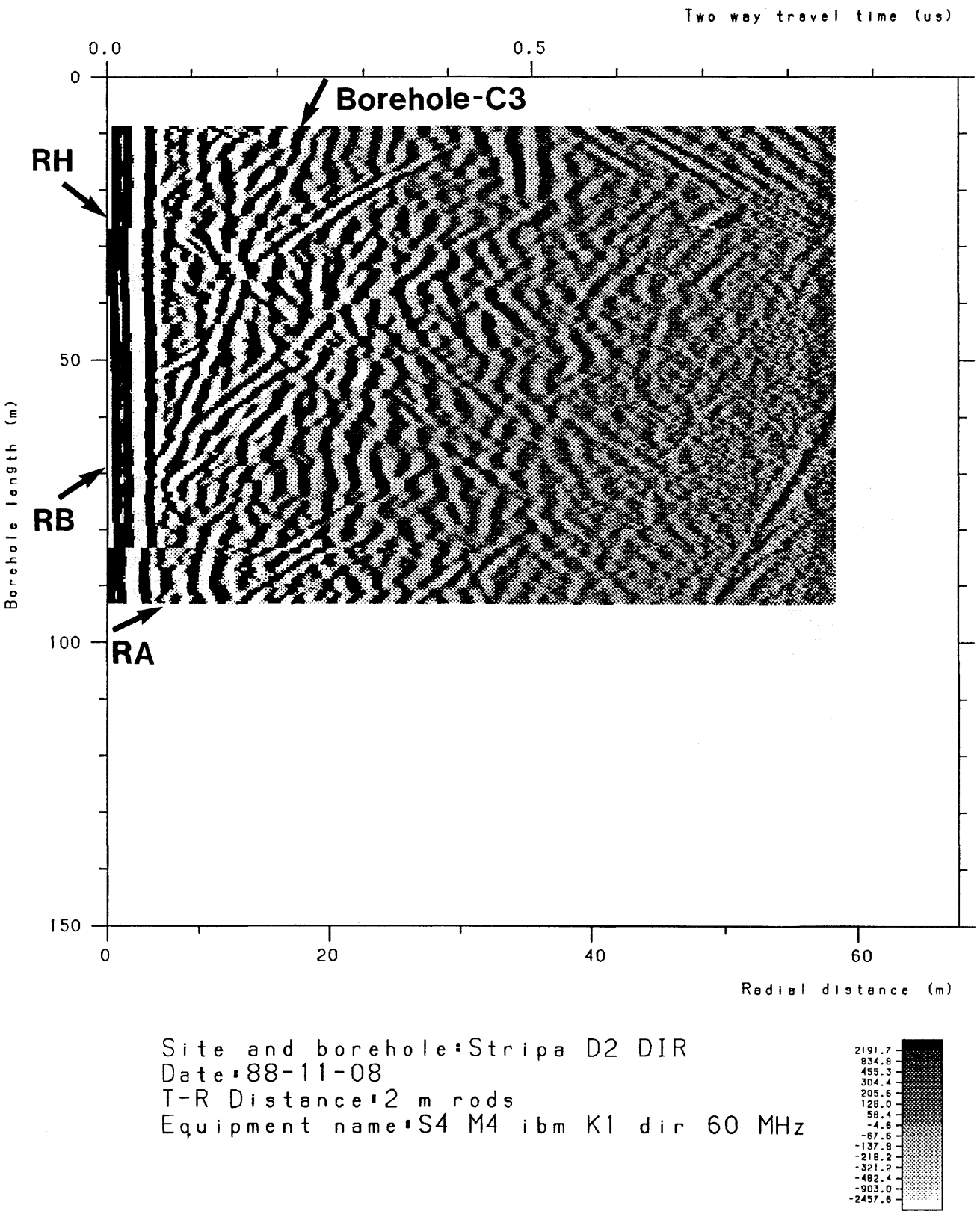

Figure A.15 Radar reflection map from the borehole D2 measured with a centre frequency of 60 MHz. Directional antenna and bandpass filter. Dipole component.

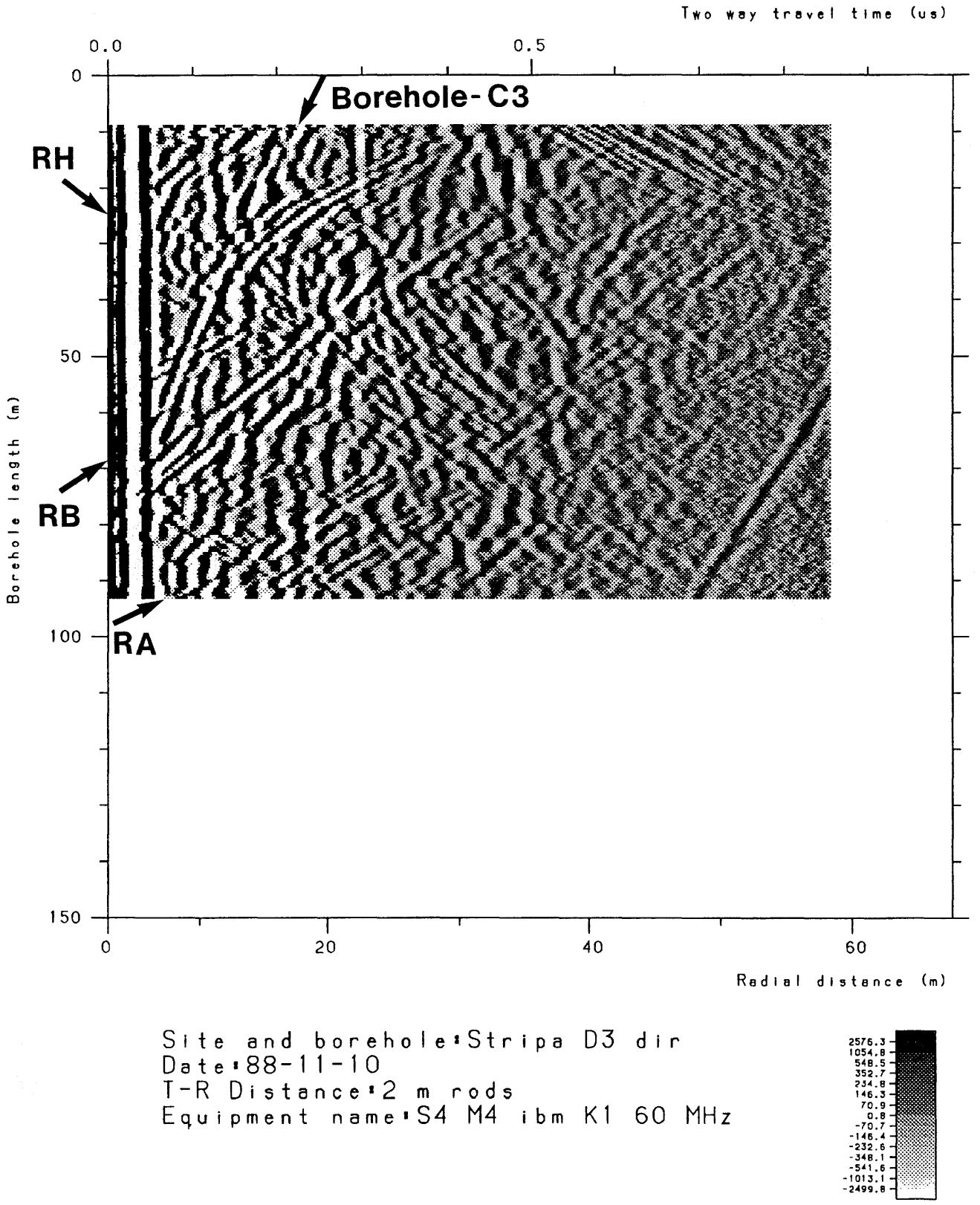

Figure A.16 Radar reflection map from the borehole D3 measured with a centre frequency of 60 MHz. Directional antenna and bandpass filter. Dipole component.

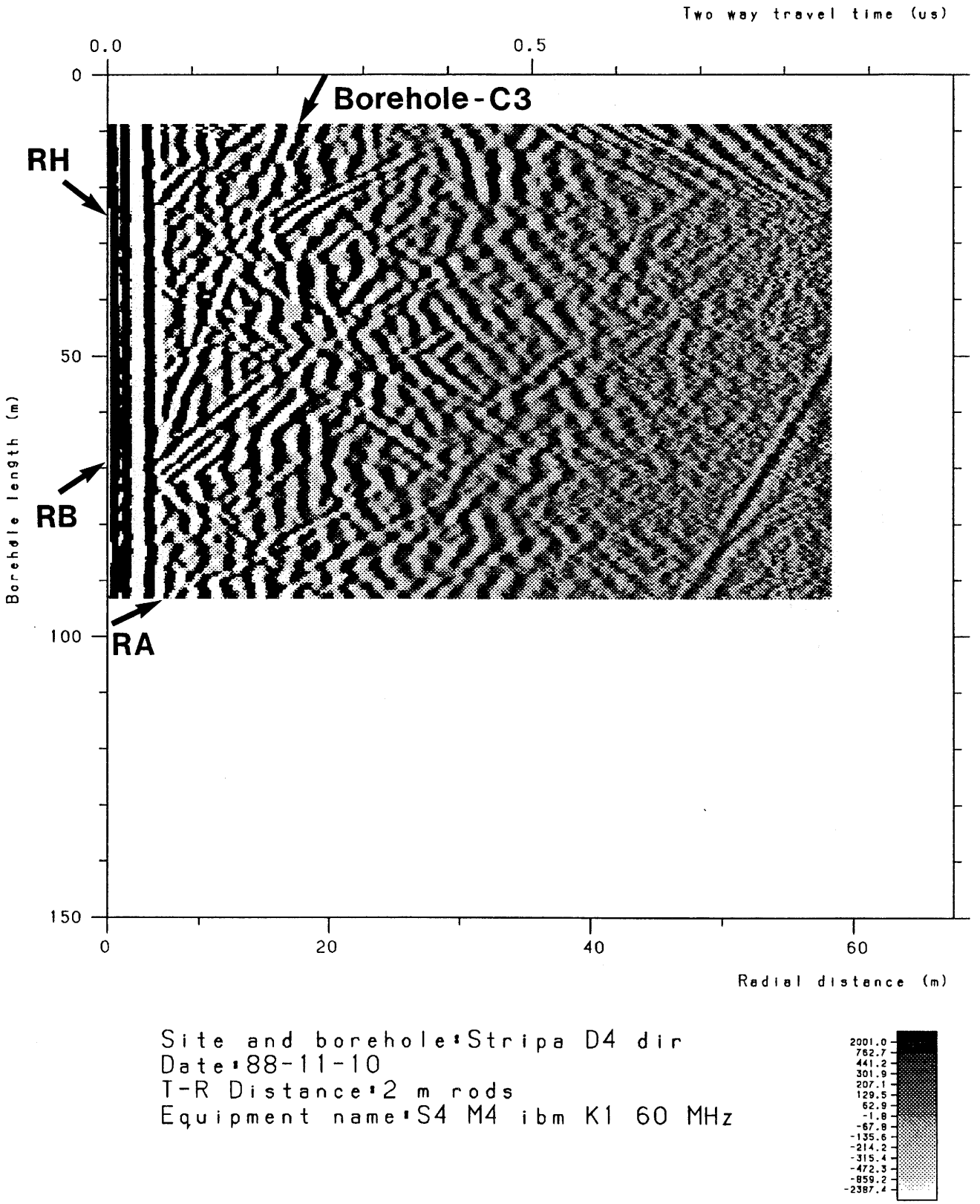

Figure A.17 Radar reflection map from the borehole D4 measured with a centre frequency of 60 MHz. Directional antenna and bandpass filter. Dipole component.

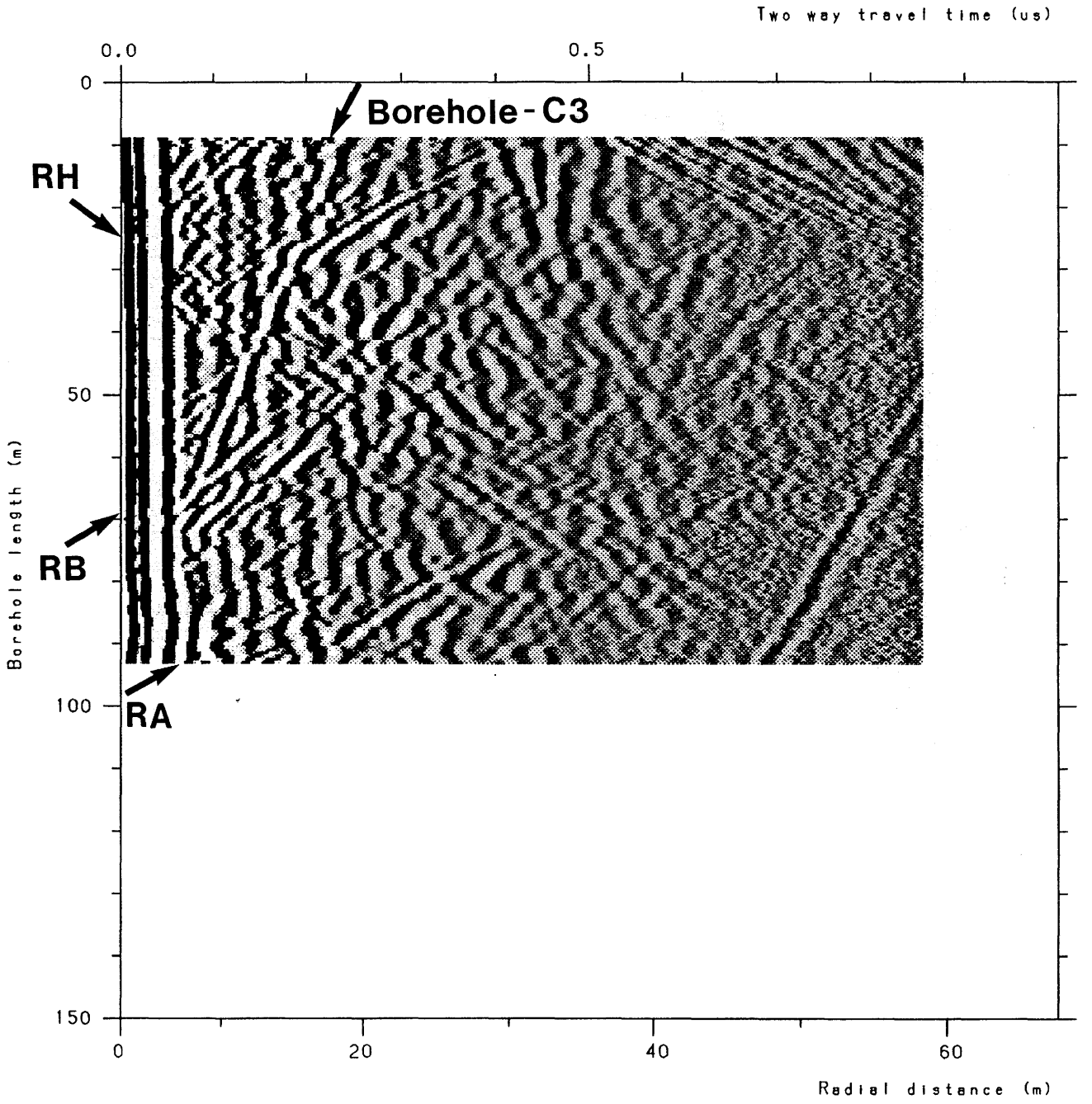

Figure A.18 Radar reflection map from the borehole D5 measured with a centre frequency of 60 MHz. Directional antenna and bandpass filter. Dipole component.

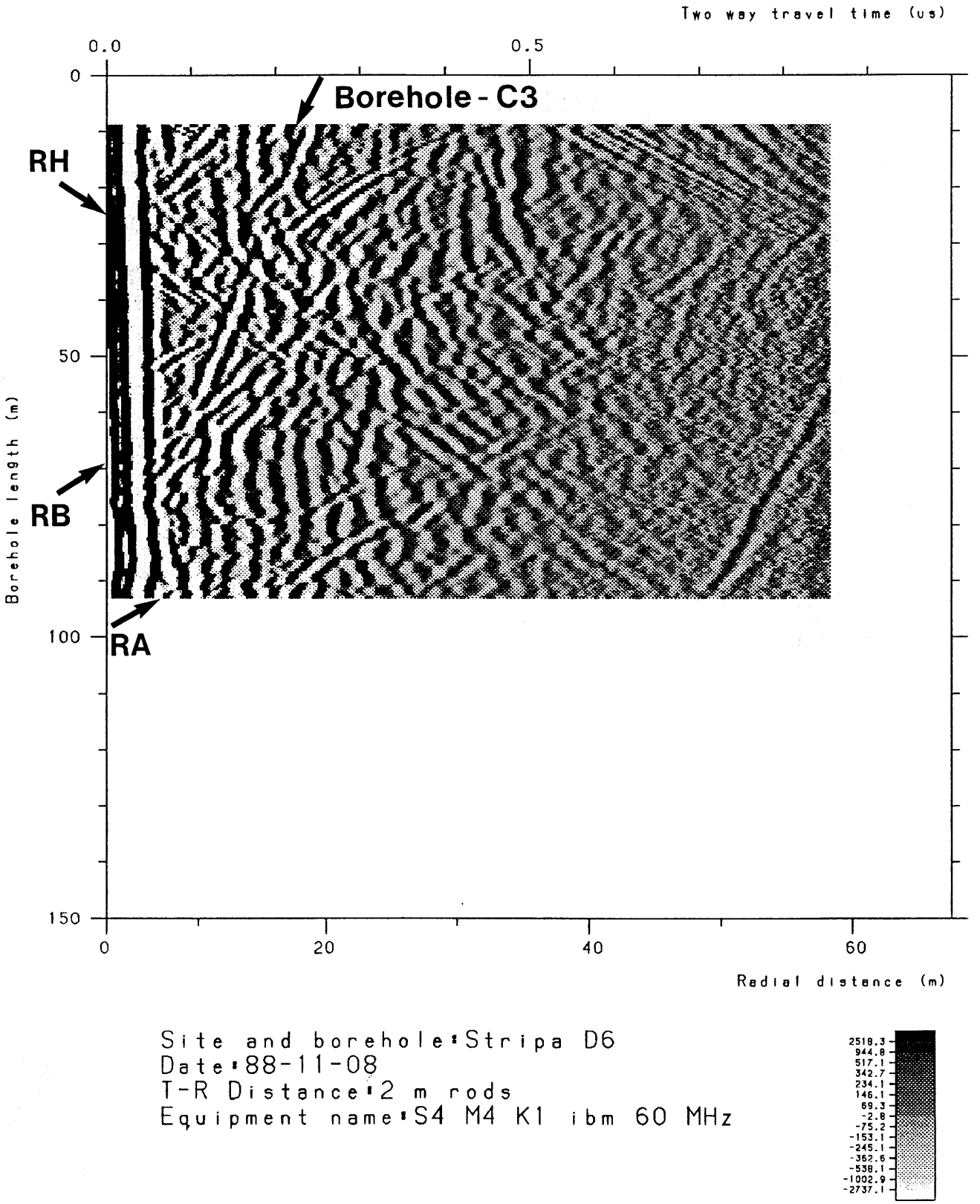

Figure A.19 Radar reflection map from the borehole D6 measured with a centre frequency of 60 MHz. Directional antenna and bandpass filter. Dipole component.

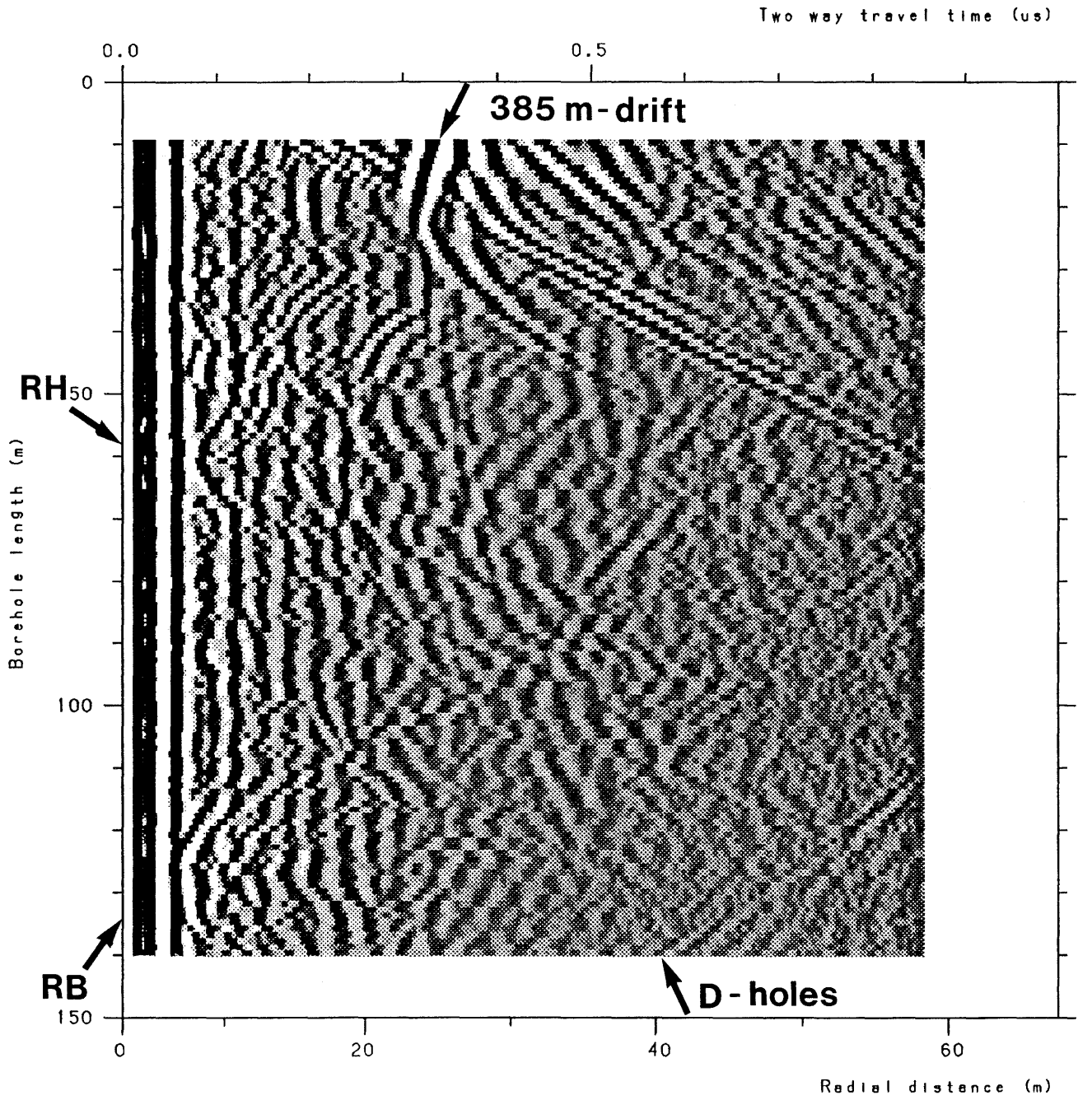

Figure A.20 Radar reflection map from the borehole W1 measured with a centre frequency of 60 MHz. Directional antenna and bandpass filter. Dipole component.

NOMOGRAM FOR PLANE REFLECTORS

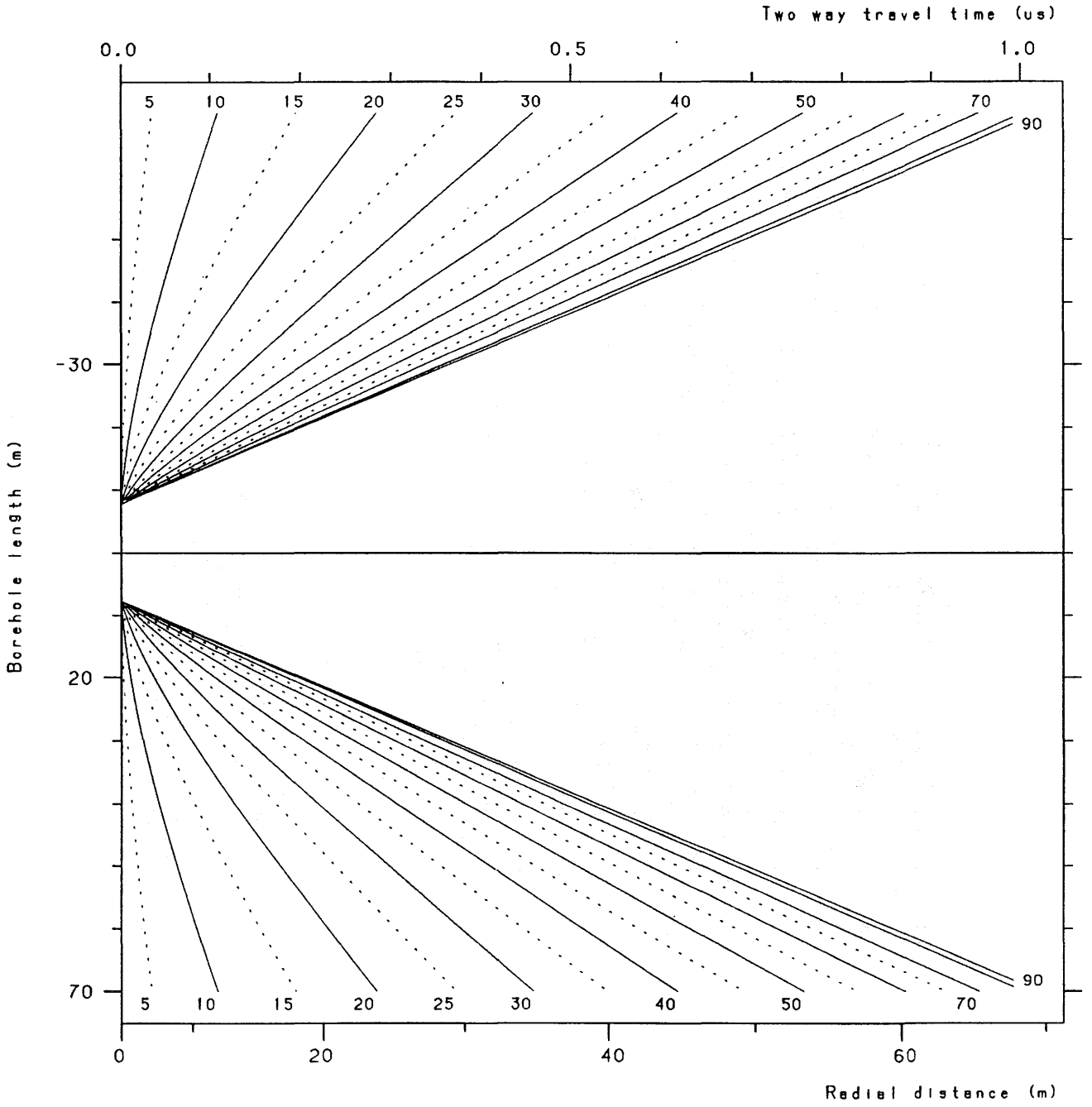

Site and borehole: STRIPA C1
Date: 88-10-10
T-R Distance: 10 M RODS
Equipment name: S2 M2 K1 C3 22 MHz

Figure A.21 Radar reflection nomogram for the 22 MHz measurements.

NOMOGRAM. Nominal velocity 122.1 m/us T-R separation 15.36 m

NOMOGRAM FOR PLANE REFLECTORS

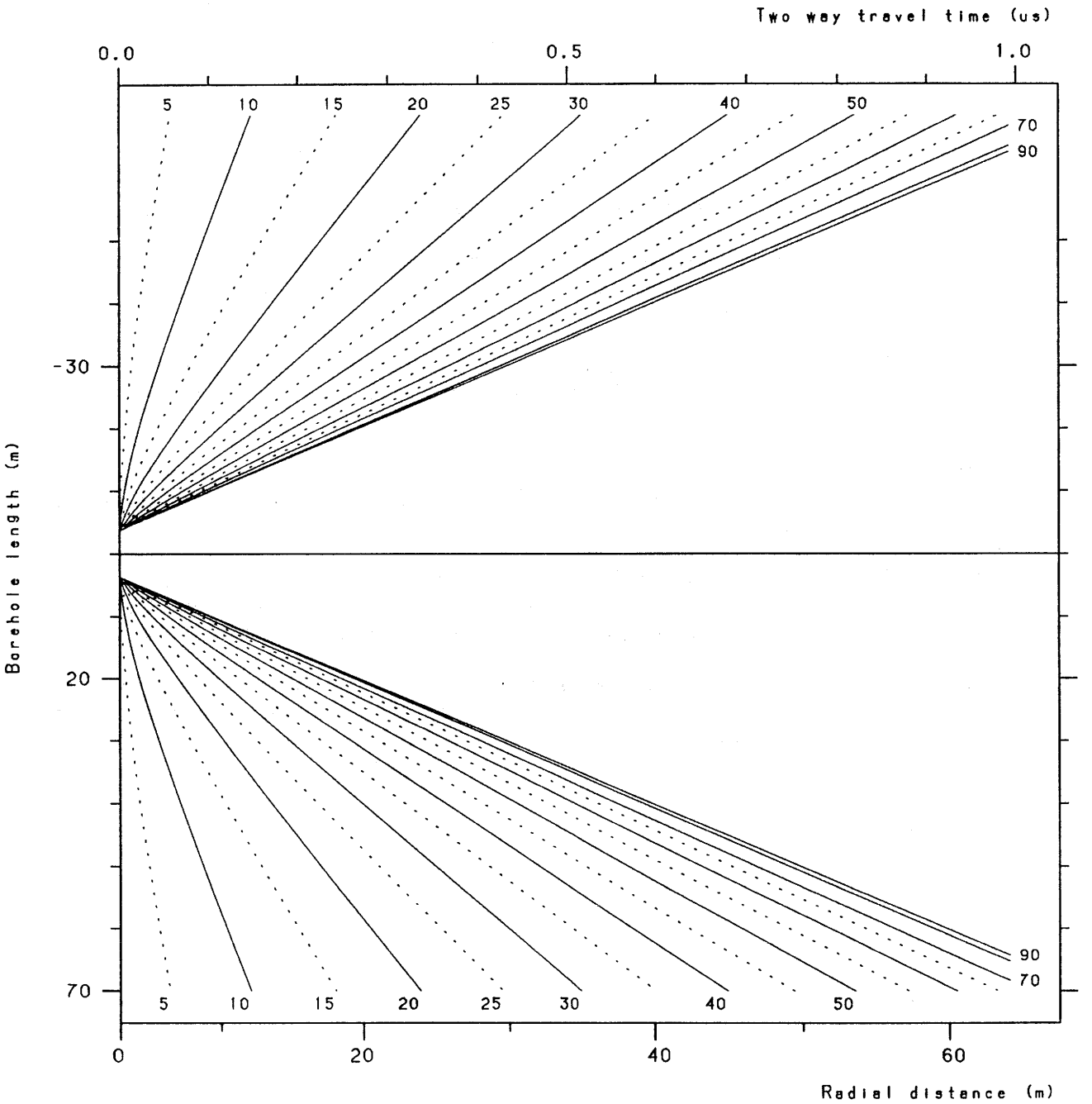

Site and borehole: Stripa D1 dir
Date: 88-11-09
T-R Distance: 2 m rods
Equipment name: S4 M4 ibm K1 60 MHz

Figure A.22 Radar reflection nomogram for the 60 MHz measurements.

NOMOGRAM, Nominal velocity 122.1 m/us T-R seperation 7.36 m

11 APPENDIX B

LIST OF RADAR TOMOGRAPHY MEASUREMENTS

Figure B.1 Residual attenuation (made on the signal envelop) tomogram for the borehole section W1-C1 made with the center frequency of 60 MHz.

Figure B.2 Residual slowness tomogram for the borehole section W1-C1 made with the center frequency of 60 MHz.

Figure B.3 Residual attenuation tomogram for the borehole section W1-C2 made with the center frequency of 60 MHz.

Figure B.4 Residual slowness tomogram for the borehole section W1-C2 made with the center frequency of 60 MHz.

Figure B.5 Residual attenuation (made on the signal envelop) tomogram for the borehole section C1-C2 made with the center frequency of 60 MHz.

Figure B.6 Residual slowness tomogram for the borehole section C1-C2 made with the center frequency of 60 MHz.

STRIPA W1C1 ENVELOP ATTENUATION (dB/km)

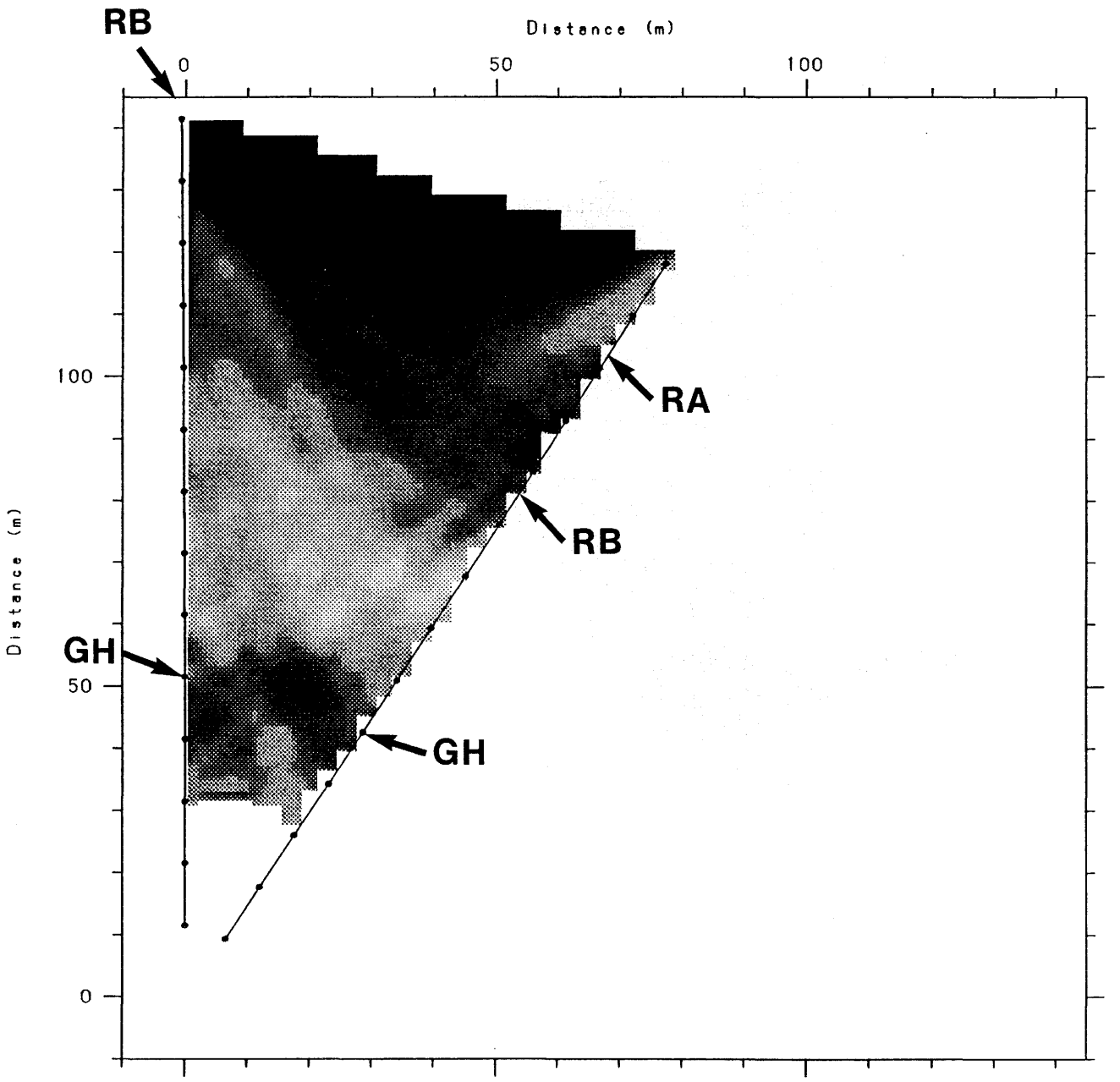

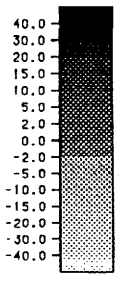

**** TOMOCG *** status and solution file ***

Input Data file: DATA.001

DATA FILE INFO:
* DATA CORRECTIONS Tmax 0 Tmin 0 Vel 0 Att 0 TPower -3.2
* DATA CORRECTIONS Aver vel 122.1 Aver att .42 Anis dir 0 Anis ampl 0
No of rows and columns: 60 30
Cell size (Z,X): 3.000 3.000
Damping factor: 100.00 Damping distr param: 1.0

Number of lines and parameters is: 759 650
Damping factor : 100.000 Damping distribution parameter: 1.00000

Figure B.1 Residual attenuation (made on the signal envelop) tomogram for the borehole section W1-C1 made with the center frequency of 60 MHz.

STRIPA W1C1 RESIDUAL SLOWNESS (ns/km)

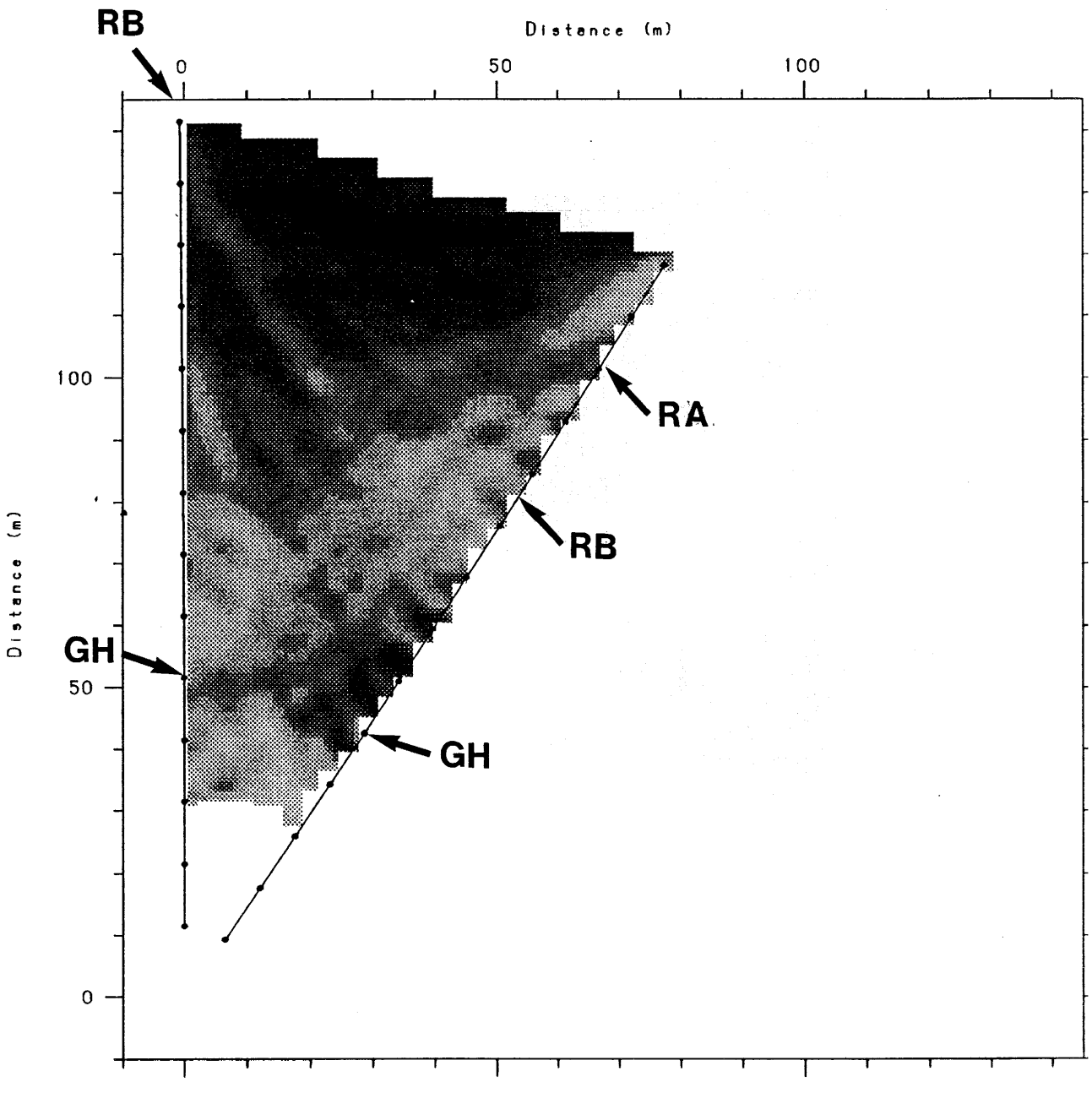

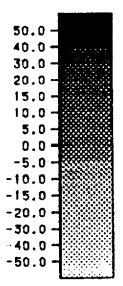

**** TOMOCG *** status and solution file ***

Input Data file: DATA.001

DATA FILE INFO:
* DATA CORRECTIONS Tmax -1.07474E-02 Tmin 0 Vel 0 Att 0 TPower 0
* Offset 0.001 Slope -0.000019 Aver 0.420000 Direc 0.0 Anis 0.0
No of rows and columns: 60 30
Cell size (Z,X): 3.000 3.000
Damping factor: 100.00 Damping distr param: 1.0

Number of lines and parameters is: 760 650
Damping factor : 100.000 Damping distribution parameter: 1.00000

Figure B.2 Residual slowness tomogram for the borehole section W1-C1 made with the center frequency of 60 MHz.

STRIPA W1C2 RESIDUAL ATTENUATION (dB/km)

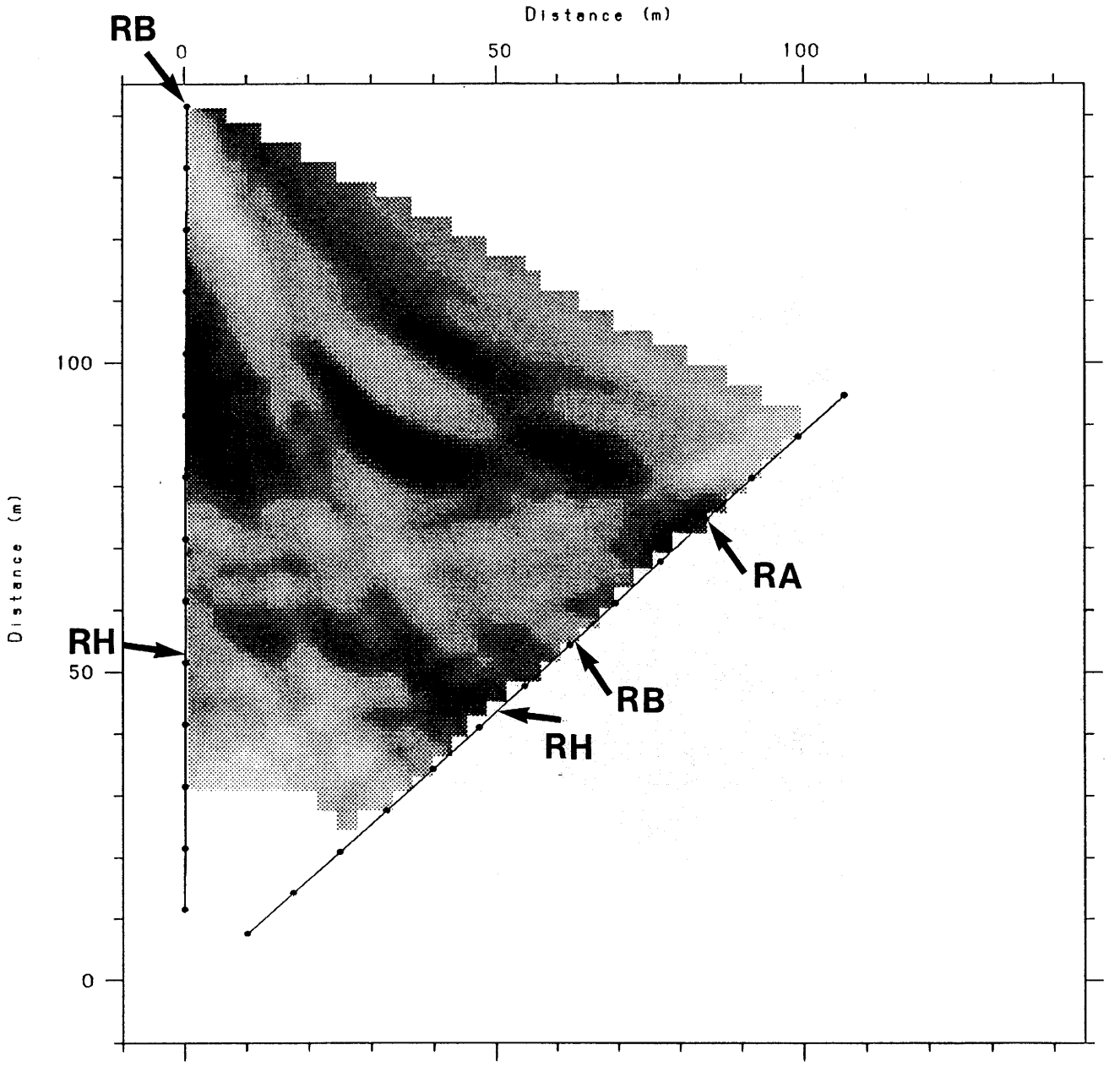

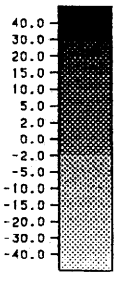

**** TOMOCG *** status and solution file ***

Input Data file: DATA.001

DATA FILE INFO:
* DATA CORRECTIONS Tmax -.011179 Tmin 0 Vel 5.4589E-05 Att 0 TPower -
* DATA CORRECTIONS Aver vel 122.1 Aver att .42 Anis dir 0 Anis ampl 0
No of rows and columns: 60 45
Cell size (Z,X): 3.000 3.000
Damping factor: 100.00 Damping distr param: 1.0

Number of lines and parameters is: 729 829
Damping factor : 100.000 Damping distribution parameter: 1.00000

Figure B.3 Residual attenuation tomogram for the borehole section W1-C2 made with the center frequency of 60 MHz.

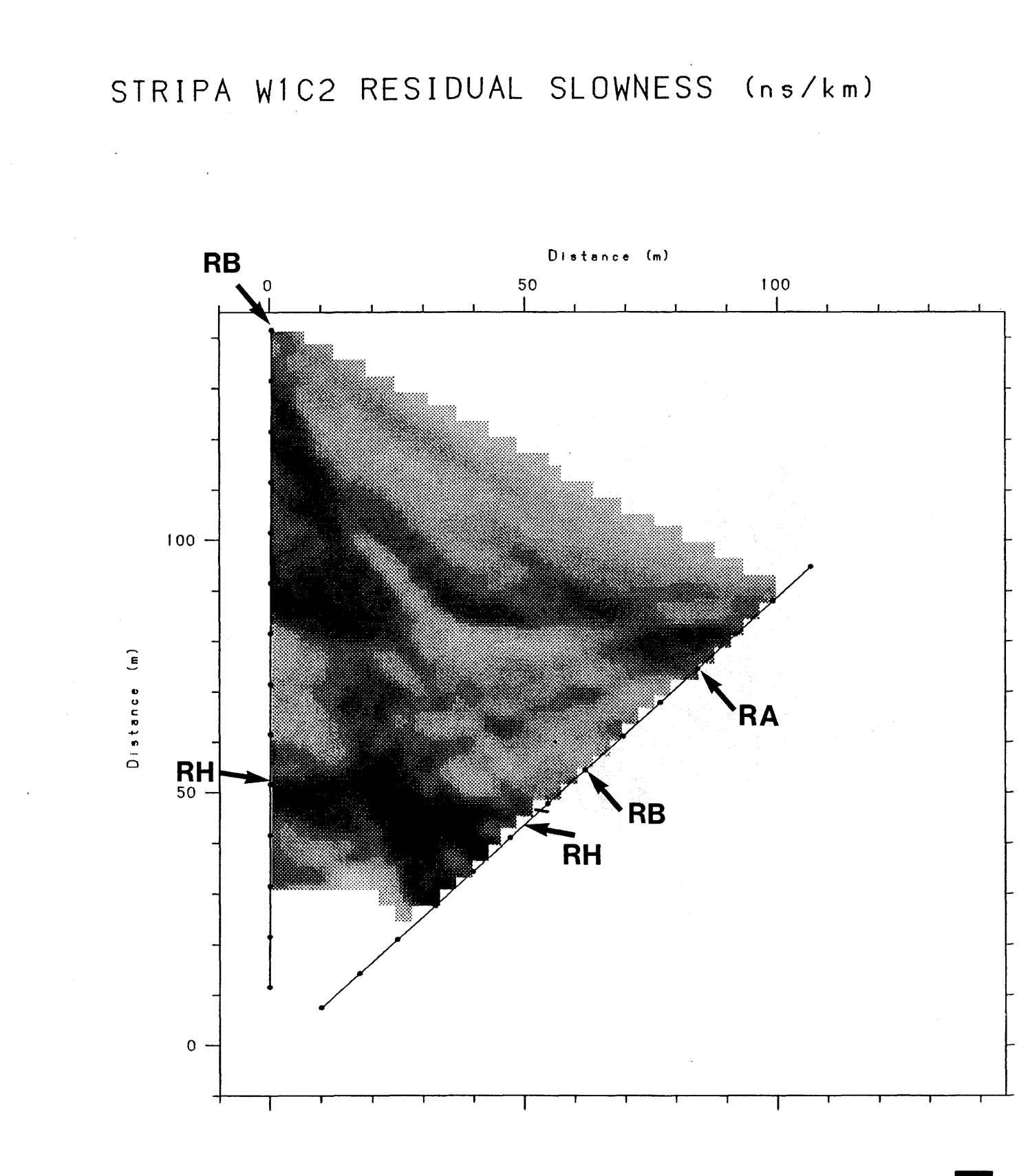

Figure B.4 Residual slowness tomogram for the borehole section W1-C2 made with the center frequency of 60 MHz.

STRIPA C1C2 ENVELOP ATTENUATION (dB/km)

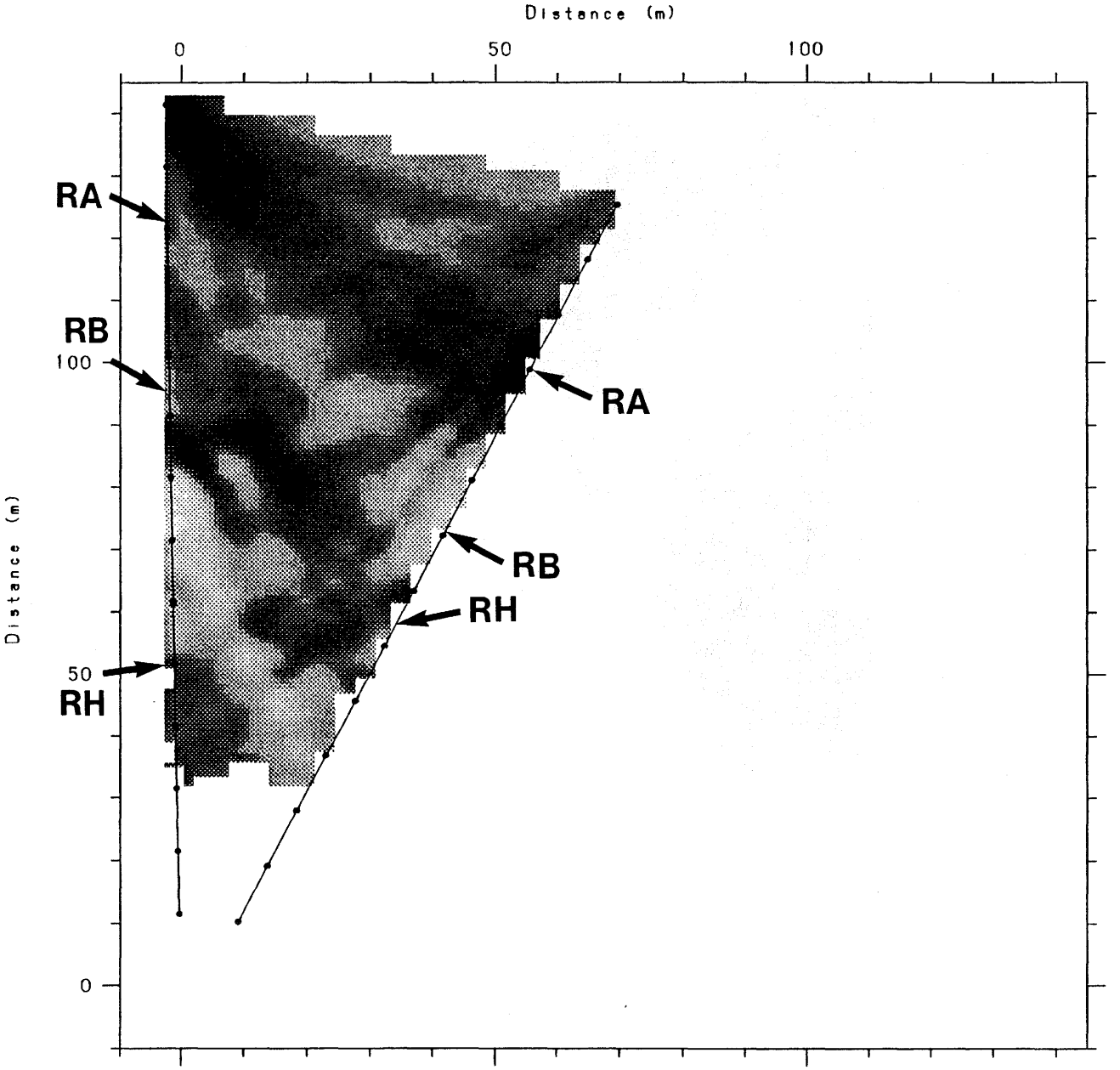

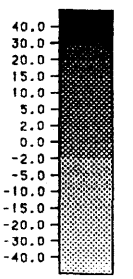

**** TOMOCG *** status and solution file ***

Input Data file: DATA.001

DATA FILE INFO:
* DATA CORRECTIONS Tmax 0 Tmin 0 Vel 0 Att 0 TPower 0
* DATA CORRECTIONS Aver vel 122.1 Aver att .42 Anis dir 105 Anis ampl
No of rows and columns: 60 30
Cell size (Z,X): 3.000 3.000
Damping factor: 100.00 Damping distr param: 1.0

Number of lines and parameters is: 759 621
Damping factor : 100.000 Damping distribution parameter: 1.00000

Figure B.5 Residual attenuation (made on the signal envelop) tomogram for the borehole section C1-C2 made with the center frequency of 60 MHz.

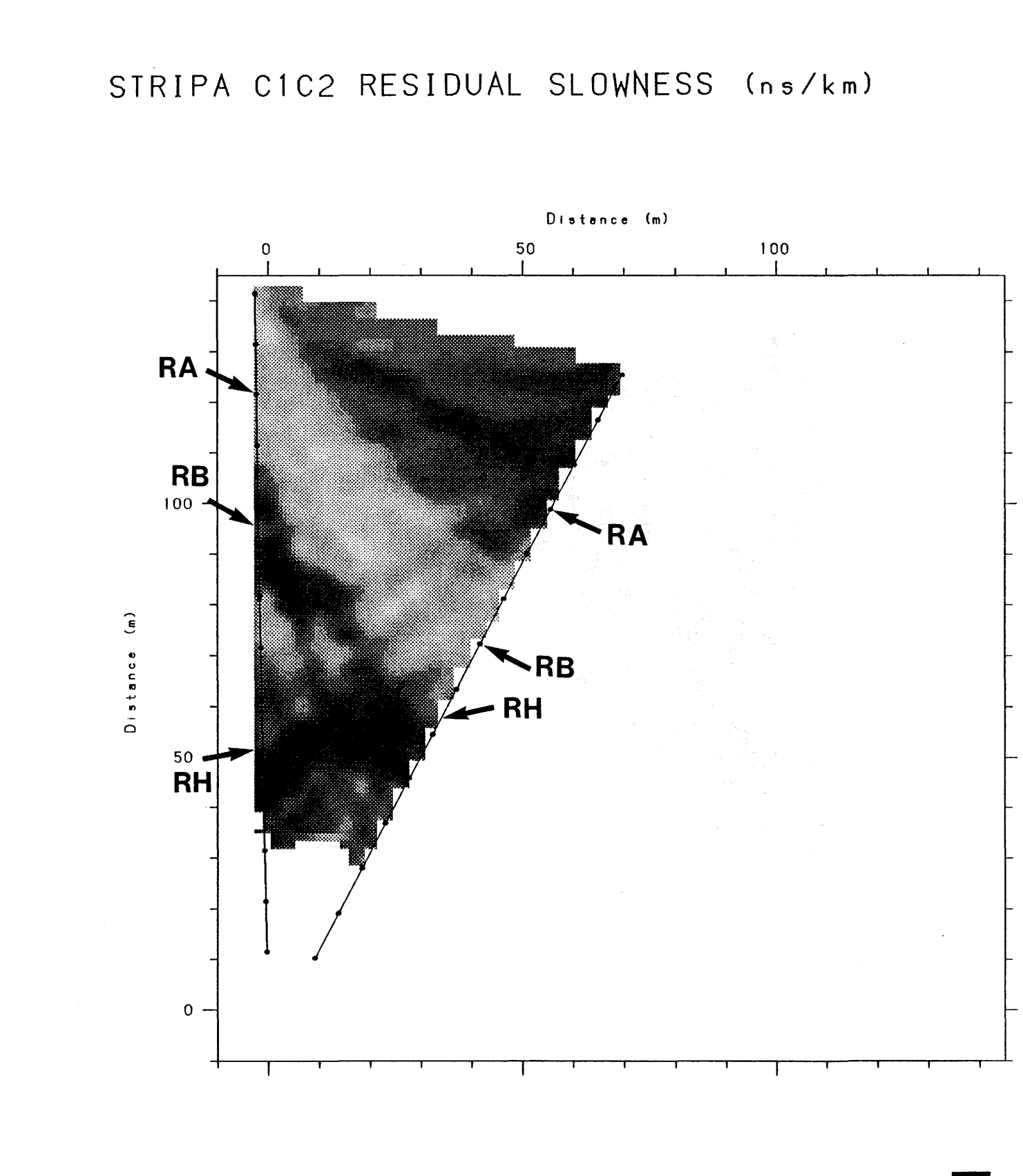

Figure B.6 Residual slowness tomogram for the borehole section C1-C2 made with the center frequency of 60 MHz.